UNIVERSITÀ DEGLI STUDI DI PARMA

Dipartimento di Chimica

Ph.D. in Science and Technology of Innovative Materials

XXVI Cycle

Cavitand Based Receptors for Sensing and Polymers

Daniele Masseroni

Coordinator: **Prof. Enrico Dalcanale**

Supervisor: **Prof. Enrico Dalcanale**

Tutor: **Dr. Elisa Biavardi**

Author: **Daniele Masseroni**

Ai miei genitori e per chi
crede sempre in me

We are not permitted to choose the frame of our destiny,
but what we put into it is ours.

Dag Hammarskjöld

Contents

Materials and Methods

Chapter 1

General Introduction

1.1 Introduction

Molecular chemistry has created a wide range of molecules and materials and has developed a variety of procedures for constructing them from atoms linked by covalent bonds.[1] Beyond the molecules, supramolecular chemistry aims at developing highly complex chemical systems from different molecular components held together by non-covalent intermolecular forces.[2]
Based on the principles of molecular recognition[3] and self-assembly,[4] the multidisciplinary domain of supramolecular chemistry is intrinsically dynamic which allows the spontaneous but information-directed generation of organized structures under equilibrium conditions. Thanks to a constant and continuous development, supramolecular chemistry has expanded the playground of the researchers in the material science field. In this regard, thanks to its capability to manipulate the non-covalent intermolecular forces that hold together different constituents, supramolecular chemistry is a powerful strategy for the creation of new materials with outstanding properties. In fact, by mastering molecular recognition processes, chemists can impart and finely tune new active functions leading to advanced functional materials that are hardly achievable with other methods. Simple system are replaced by even more complex ones, building blocks become more intricate, with respect to both structure and function.

Nowadays supramolecular chemistry is even more an application oriented science,[5] because has a central role in the generation of structures capable of advanced tasks. The aim of the present thesis is to synthesize new building blocks with specific functionalities in order to generate supramolecular polymers, fluorescent sensors, and supramolecular vesicles, exploiting the molecular recognition paradigm.

1.2 Molecular Receptors

Molecular recognition can be defined as the selective recognition of substrate molecules (guests) by synthetic receptors (hosts). Molecular receptors bearing specific recognition functions are the fundamental units that allow the assembly of supramolecular aggregates. Conventional approaches for designing molecular receptors have been made using the *lock and key* theory (a steric fit concept enunciated by Emil Fischer in 1894).[6] Indeed, as for biological systems, the concepts of size, shape and chemical complementarity are crucial for successful molecular recognition processes in artificial host-guest systems. In the late 1960s, Pedersen,[7] Lehn,[2] Cram[8] and others, reported on the synthesis of

numerous receptors, differently pre-organized, capable of binding specific substrates.
Considerable attention has been paid to molecular receptors named cavitands. According to Cram, they are synthetic organic compounds having enforced cavities large enough to complex complementary organic molecules or ions.[9] The present thesis takes its place in this context, and it shows, by harnessing non-covalent interactions within different building blocks, how it is possible to generate functional materials.
In the following paragraphs we will illustrate the synthesis, structural properties and molecular recognition features of two classes of molecular receptors: tetraphosphonate cavitands and cucurbit[*n*]urils. These two macrocyclic receptors will be exploited throughout the thesis as structural subunits to assembly advanced materials.

1.2.1 Tetraphosphonate Cavitands

A suitable scaffold for the synthesis of cavitands that can be exploited for recognition process is the resorcin[*4*]arene macrocycle, prepared by an acid condensation between resorcinol and an appropriate aldehyde.[10] The choice of a different R group in the resorcinol or in the aldehyde (R_1 or R_2, Figure 1.1) provides different points for derivatizations both at the upper and at the lower rim. However, the resorcin[*4*]arene scaffold is too flexible to be used in host-guest chemistry, whereas bridging the phenolic groups with a proper functionality leads to a rigid cavity, improving complexation capability. Among the possible bridging groups, phosphonate moieties impart special recognition features toward positively charged species such as alkaline-earth cations,[11] *N*-methylammonium or *N*-methylpyridinium species.[12]

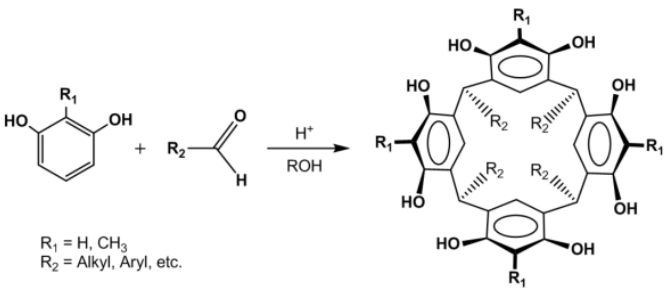

Figure 1.1 *Resorcin[4]arene synthesis.*

The presence of four stereogenic centers in the tetraphosphonate cavitands gives rise to six possible diasteroisomers, differing from each other for the orientation of the P=O moieties, inward (i) or outward (o) the cavity (Figure 1.2; for complete nomenclature see ref. 13). Stereochemistry is pivotal to determine the cavitand complexing capability. In particular, considering the ammonium salts class as target guests, the cavitand that presents the best recognition properties is the one with all the four P=O moieties oriented inward with respect to the cavity (**Tiiii**).

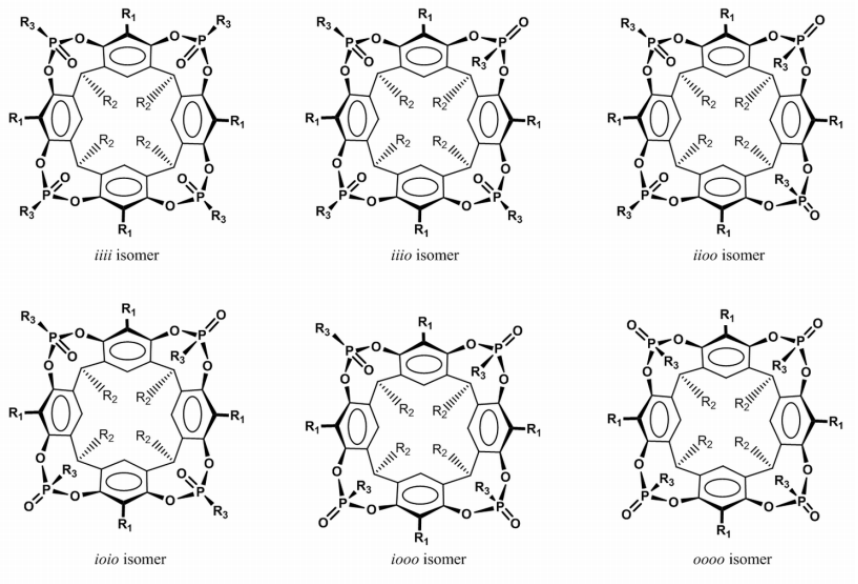

Figure 1.2 *Isomers of tetraphosphonate bridged cavitands.*

The main specific interactions responsible for its complexation ability, which can be activated either individually or in combination are: (i) multiple ion-dipole interactions between the inward facing P=O and the positively charged species, (ii) single or multiple H-bonding involving the P=O groups and the nitrogen protons, and (iii) CH_3-π interactions between an acidic *N*-methyl group of the guest and the π-basic cavity of the host. In Figure 1.3 are illustrated the complexation mode of tetraphosphonate cavitand towards *N*-methylpyridinium (left) and *N*-alkylammonium salts (right). The interactions involved in the first case are two, namely cation-dipole and CH-π interactions, while in the second case all the three interactions operate in a synergistic

fashion, causing the higher affinity of the *N*-methylammonium towards the cavity.[14]

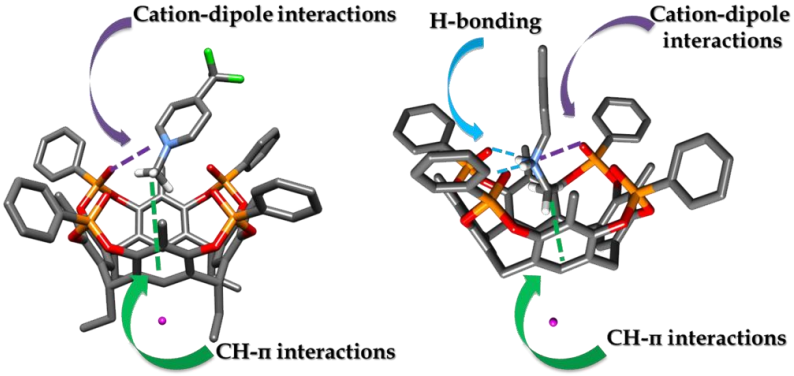

Figure 1.3 *Complexation mode of tetraphosphonate cavitands towards N-methylpyridinium salts (left) and N-alkylammonium salts (right).*

As already discussed, the stereochemistry of tetraphosphonate cavitand is fundamental to determine its complexation ability, demanding an appropriate synthetic path that can lead to the synthesis of the **Tiiii** stereoisomer as the major product.

The group of Dutasta was the first able to synthesized the right stereoisomer, performing the reaction in toluene with *P,P*-dichlorophenylphosphine oxide and *N*-methylpyrrolidinium as templating agent (Figure 1.4).[15] In this reaction the use of a less reactive P(V) reagent leads to a low yield of the desired isomer and the simultaneous formation of the **Tiiio** isomer, albeit in a low amount.

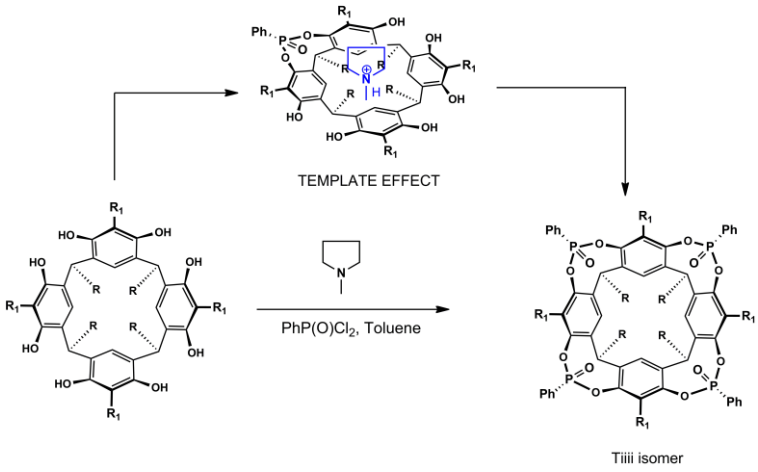

Figure 1.4 ***Tiiii*** *isomer synthesis via template effect.*

These shortcomings have been addressed by employing a stereospecific synthesis. This reaction necessitates bridging the resorcin[4]arene scaffold with four P(III) units and then oxidizing them *in situ* with hydrogen peroxide (Figure 1.5).[16] The outcome of the one pot two steps reaction is the desired product in high yield (up to 90%). The stereospecificity of the reaction is related to the formation of an intermediate based on P(III), where all the electrons lone pairs point inside the cavity.[17]

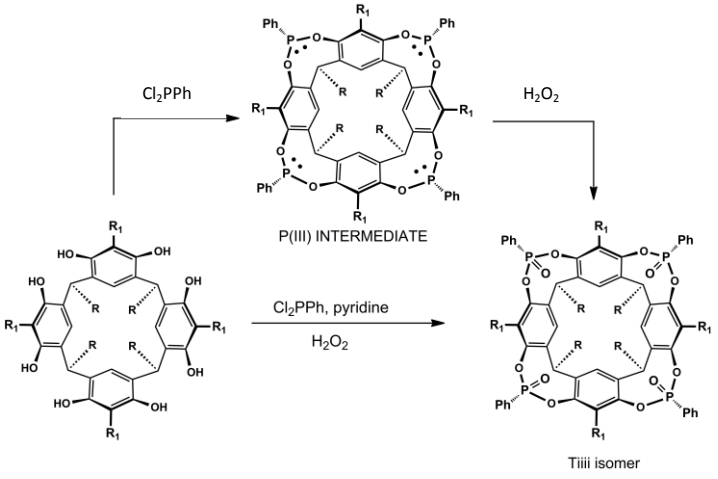

Figure 1.5 ***Tiiii*** *isomer synthesis via P(III) intermediate.*

When the P=O moieties are replaced by the P=S ones, the structurally related tetrathiophosphonate cavitands[18] are obtained (Figure 1.6). Those receptors have been synthesized via oxidation *in situ* of the tetraphosphonite cavitand with S_8. The presence of four P=S groups shift the molecular recognition properties toward other guests like soft metals (Ag^+, Hg^{2+} *etc.*).[19] There is no recognition process with the ammonium and pyridinium guests because sulphur has lower electronic density with respect to the oxygen and consequently it is less prone to H-bonding interactions.[20]

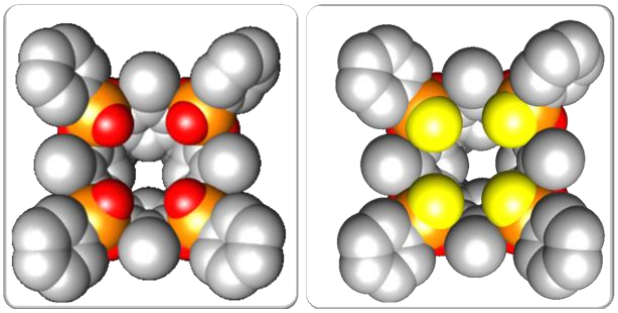

Figure 1.6 *Top view of tetraphosphonate (left) and tetrathiophosphonate cavitands (right).*

The well known recognition properties of tetraphosphonate cavitands make this molecule a suitable host for the two basic research lines of supramolecular chemistry: molecular recognition and self organization processes.
A clever application of the molecular recognition properties of **Tiiii** cavitand has been reported in a recent paper by Dalcanale *et al.*,[21] demonstrating the specific detection of sarcosine, a methylated form of glycine, recently linked to the occurrence of aggressive prostate cancer forms,[22] in water and urine. The recognition processes has been investigated in the solid state, in solution, and at the solid–liquid interface. The decisive step in this work has been grafting the receptor on a silicon wafer (**Tiiii**-Si), hence transferring the complexation features of **Tiiii** onto surface. The functionalized surface has been tested in urine with XPS and fluorescence guest displacement tests, that have demonstrated the selectivity of **Tiiii**-Si towards sarcosine.

In this thesis the tetraphosphonate receptors will be exploited in Chapters 2 and 3 for the construction of supramolecular soft materials. In particular in Chapter 2 we will introduce a new class of host-guest supramolecular polymer responsive to chemical stimuli, while in Chapter 3 we will use

tetraphosphonate cavitands to manipulate the macroscopic properties of polymer blends.
In Chapter 4 we will demonstrate the capability of these molecules to act as recognition unit in a fluorescent chemical sensor for illicit and designer drugs detection.

1.2.2 Cucurbit[*n*]urils

Cucurbit[*n*]urils (*n* = 5-8 and 10; CB[*n*]) are water soluble cyclic methylene-bridged glycouril oligomers whose shape resemble a pumpkin. These receptors are symmetric and barrel like in shape with two identical portal regions laced by ureido-carbonyl oxygens.[23] The number of glycouril determines the size of the CB[*n*] cavity without affecting the height of the molecular container (approximately 0.9 nm), similar to cyclodextrin family (Figure 1.7).

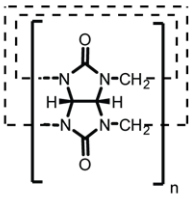

CB[*n*]: n = 5, 6, 7, 8

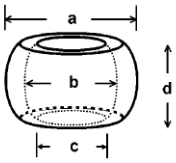

		CB[5]	CB[6]	CB[7]	CB[8]
outer diameter (Å)	a	13.1	14.4	16.0	17.5
cavity (Å)	b	4.4	5.8	7.3	8.8
	c	2.4	3.9	5.4	6.9
height (Å)	d	9.1	9.1	9.1	9.1
cavity volume (Å^3)	-	82	164	279	479

Figure 1.7 *CB[n] homologues.*

The synthetic protocol of CB homologues requires reacting glycouril with formaldehyde in mineral acids, such as 9 M H_2SO_4 or conc. HCl at 75-90 °C for 24 hours. The reaction mixture contains a family of CB[*n*] mostly from pentamer to octamer, with typical contents being: 10-15% CB[*5*], 50-60% CB[*6*], 20-25% CB[*7*] and 10-15% CB[*8*]. These four homologues are separated in pure form using fractional crystallization and dissolution.[24]

CB[5] and CB[7] are quite soluble in water, while CB[6] and CB[8] are poorly soluble in water. However, all the CBs are soluble in acidic water, as well as in an aqueous solutions of alkali metals. The solubility of cucurbiturils in common organic solvents is less than 10^{-5} M, and therefore the host–guest chemistry of these macrocycles has mainly been studied in aqueous media. Several intermolecular interactions promote the binding of guests by cucurbiturils. First, a hydrophobic effect due to the release of "high-entropy water" upon inclusion of non polar organic residues.[25] Second, ion-dipole interactions and hydrogen bondings may come into play with organic ammonium ions with any of the two ureido carbonyl rims (Figure 1.8).

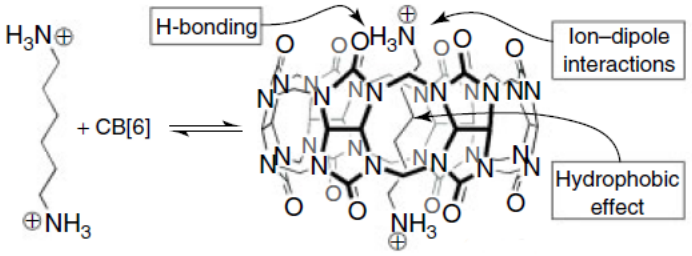

Figure 1.8 *Non-covalent interactions driving the formation of CB[6]@diammine.*

Smaller homologues of the CB[*n*] family (*i.e.* CB[5], CB[6] and CB[7]) are able of binding single guests (cationic amines, ion metals, imidazolium ions or small drugs).[26] In contrast to these receptors, CB[8] presents a larger cavity volume (479 Å)[27] capable of accommodating two planar and hydrophobic guests in a π-π stacking geometry (Figure 1.9).[28]

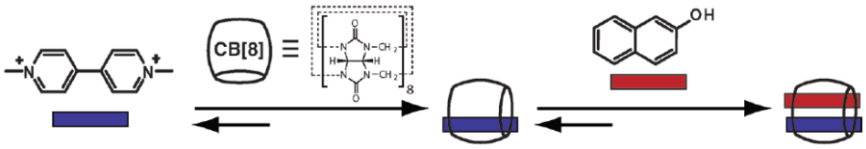

Figure 1.9 *Schematic of the two-step, three-component binding of cucurbit[8]uril in water.*

This host has been exploited mostly in a 1:1:1 ternary complex using an electron deficient first guest such as methyl viologen (MV) and an electron rich second guest such as naphthol, pyrene or dibenzylfuran.[29] The formation of the hetero-complex occurs in a stepwise binding process whereby the electron-poor guest enters first (K_{a1}) followed by the electron-rich guest (K_{a2}).

Therefore the ability of CB[*8*] host to act as dynamic *handcuff* along with its high binding constant in water makes it attractive for the constructions of: aqueous based materials such as multivalent receptors,[30] supramolecular block copolymers[31] and sensors for aromatic analytes.[32]

A well-designed example of the exploitation of the molecular recognition properties of CB[*8*] in material science has been demonstrated by Scherman *et al.*[33] They reported a thermo-sensitive supramolecular polymer hydrogel, which was designed by using as handcuff the macrocyclic host CB[*8*] to facilitate reversible cross-linking of multivalent copolymers, which contained either pendant methyl viologen (MV) units or naphthoxy (Np) moieties with high binding constants ($K_a > 10^{11}$–10^{12} M^{-2}, Figure 1.10).

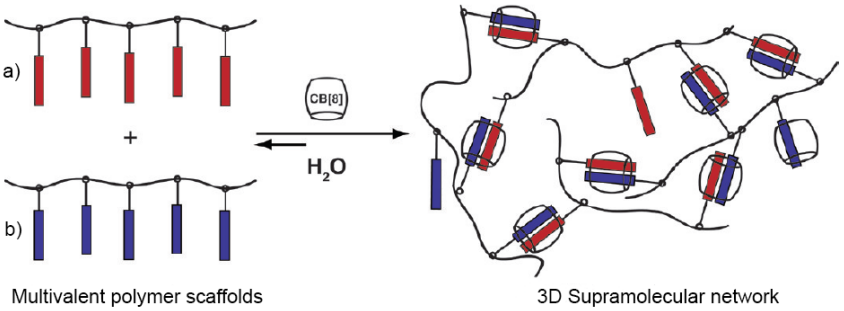

Figure 1.10 *a) Methyl viologen functionalized polymer; b) naphthoxy-functionalized polymer and cartoon representation of the formation of a 3D supramolecular network from them crosslinked by cucurbit[8]uril.*

The resulting supramolecular hydrogels exhibited thermal reversibility because of the dynamic cross-links (1:1:1 supramolecular ternary complexes of CB[*8*]:viologen:naphthoxy), which can be qualitatively characterized by probing the hydrogel microstructures. Upon heating, the hydrogel undergoes a gel-to-sol transition, which can reform upon cooling or adding more CB[*8*]. The fundamental methodology obtained from this study will facilitate the development of smart supramolecular polymeric materials.

In Chapter 5 of this thesis, we will exploit the versatility of the CB[*8*] host for the synthesis of biologically relevant soft materials, specifically as building block for the self-assembly of peptide based supramolecular vesicles.

1.3 References and Notes

[1] J. M. Lehn, *Proc. Natl. Acad. Sci. U.S.A.* **2002**, *99*, 4763-4768.

[2] J. M. Lehn, *Angew Chem. Int. Ed.* 1988, *27*, 89-112.

[3] J. M. Lehn, *Science* **2002**, *295*, 2400-2403.

[4] a) G. M. Whitesides, J. P. Mathias, C. T. Seto, *Science* **1991**, *254*, 1312-1319; b) G. M. Whitesides, M. Boncheva, *Proc. Natl. Acad. Sci. U.S.A.* **2002**, *99*, 4796-4774.

[5] a) X. Yan, F. Wang, B. Zheng, F. Huang, *Chem. Soc. Rev.* **2012**, *41*, 6042-6065; b) K. Liu, Y. Kang, Z. Wang, X. Zhang, *Adv. Mater.* **2013**, *25*, 5530-5548.

[6] E. Fischer, *Ber. Dtsch. Chem. Ges.* **1894**, *27*, 2985.

[7] C. J. Pedersen, *Angew Chem. Int. Ed.* **1988**, *27*, 1021-1027.

[8] D. J. Cram, *Angew Chem. Int. Ed.* **1988**, *27*, 1009-1020.

[9] D. J. Cram, J. M. Cram in *Container Molecules and Their Guests* **1994**, The Royal Society of Chemistry, Cambridge, Chap. 5.

[10] L. M. Tunstad, J. A. Tucker, E. Dalcanale, J. Weiser, J. A. Bryant, J. C. Sherman, R. C. Helgeson, C. B. Knobler, D. J. Cram, *J. Org. Chem.* **1989**, *54*, 1305-1312.

[11] a) P. Delangle, J. C. Mulatier, B. Tinant, J. P Declercq., J. P. Dutasta, *Eur. J. Org. Chem*. **2001**, 3695-3704; b) J. P Dutasta., *Top. Curr. Chem*. **2004**, *232*, 55-91.

[12] E. Biavardi, M. Favazza, A. Motta, I. L. Fragalà, C. Massera, L. Prodi, M. Montalti, M. Melegari, G. C. Condorelli, E. Dalcanale, *J. Am. Chem. Soc.* **2009**, *131*, 7447-7455.

[13] R. Pinalli, M. Suman, E. Dalcanale, *Eur. J. Org. Chem.* **2004**, *3*, 451-462.

[14] D. Menozzi, E. Biavardi, C. Massera, F. P. Schmidtchen, A. Cornia, E. Dalcanale, *Supramol. Chem.* **2010**, *22*, 768-775.

[15] P. Delangle, J. P. Dutasta, *Tetrahedron Lett.* **1995**, *36*, 9325-9328.

[16] E. E. Nifantyev, V. I. Maslennikova, R. V. Merkulov, *Acc. Chem. Res.* **2005**, *38*, 108-116.

[17] W. Xu, J. P. Rourke, R. J. Puddephatt, *J. Chem. Soc., Chem. Commun.* **1993**, 145-147.

[18] R. M. Yebeutchou, F. Tancini, N. Demitri, S. Geremia, R. Mendichi, E. Dalcanale, *Angew. Chem. Int. Ed.* **2008**, *47*, 4504-4508.

[19] B. Bibal, J. P. Declercq, J. P. Dutasta, B. Tinant, A. Valade, *Tetrahedron* **2003**, *59*, 5849-5854.

[20] D. Reyntjens-Van Damme, T. Zeegers-Huyskens, *J. Phys. Chem.* **1980**, *84*, 282-285.

[21] E. Biavardi, C. Tudisco, F. Maffei, A. Motta, C. Massera, G. G. Condorelli, E. Dalcanale, *Proc. Natl. Acad. Sci. U.S.A.* **2012**, *109*, 2263-2268.

[22] A. Sreekumar, L. M. Poisson, T. M. Rajendiran, A. P. Khan, Q. Cao, J. Yu, B. Laxman, R. Mehra, R. J. Lonigro, Y. Li, M. K. Nyati, A. Ahsan, S. Kalyana-Sundaram, B. Han, X. Cao, J. Byun, G. S. Omenn, D. Ghosh, S. Pennathur, D. C. Alexander, A. Berger, J. R. Shuster, J. T. Wei, S. Varambally, C. Beeche, A. M. Chinnaiyan, *Nature* **2009**, *457*, 910-914.

[23] J. Lagona, P. Mukhopadhyay, S. Chakrabarti, L. Isaacs, *Angew Chem. Int. Ed.* **2005**, *44*, 4844-4870.

[24] J. W. Lee, S. Samal, N. Selvapalam, H. J. Kim, K. Kim, *Acc. Chem. Res.* **2003**, *36*, 621-630.

[25] F. Biedermann, V. D. Uzunova, O. A. Scherman, M. Nau, M. Werner, A. De Simone, *J. Am. Chem. Soc.* **2012**, *134*, 15318-15323.

[26] K. Kim, N. Selvapalam, Y. H. Ko, K. M. Park, D. Kim, J. Kim, *Chem. Soc. Rev.* **2007**, *36*, 267-279.

[27] a) F. Biedermann, V. D. Uzunova, O. A. Scherman, W. M. Nau, A. De Simone, *J. Am. Chem. Soc.* **2012**, *134*, 15318-15323; b) W. M. Nau, M. Florea, K. I. Assaf, *Isr. J. Chem.* **2011**, *51*, 559-577.

[28] a) A. Day, A. P. Arnold, R. J. Blanch, B. Snushall, *J. Org. Chem.* **2001**, *66*, 8094-8100; b) J. Kim, I. S. Jung, S. Y. Kim, E. Lee, J. K. Kang, S. Sakamoto, K. Yamaguchi, K. Kim, *J. Am. Chem. Soc.* **2000**, *122*, 540-541.

[29] a) H. J. Kim, J. Heo, W. S. Jeon, E. Lee, J. Kim, S. Sakamoto, K. Yamaguchi, K. Kim, *Angew Chem. Int. Ed.* **2001**, *40*, 1526-1529; b) U. Rauwald, F. Biedermann, S. Deroo, C. V. Robinson, O. A. Scherman, *J. Phys. Chem. B* **2010**, *114*, 8606-8615; c) F. Biedermann, O. A. Scherman, *J. Phys. Chem. B* **2012**, *116*, 2842-2849.

[30] J. J. Reczek, A. A. Kennedy, B. T. Halbert, A. R. Urbach, *J. Am. Chem. Soc.* **2009**, *131*, 2408-2415.

[31] U. Rauwald, O. A. Scherman, *Angew. Chem. Int. Ed.* **2008**, *47*, 3950-3953.

[32] a) J. W. Lee, S. Samal, N. Selvapalam, H. Kim, K. Kim, *Acc. Chem. Res.* **2003**, *36*, 621-630; b) M. E. Bush, N. D. Bouley, A. R. Urbach, *J. Am. Chem. Soc.* **2005**, *127*, 14511-14517; c) Y. Ling, W. Wang, A. E. Kaifer, *Chem. Commun.* **2007**, 610-612.

[33] E. A. Appel, U. Ruwald, S. Jones, J. M. Zayed, O. A. Scherman, *J. Am. Chem. Soc.* **2010**, *132*, 14251-14260.

Chapter 2

Self-assembly of an Acid-Base Responsive Host-Guest Homopolymer

2.1 State of the Art

Supramolecular polymer chemistry, the result of a close integration of supramolecular chemistry and polymer science, has garnered widespread attention for its capability of producing materials with new attractive functions. Polymers based on these concepts combine many attractive characteristics of conventional polymers with properties that result from the dynamic nature of non-covalent interactions. According to the definition proposed by E. W. Meijer, "*supramolecular polymers are polymeric arrays of monomeric units held together by reversible and highly directional secondary interactions, resulting in polymeric properties in diluted and concentrated solution as well as in the bulk*".[1]
Tuning the strength and directionality of interactions among molecular units is the key feature for designing supramolecular polymers. High association constants are required to obtain a significant polymerization degree. It must also be considered the lifetime of non covalent interactions. In fact, when the lifetime of these bonds is too short ($\tau < 1$ μs) a robust 1D assembly that resembles a polymer does not exist, whereas too long lifetime ($\tau > 1$ min) form materials without interesting dynamic behavior.[2] In an intermediate range of bond lifetimes it is possible to modulate the dynamic properties of the materials such as: adaptability, self-repair and responsiveness.
Hydrogen bonding is one of the most used weak interactions for constructing supramolecular polymers due to its tunable, directional bonds. Indeed, this system was cleverly used by Sijbesma *et al.*[3] to construct a supramolecular polymer based on a self complementary ureido-pyrimidone that form a quadruple hydrogen bonding unit (Figure 2.1). The formation of high molecular weight species due to the high association constant ($K_a > 10^6$) was demonstrated by viscosimetry, which revealed an exponential relationship between viscosity and concentration.

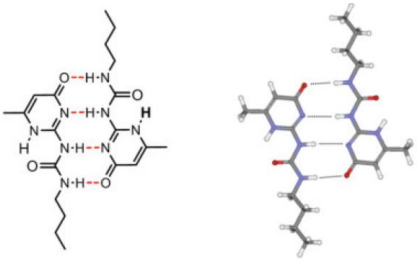

Figure 2.1 *Homodimer of ureido-pyrimidone units.*

Another ideal multiple and cooperative non-covalent interaction is the host-guest complexation. Molecular receptors are ideal candidates as components of supramolecular polymers thanks to their synthetic and binding versatility. So far many different hosts have been employed such as: ciclodextrins,[4] cucurbiturils,[5] calixarenes[6] and crown ethers.[7]
A further class of molecular receptor that fulfill the requirement of high association constants between the host and the guest is that of cavitands. These molecules are appealing because they can be functionalized both at the upper and at the lower rim, allowing to embed multiple self-assembly motifs on the same molecule, thus leading to complex supramolecular architectures, featuring orthogonal switching modes. On the basis of structural considerations, cavitand monomers can be classified into four main classes (Figure 2.2).

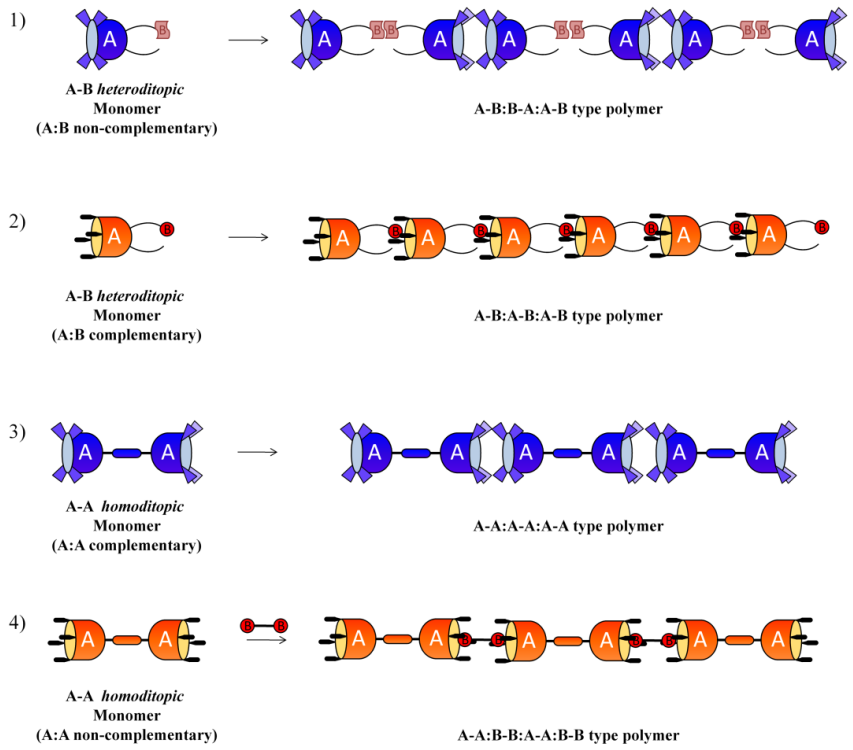

Figure 2.2 *Supramolecular polymerization motifs in cavitands.*

In the first class heteroditopic A-B monomers can be found, in which A:A and B:B interactions are respectively complementary. In this case a single monomer is present, but two interaction modes are active, leading to the formation of A-

B:B-A:A-B type polymers. A second class includes heteroditopic A-B monomers, in which A:B interaction is complementary in nature. Also in this case a single monomer is involved, but just one interaction mode is active, and A-B:A-B:A-B type polymers are formed. The third class collects the homoditopic A-A monomers, in which the A:A interaction is self-complementary. A single monomer and a single interaction are involved, leading to the formation of A-A:A-A:A-A type polymers. Finally, the fourth class includes the A-A monomers, in which the A:A interaction is not self-complementary. In this case two different homoditopic monomers are required, namely A-A and B-B, and the polymerization process proceeds thanks to the complementarity of the A:B interaction, leading to A-A:B-B:A-A:B-B copolymers.[8]

Tetraphosphonate cavitands are macrocyclic host molecules that have shown intriguing properties particularly in self assembled structures. Their noteworthy complexation and plasticity properties can be exploited to enrich polymers with some relevant qualities, including responsiveness to environmental stimuli, self-healing and adaptability.
In a previous work,[9] our research group has designed and synthesized a self-complementary heteroditopic monomer, that exploited the molecular recognition properties of tetraphosphonate cavitands toward *N*-methylpyridinium guests to form a supramolecular array by isodesmic polymerization. In particular, the designed monomer was a cavitand bearing four inward facing P=O groups at the upper rim, and a single *N*-methylpyridinium moiety at the lower rim (Figure 2.3). The corresponding polymer featured guest-triggered reversibility and template driven conversion from linear into star-branched form.

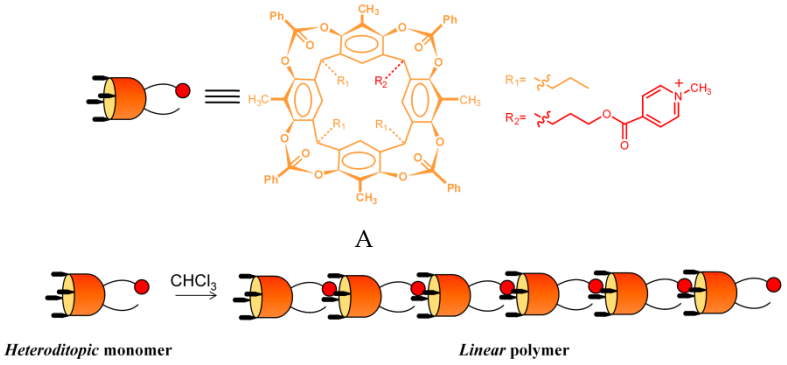

Figure 2.3 *A-B heteroditopic polymerization mode of cavitand* ***A****.*

2.2 Introduction

To further expand the scope of tetraphosphonate cavitands as building blocks in supramolecular polymer chemistry we sought to design a new A-B heteroditopic monomer. Cavitands bridged with phosphonate groups present remarkable recognition properties not only toward *N*-methylpyridinium salts, but they complex even better *N*-methylammonium salts through three interaction modes: (i) $N^{+}\bullet\bullet\bullet O{=}P$ cation–dipole interactions, (ii) CH_3-π interactions of the acidic $^{+}NH_2$-CH_3 group with the π basic cavity, (iii) two simultaneous hydrogen bonds between two adjacent P=O bridges and the two nitrogen protons.[10] These complexes exhibit an high association constant (≈ 4 × 10^5 M^{-1}, in methanol[11] and even higher K_a in chlorinated solvents) making them ideal candidates for the self-assembly of supramolecular aggregates. Indeed, to obtain an high degree of polymerization the K_a of the supramolecular complex should be ≥ 10^5. Moreover the exploitation of this complex allowed the formation of responsive polymer towards simple chemical stimuli such as acid/base substances.

Herein we report the synthesis and self-assembly process of a tetraphosphonate cavitand functionalized with a sarcosine moiety **Tiiii [3 C_3H_7, 1 sarcosine, CH_3, Ph]** (**I**) at the lower rim (Figure 2.4). The protonation of sarcosine allowed the self-assembly of an A-B:A-B:A-B type homopolymer thanks to the interaction between the phosphonate groups and the methylammonium ion. The formation of the supramolecular polymers is controlled by simple chemical stimuli such as acid/base treatments.

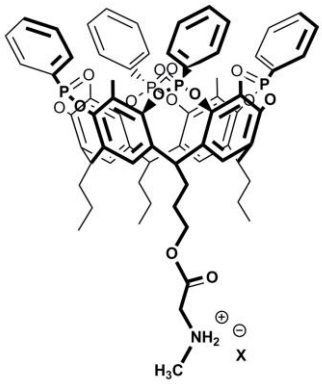

Figure 2.4 ***Tiiii [3 C_3H_7, 1 sarcosine, CH_3, Ph], I.***

The self-assembly process was monitored by ^{1}H and ^{31}P NMR spectroscopy, static and dynamic light scattering and TEM. All these techniques granted evidence for the formation of supramolecular oligomers in solution.

2.3 Results and Discussion

2.3.1 Synthesis of the Homopolymer

The target cavitand **Tiiii [3 C_3H_7, 1 sarcosine, CH_3, Ph]** (**I**) was synthesized in four steps and 22% overall yield (Scheme 2.1). The key step of the synthesis was the insertion of the sarcosine moiety (Boc protected) at the lower rim of the resorcinarene scaffold **II** under Steglich conditions.[12]

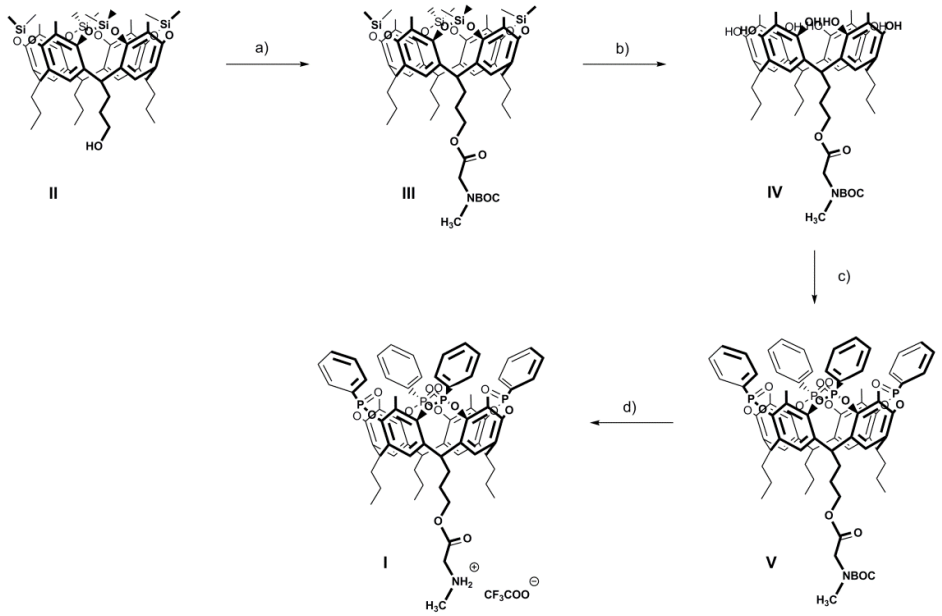

Scheme 2.1 *Synthesis of* ***Tiiii [3 C_3H_7, 1 sarcosine, CH_3, Ph]****, **I**: a) N-Boc-Sarcosine, DCC/DMAP, $CHCl_3$, r.t., 12 h, 40%; b) TBAF, THF, r.t., 1 h, 60%; c) 1) $PhPCl_2$, Py, 75 °C, 3h; 2) H_2O_2, r.t., 1h, 92% (over two steps); d) TFA, DCM, r.t., 3h, quantitative.*

The carbamate protecting group allowed an orthogonal deprotection of the upper rim of **III** using tetra butylammonium fluoride. The four inward phosphonate groups were introduced by reacting the resorcinarene **IV** with dichlorophenylphosphine and oxidizing the tetraphosphonate intermediate *in situ* with hydrogen peroxide. Finally cavitand **V** was treated with trifluoro-

acetic acid to remove the carbamate protecting group and protonate the amine functional group. This reaction provided the corresponding monomer **I** quantitatively.

2.3.2 ^{1}H and ^{31}P NMR Complexation Studies

The self-assembly of the cavitand based monomer can be easily monitored by ^{1}H and ^{31}P NMR spectroscopy. In Figure 2.5 is reported the proton NMR spectrum of the protected cavitand **V** before (Figure2.5a) and after (Figure2.5b) the acidic treatment.

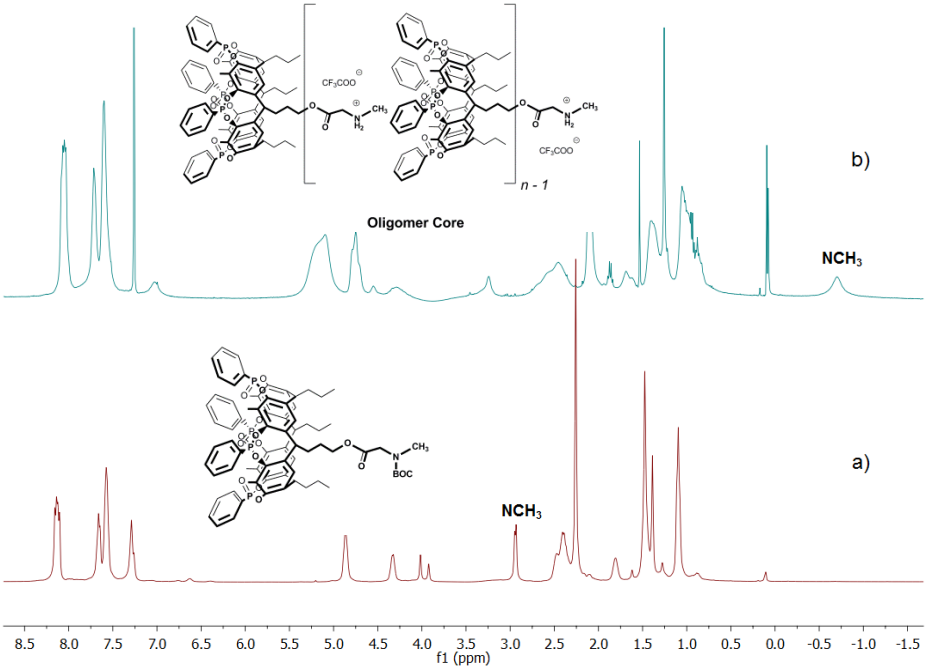

Figure 2.5 *^{1}H NMR spectra ($CDCl_3$, 400 MHz, 10 mM, 25 °C) of: a) monomer BOC protected **V**; b) homopolymer.*

As expected, removal of BOC protecting group and protonation of the amine caused the intermolecular inclusion process between the methylammonium moiety of one cavitand monomer and the cavity of another. In fact the proton of the methyl group of the sarcosine experienced a remarkable up-field shift, from 3 to -0.6 ppm, due to the shielding effect of the cavity.

The phosphorous signal of **V** is formed by two singlets because the four phosphorous of the cavitand are not magnetically equivalent (Figure 2.6). After

the acidic treatment the ^{31}P signal of the phosphonate groups of the cavitand **I** experiences a down-field shift thanks to the inclusion of the cationic part of the guest in the cavity.

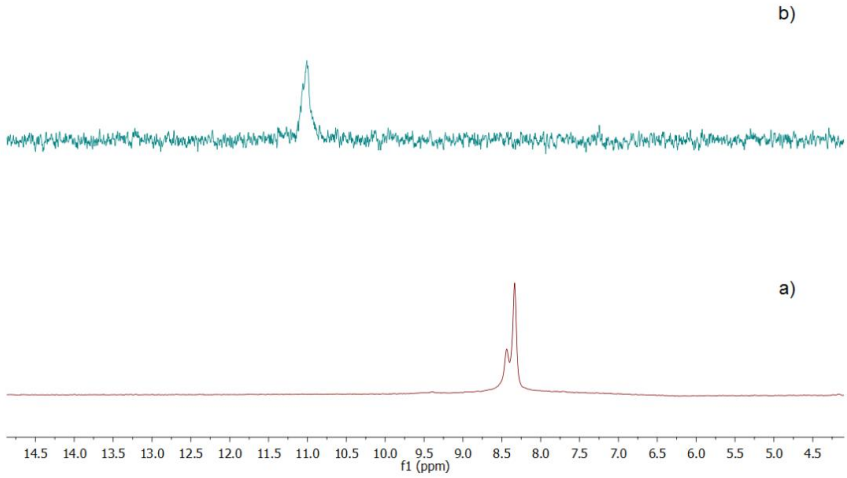

Figure 2.6 *$^{31}P\{^1H\}$NMR spectra ($CDCl_3$, 400 MHz, 10 mM, 25 °C) of: a) monomer Boc protected **V**; b) homopolymer.*

Also MALDI-TOF spectrum highlighted the aggregation tendency of the monomer. In the spectrum, even under adverse conditions, the peak of the dimer was detected (see Experimental Section, Figure 2.7).

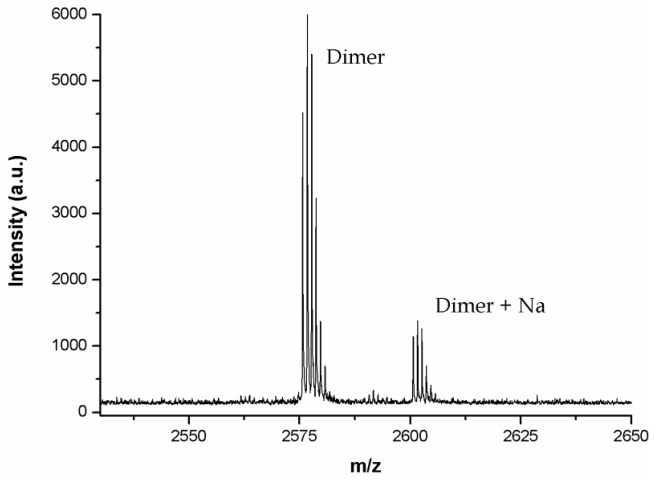

Figure 2.7 *MALDI-TOF spectrum of the homopolymer.*

Tiiii V is able to respond to simple chemical stimuli such as an acid-base treatment, causing the assembly and disassembly of the homopolymer. Compound **V** was easily deprotonated with 3 eq. of 1,8-diazabicyclo[5.4.0]undec-7-ene (DBU) a non-nucleophic hindered base that when protonated does not fit into the cavity of the molecule. Additionally the deprotonated cavitand can be reconverted to the homopolymer upon subsequent exposure to 5 eq. of trifluoro-acetic acid (TFA). This process was followed by two complementary techniques: NMR spectroscopy and dynamic light scattering (paragraph 2.3.3).
The ^{31}P NMR spectroscopy records an high-field shift of the signal after the basic treatment and consequent reappearing of the characteristic pattern of the phosphorous signal similar to that of the protected monomer **V** (Figure 2.8b). The addition of TFA restored the phosphorous signal at low-field (Figure 2.8c). The reversible response of our system to chemical stimuli was also confirmed by ^{1}H NMR spectroscopy: the spectra in Figure 2.9 show the shift of the methyl group of the secondary amine below and above 0 ppm during the acid-base treatment.

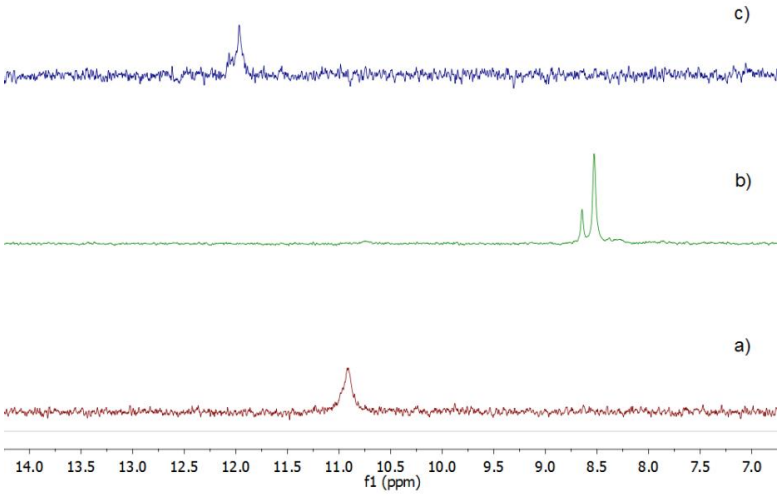

Figure 2.8 *^{31}P{^{1}H}NMR spectra ($CDCl_3$, 400 MHz, 10 mM, 25 °C) of: a) homopolymer; b) homopolymer + 3 eq. DBU; c) homopolymer + 3 eq. DBU+ 5 eq. of TFA.*

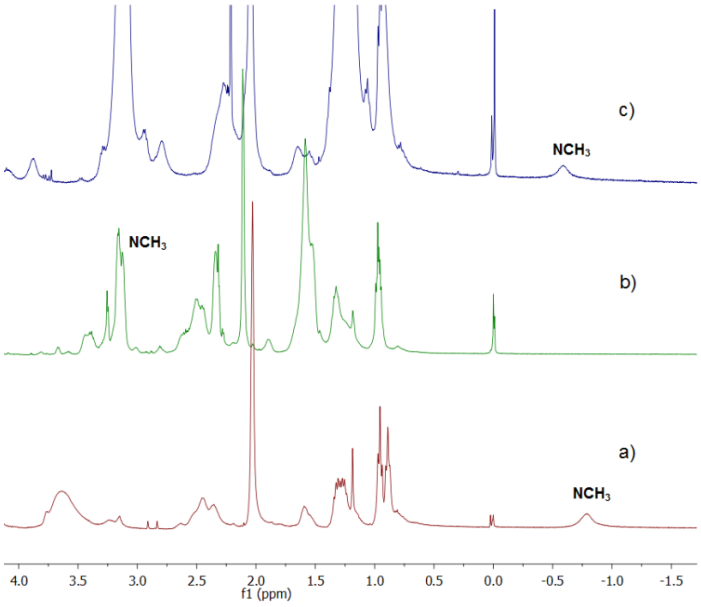

Figure 2.9 *^{1}H NMR spectra ($CDCl_3$, 400 MHz, 10 mM, 25 °C) of: a) homopolymer; b) homopolymer + 3 eq. DBU; c) homopolymer + 3 eq. DBU+ 5 eq. of TFA.*

2.3.3 Light scattering Studies

To obtain further insight into the self-assembly process a series of static and dynamic light scattering experiments were performed. These two types of methods are well-established for determination of molecular weight and hydrodynamic radius of macromolecules.[13]

The static light scattering (SLS) measurement allows to obtain the weight-average molecular weight (M_w) of the aggregates in solution by measuring the intensity of the scattered light, which is also related to the concentration of the macromolecules. In the case of **Tiiii** supramolecular polymer, SLS measurements were performed in chloroform in the concentration range of 9.0-40.0 mg mL^{-1}.

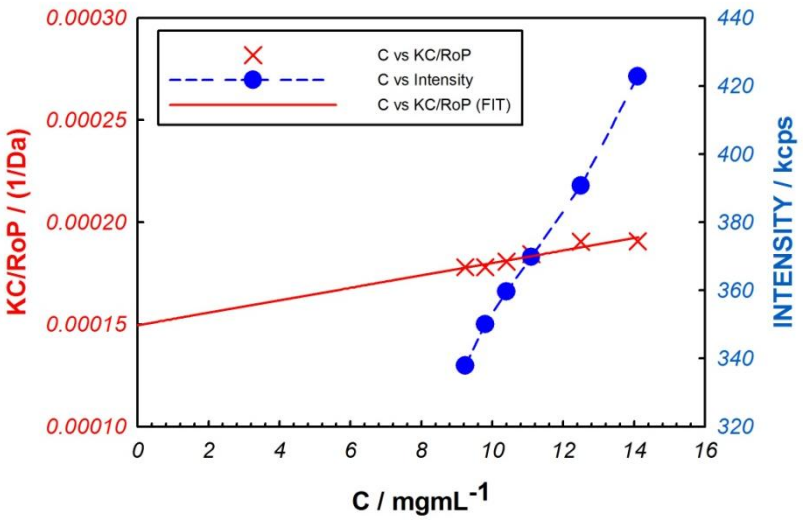

Figure 2.10 *Debye plot for the SLS analysis (chloroform, 25 °C) of* ***Tiiii*** *supramolecular polymer in the 9.2-14.1 mg mL^{-1} concentration range (M_w = 7 ± 1 KDa).*

Due to the presence of complexation equilibria within the supramolecular polymer, M_w estimation by SLS measurements were made in quite narrow concentration windows, in order to have an approximate value of the average molecular weight in the considered concentration regime. In particular the Debye plots for the 9.2-14.1 mg mL^{-1} (M_w = 7 ± 1 KDa) and 25.5-36.7 mg mL^{-1} (M_w = 11 ± 1 KDa) are reported in Figure 2.10 and 2.11. An incremental refractive index (dn/dC) of 0.152 mL g^{-1} and toluene as scattering standard were used for these measurements. The SLS experiments in the two concentration ranges show that the homopolymer presents a polymerization degree of about 7-10 monomers, confirming the formation of high supramolecular oligomers in solution.

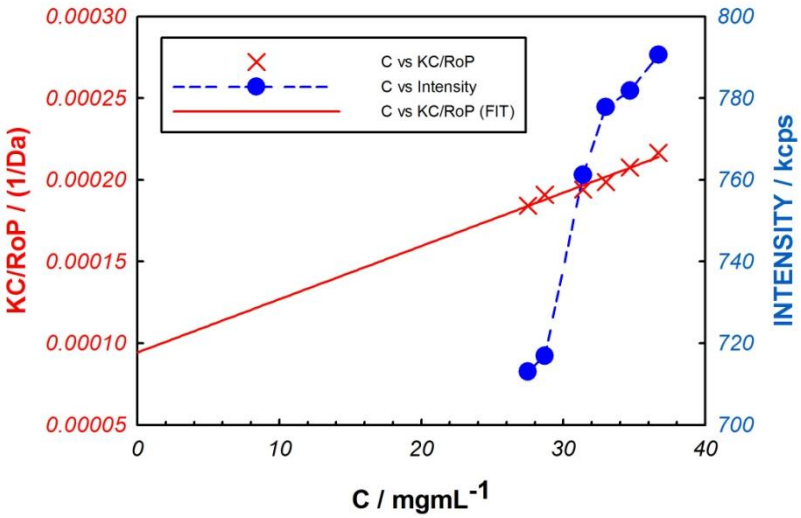

Figure 2.11 *Debye plot for the SLS analysis (chloroform, 25 °C) of* ***Tiiii*** *supramolecular polymer in the 25.5-36.7 mg mL^{-1} concentration range (M_w = 11 ± 1 KDa)*

The dynamic light scattering (DLS) is a popular technique for determining the size distribution profiles of small particles such as micelles, polysaccharides and supramolecular aggregates like supramolecular polymers.
The DLS experiment at various concentration shows a monodisperse system at room temperature (Figure 2.12). The one size population increases its hydrodynamic radius (ranging from 5 to 10 nm) as expected for a supramolecular polymer. Moreover we found a low and reproducible polydispersity index for all the concentration range. The size distribution of the supramolecular polymers found at various concentrations are in good agreement with the SLS data.

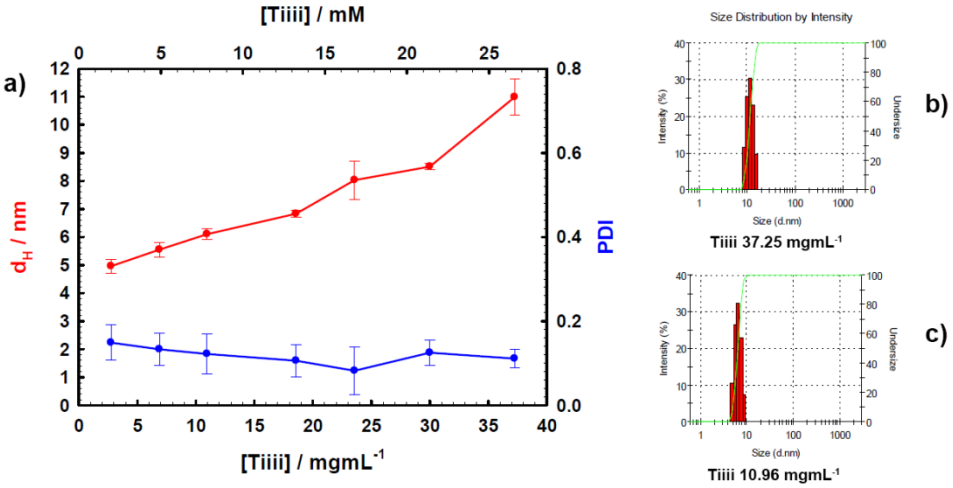

Figure 2.12 *DLS analysis (chloroform, 25 °C): a) hydrodynamic radius of the homopolymer as function of concentration; b),c) examples of size intensity distributions.*

The size distribution of the supramolecular aggregates can be triggered by an acid-base stimuli, as previously demonstrated in the ^{1}H and ^{31}P NMR studies (paragraph 2.3.2). The dynamic light scattering spectrum presents a drop in the size distribution of the homopolymer after the basic treatment (Figure 2.13). The size of the aggregates observed is consistent with the dimension of one monomer. Subsequently, the addition of triflic acid restored the initial size distribution demonstrating the reproducible responsiveness of this system.

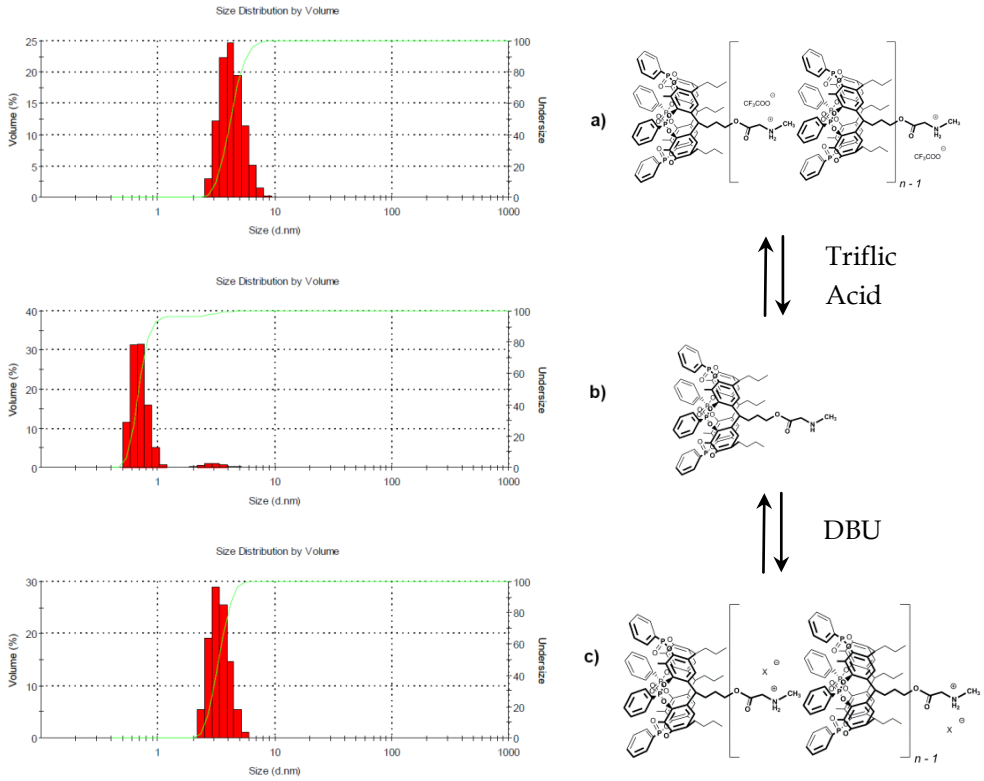

Figure 2.13 *DLS reversibility (chloroform, 10.5 mM, 25 °C) : a) homopolymer; b) homopolymer + DBU (excess); c) homopolymer + DBU + triflic acid.*

The size distribution of the homopolymer was measured at various temperatures to assure the stability of the aggregates. The experiment was performed in 1,1,2,2-tetrachloroethane, which has an high boiling point, using two different concentrations (4.2 and 36.7 mg mL^{-1}) and a wide range of temperature, from 1 °C to 80 °C. For both concentrations we observed from 20 °C to 80 °C a stable PolyDispersity Index (PDI) and an hydrodynamic radius of about 10 nm. Interestingly, before 20 °C we noted a bimodal size distribution, one size distribution centered at about 10 nm and the other one centered at about 200 nm. Lowering the temperature until 2 °C promotes the formation of largest aggregates. For both concentrations the high size distribution increases reaching 230 and 300 nm, while the low size distribution disappears (Figures 2.14 and 2.15).

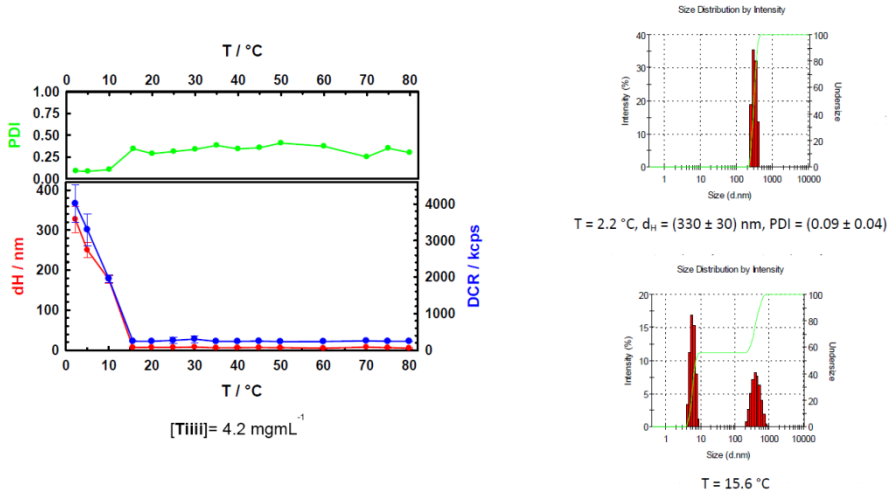

Figure 2.14 *DLS as function of temperature (1,1,2,2-tetrachloroethane),* ***[Tiiii]****= 4.2 mg mL-1.*

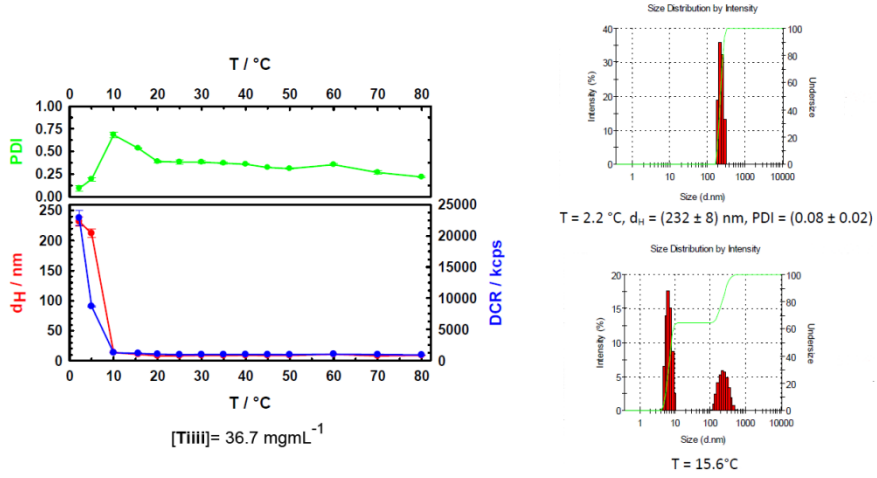

Figure 2.15 *DLS as function of temperature (1,1,2,2-tetrachloroethane),* ***[Tiiii]****= 36.7 mg mL-1.*

These results can be interpreted considering that the polymer chains interact longitudinally to form bundles. These large objects are composed by four polymeric chains held together by quadrupolar interactions between the chains and the counterions (Figure 2.16). The generation of this aggregates has been observed also for the supramolecular homopolymers based on

tetraphosphonate cavitands functionalized at the lower rim with a *N*-methylpyridinium moiety.[8]

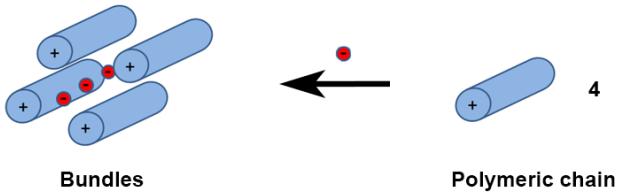

Figure 2.16 *Formation of bundles from quadrupole interactions between four polymeric chains and the counterions.*

The same behavior was not observed in chloroform. We measured the hydrodynamic radius of the homopolymer at low temperature in chloroform, in this case the aggregates present a size distribution that does not exceed 10 nm.

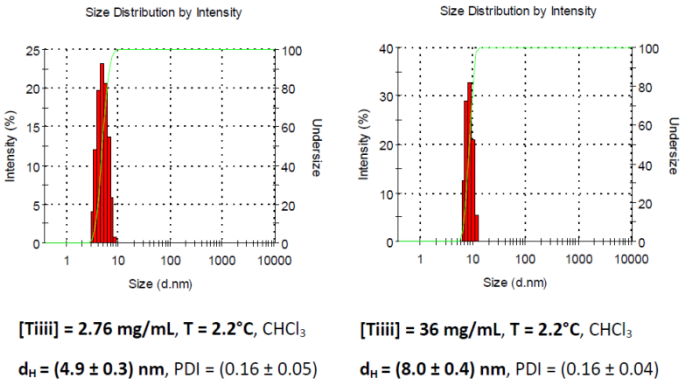

Figure 2.16 *DLS at low temperature (chloroform).*

With these experiments we demonstrated the ability of the supramolecular homopolymer to form large aggregates, that are temperature and solvent dependent. In fact the combination of lower temperature and the solvent assists the formation of these aggregates. To confirm our hypothesis other experiments like DOSY measurements are ongoing.

2.3.4 TEM Measurements

In order to further study the supramolecular aggregates at low temperature we tried to obtain images using transmission electron microscopy (TEM). We took a solution 4.2 mg mL^{-1} at 2.2 °C in 1,1,2,2-tetrachloroethane (d_H= (110 ± 5) nm from DLS) and we deposited this solution on a copper/carbon grid, the solvent was evaporated under reduced pressure. The aggregates observed in the images seem to being formed by smaller sub-units which are organized in a linear fashion (Figure 2.17). Although temperature and evaporation of the solvent cannot be precisely controlled, the size of the aggregates observed in the experiment are in line with the size distribution obtained in solution with DLS at low temperature. Hence is an indirect proof of the assembly of large supramolecular aggregates.

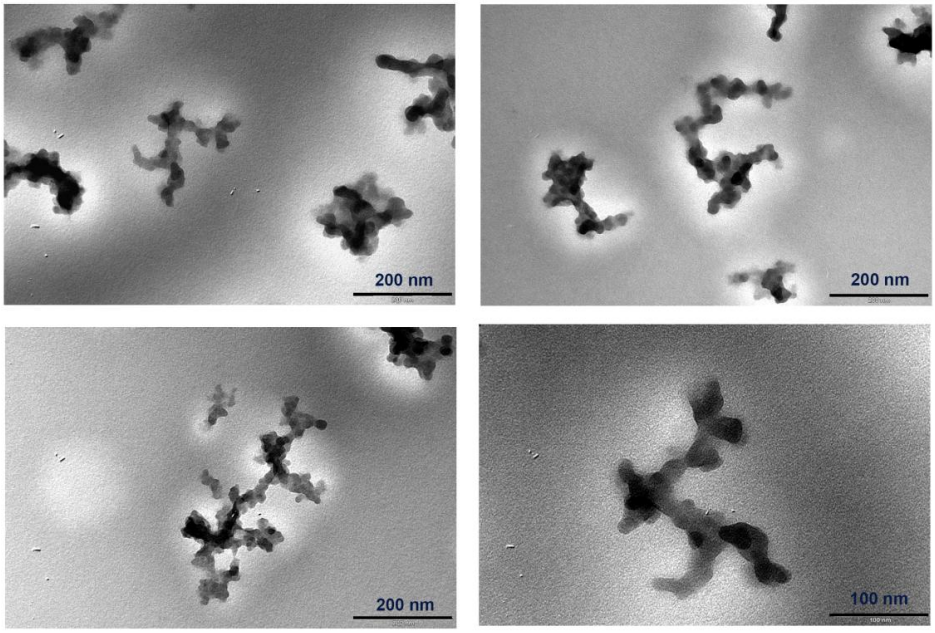

Figure 2.17 *TEM (80 kV) images obtained on copper/carbon grid, staining effectuated with uranyl acetate 2% w/w in water.*

2.4 Conclusions

In conclusion, a new stimuli responsive supramolecular homopolymer has been designed and synthesized. The monomer based on the resorcinarene scaffold presents four P=O groups at the upper rim and a sarcosine moiety at the lower rim. The self-assembly properties of this supramolecular polymer have been investigated with several techniques (^{1}H and ^{31}P NMR spectroscopy, light scattering measurements, TEM). The combination of these experiments have provided numerous evidences on the formation of supramolecular homopolymer in solution. Furthermore, we have proved that the polymers assembly can be controlled by means of acid-base treatment demonstrating the reversibility of the system. Interestingly, we have found that our system is solvent and temperature dependent, in fact larger aggregates were observed in tetrachloroethane.
This host-guest counterpart will be embedded in polymers in Chapter 3 to test its ability to promote polymer blending, and to investigate the responsiveness of this complex in truly polymeric materials.

2.5 Acknowledgments

Special thanks to Dr. Enrico Rampazzo from Department of Chemistry "G. Ciamician", University of Bologna for light scattering measurements.

2.6 Experimental Section

***N*-Boc-sarcosine**

To a solution of sarcosine (0.4 g, 4.49 mmol) in acetonitrile, triethylamine (0.68 mL, 4.94 mmol) and di-tert-butyl dicarbonate (1.13 mL, 4.94 mmol) were added. The solution was heated to reflux for 4 hours and the solvent removed *in vacuo*. The crude oil was dissolved in dichloromethane and extracted with water (2 x 30 mL). Then the organic phase was dried with anhydrous $CaCl_2$ and evaporated under reduced pressure to give the product as colorless oil (0.407 g, 2.15 mmol, 48%).

^{1}H NMR ($CDCl_3$, 400 MHz): δ (ppm) = 9.56 (s, 1H, O**H**), 3.87 (d, J=33.4 Hz, 2H, NC**H$_2$**), 2.83 (s, 3H, NC**H$_3$**), 1.34 (s, 9H, C(C**H$_3$**)$_3$); **ESI-MS**: m/z 190.1 $[M+H]^+$.

***N*-Boc-sarcosine based silylcavitand (III)**

N-Boc-sarcosine (0.318 g, 1.68 mmol) DCC (0.346 g, 1.68 mmol) and DMAP (0.205 g, 1.68 mmol) were dissolved in dry chloroform with stirring for 15 minutes. Following, monohydroxy footed silylcavitand **II** (0.8 g, 0.839 mmol) was added into the reaction mixture and stirred overnight at room temperature. Saturated NH_4Cl solution was added and the organic phase was extracted with water (2 x 20 mL) dried with anhydrous Na_2SO_4, and the solvent removed *in vacuo*. Purification by silica gel column chromatography (hexane:ethyl acetate 85:15) yielded the desired product as white solid (0.377 g, 0.336 mmol, 40%).

^{1}H NMR ($CDCl_3$, 300 MHz): δ (ppm) = 7.20 (s, 2H, Ar**H**), 7.18 (s, 2H, Ar**H**), 4.64 (t, J=8 Hz, 4H, ArC**H**), 4.28-4.20 (m, 2H, C**H$_2$**OC(O)), 3.96 (d, J= 40 Hz, 2H, N C**H$_2$**), 2.85 (d, J=10.3 Hz, 3H, N C**H$_3$**), 2.27-2.01 (m, 10H, C**H$_2$**CH_2CH_2OC(O), C**H$_2$**CH_2CH_3), 1.85 (s, 12H, Ar C**H$_3$**); 1.67-1.14 (m, 17H, C**H$_2$**CH_2OC(O), C(C**H$_3$**)$_3$, CH_2C**H$_2$**CH_3), 0.98-0.82 (m, 9H, CH_2CH_2C**H$_3$**), 0.54 (s, 12H, Si C**H$_{3,out}$**), -0.64 (s, 12H, Si C**H$_{3,in}$**); **ESI-MS**: m/z 1164.1 $[M+K]^+$.

***N*-Boc-sarcosine based resorcinarene (IV)**

To a solution of *N*-Boc-sarcosine based silylcavitand **II** (0.39 g, 0.347 mmol) in dry THF, TBAF (1.36 g; 5.2 mmol) was added under argon atmosphere at 0 °C. After 1 hour the reaction mixture was quenched by adding saturated NH_4Cl solution. The crude was diluted with ethyl acetate and the organic phase extracted with sat. aq. $NaHCO_3$ and water. The organic phase was dried with anhydrous Na_2SO_4 and the solvent removed *in vacuo*. Purification by silica gel column chromatography (hexane:ethyl acetate 1:1) afforded the pure product as yellow pale solid (0.188 g, 0.208 mmol, 60%).

^{1}H NMR ($(CD_3)_2CO$, 300 MHz): δ (ppm) = 7.84 (s, 2H, O**H**), 7.46 (s, 2H, Ar**H**), 7.44 (s, 2H, Ar**H**), 4.41 (t, J=9 Hz, 4H, ArC**H**), 4.24-4.11 (m, 2H, C$\mathbf{H_2}$OC(O)), 3.97 (d, J=14.5 Hz, 2H, NC$\mathbf{H_2}$), 2.91 (d, J=9 Hz, 3H, NC$\mathbf{H_3}$), 2.45-2.00 (m, 20H, C$\mathbf{H_2}CH_2CH_2OC(O)$, C$\mathbf{H_2}CH_2CH_3$, ArC$\mathbf{H_3}$), 1.71-1.55 (m, 2H, C$\mathbf{H_2}CH_2OC(O)$), 1.50-1.18 (m, 15H, C(C$\mathbf{H_3}$)$_3$, $CH_2C\mathbf{H_2}CH_3$), 0.95 (t, J=9 Hz, 9H, $CH_2CH_2C\mathbf{H_3}$); **ESI-MS**: m/z 922.8 $[M+Na]^+$, 939 $[M+K]^+$.

Tiiii [3 C_3H_7, 1 Boc-sarcosine, CH_3, Ph] (V)

To a solution of *N*-Boc-sarcosine based resorcinarene **III** (0.19 g, 0.21 mmol) in freshly distilled pyridine, dichlorophenylphosphine (0.13 mL, 0.882 mmol) was added slowly, at room temperature under argon atmosphere. After 3 hours of stirring at 75 °C, the solution was allowed to cool at room temperature and 2 mL of aqueous H_2O_2 (30%) was added. The resulting mixture was stirred for 1 hour at room temperature, then addition of water resulted in the precipitation of a white powder. The solid was recovered by suction filtration to give pure **IV** (0.45 g, 0.33 mmol, 92%).

^{1}H NMR ($CDCl_3/D_2O$, 400 MHz): δ (ppm) = 8.15-8.01 (m, 8H, P(O)Ar$\mathbf{H_o}$), 7.72-7.61 (m, 4H, P(O)Ar$\mathbf{H_p}$), 7.61-7.47 (m, 8H, P(O)Ar$\mathbf{H_m}$), 7.24-7.13 (m, 4H, Ar**H**), 4.85-4.72 (m, 4H, ArC**H**), 4.35-4.24 (m, 2H, C$\mathbf{H_2}$OC(O)), 3.97 (d, J=36 Hz, 2H, NC$\mathbf{H_2}$), 2.90 (s, 3H, NC$\mathbf{H_3}$), 2.44-2.21 (m, 8H, C$\mathbf{H_2}CH_2CH_3$, C$\mathbf{H_2}CH_2CH_2OC(O)$), 2.14 (s, 12H, ArC$\mathbf{H_3}$), 1.82-1.69 (m, 2H, C$\mathbf{H_2}CH_2OC(O)$), 1.50-1.21 (m, 15H, C(C$\mathbf{H_3}$)$_3$, $CH_2C\mathbf{H_2}CH_3$), 1.12-0.98 (m, 9H, $CH_2CH_2C\mathbf{H_3}$); **^{31}P{^{1}H}NMR** ($CDCl_3/D_2O$, 161.9 MHz): δ (ppm) = 8.44 (s, 1P, P=O) 8.34 (s, 3P, P=O); **HR-ESI-MS**: m/z calcd. for $C_{76}H_{81}NO_{16}P_4Na$: 1410.4403; found: 1410.4398.

Tiiii [3 C_3H_7, 1 sarcosine, CH_3, Ph] (I)

V (20 mg, 0.014 mmol) was treated with 10 equivalent of trifluoroacetic acid in $CHCl_3$. After 3 hours the solvent was removed *in vacuo* and the crude was dried under reduced pressure (quantitative yield).

^{1}H NMR ($CDCl_3$, 400 MHz): δ (ppm) = 8.15-8.01 (m, 8H, P(O)Ar$\mathbf{H_o}$), 7.72-7.61 (m, 4H, P(O)Ar$\mathbf{H_p}$), 7.61-7.47 (m, 8H, P(O)Ar$\mathbf{H_m}$), 7.24-7.13 (m, 4H, Ar**H**), 4.85-4.72 (m, 4H, ArC**H**), 4.35-4.24 (m, 2H, C$\mathbf{H_2}$OC(O)), 3.97 (d, J=36 Hz, 2H, NC$\mathbf{H_2}$), 2.90 (s, 3H, NC$\mathbf{H_3}$), 2.44-2.21 (m, 8H, C$\mathbf{H_2}CH_2CH_3$, C$\mathbf{H_2}CH_2CH_2OC(O)$), 2.14 (s, 12H, ArC$\mathbf{H_3}$), 1.82-1.69 (m, 2H, C$\mathbf{H_2}CH_2OC(O)$), 1.50-1.21 (m, 15H, C(C$\mathbf{H_3}$)$_3$, $CH_2C\mathbf{H_2}CH_3$), 1.12-0.98 (m, 9H, $CH_2CH_2C\mathbf{H_3}$); **^{31}P{^{1}H}NMR** ($CDCl_3$, 161.9 MHz): δ (ppm) = 11.01 (s, P=O); **MALDI TOF-TOF**: calcd. for $C_{71}H_{74}NO_{14}P_4$ 1288.4054 Da, found: 1288.3879 Da. The dimer was observed in the MS spectrum, calcd. for $C_{142}H_{146}N_2O_{28}P_8$ 2574,7957 Da, found 2574.7963.

Light scattering measurements

SLS and DLS measurements were performed using a Malvern Nano ZS instrument, equipped with a 633 nm laser source. All the solution were filtered with PTFE filters (4 mm x 0.2 µm, Supelco).

2.7 References and Notes

[1] L. Brunsveld, J. B. Folmer, E. W. Meijer, R. P. Sijbesma, *Chem. Rev.* **2001**, *101*, 4071-4097.

[2] T. Aida, E. W. Meijer, S. I. Stupp, *Science* **2012**, *335*, 813-817.

[3] R. P. Sijbesma, F. H. Beijer, L. Brunsveld, B. J. B. Folmer, J. H. K. K. Hirschberg, R. F. M. Lange, J. K. L. Lowe, E. W. Meijer, *Science* **1997**, *278*, 1601-1604.

[4] K. Ohga, Y. Takashima, H. Takahashi, Y. Kawaguchi, H. Yamaguchi, A. Harada, *Macromolecules* **2005**, *38*, 5897-5904; (b) M. Miyauchi, Y. Takashima, H. Yamaguchi, A. Harada, *J. Am. Chem. Soc.* **2005**, *127*, 2984-2989; (c) M. Miyauchi, T. Hoshino, H. Yamaguchi, S. Kamatori, A. Harada, *J. Am. Chem. Soc*. **2005**, *127*, 2034-2035.

[5] J. del Barrio, P. N. Horton, D. Lairez, G. O. Lloyd, C. Toprakcioglu, O. A. Scherman, *Angew. Chem. Int. Ed.* **2013**, *135*, 11760-11763.

[6] S. Pappalardo, V. Villari, S. Slovak, Y. Cohen, G. Gattuso, A. Notti, A. Pappalardo, I. Pisagatti, M. F. Parisi, *Chem. Eur. J.* **2007**, *13*, 8164-8173.

[7] F. Wang, J. Zhang, X. Ding, S. Dong, M. Liu, B. Zheng, S. Li, L. Wu, Y. Yu, H. W. Gibson, F. Huang, *Angew. Chem. Int. Ed.* **2010**, *49*, 1090-1094.

[8] F. Tancini, E. Dalcanale in *Supramolecular Polymer Chemistry*, Ch. 4, **2011**, Wiley-VCH.

[9] R. M. Yebeutchou, F. Tancini, N. Demitri, S. Geremia, R. Mendichi, E. Dalcanale, *Angew. Chem. Int. Ed.* **2008**, *47*, 4504-4508.

[10] a) P. Delangle, J. C. Mulatier, B. Tinant, J. P. Declercq, J. P. Dutasta, *Eur. J. Org. Chem.* **2001**, 3695-3704; b) E. Kalenius, D. Moiani, E. Dalcanale, P. Vainiotalo, *Chem. Commun.* **2007**, *43*, 3865-3867; c) M. Melegari, M. Suman, L. Pirondini, D. Moiani, C. Massera, F. Ugozzoli, E. Kalenius, P. Vainiotalo, J. C. Mulatier, J. P. Dutasta, E. Dalcanale, *Chem. Eur. J.* **2008**, *14*, 5772-5779.

[11] M. Dionisio, G. Oliviero, D. Menozzi, S. Federici, R. M. Yebeutchou, F. P. Schmidtchen, E. Dalcanale, P. J. Bergese, *J. Am. Chem. Soc.* **2012**, *134*, 2392-2398.

[12] B. Neises, W. Steglich, *Angew. Chem. Int. Ed.* **1978**, *17*, 522-524.

[13] Y. Liu, Z. Wang, X. Zhang, *Chem. Soc. Rev.* **2012**, *41*, 5922-5932.

Chapter 3

Morphological Studies of Host-Guest Polymer Blends

3.1 State of the Art

Challenges in polymer science has increased in recent years thanks to a growing demand of new functional materials that have the ability to reversibly adapt to the environmental stimuli and possess a wide range of responses ranging from self-healing to mechanical work.[1] Supramolecular polymer chemistry, a field based on the synergistic combination of non covalent interactions and polymer chemistry,[2] addresses adequately the multifaceted tasks of designing smart materials and further expand applications of polymers in different research areas.

The nature of the secondary weak interactions and the types of building blocks involved in the supramolecular polymer systems are pivotal to determine the responsiveness of the materials.

An interesting feature of supramolecular polymers is the capability to form reversible non-covalent cross-linked polymers. Polymer cross-linking is one of the most important features for the development of new materials because it strongly influences the physical-mechanical properties of the polymers. For instance a very high cross-link density can gives rise to materials alternatively rigid when cross-linked and flexible when polymer chains are disconnected. Although conventional cross-linking has been based on covalent chemistries, the supramolecular cross-linking approach offers a new route towards materials that are otherwise not accessible. In fact, molecular recognition processes present many advantages such as reversibility and a greater control of the network architecture. Additionally, the combination of orthogonal molecular recognition units for non-covalent cross-linking can generate multi-responsive materials.

Polymer blending is an attractive route to develop new materials that combine the desirable properties of more than one polymer.[3] Another reasons to employ polymer blending is to save costs by blending an high performance polymer with cheaper materials. Although this approach has relevant practical implications, the microscopic segregation observed in most polymer blends jeopardize their use. Indeed blending two immiscible polymers lead to an heterogeneous structure, in which there are regions of one polymer alternated to regions of the other polymer, with little adhesion between the areas. Many efforts have been made to solve the phase segregation issue using both physical and chemical compatibilization. For example the addition of a third component like a block copolymer, that is partially miscible with both constituents of the blend, can minimize the interfacial energy. Otherwise another option is the

introduction of reactive functional groups in the side chain of the polymers, which can covalently connect the macromolecules within the blend.
Recently, Zimmerman *et al.*[4] reported the use of hydrogen bonding to tackle the miscibility problem in polymer blends. In their work, two immiscible polymers,[5] polystyrene and poly(butyl)methacrylate, were functionalized with 2,7-diamido-1,8-naphthyridine (DAN) and guanosine urea (UG) respectively; the strong heterocomplex formation between the two recognition units driven the polymer blending of the immiscible polymers (Figure 3.1). This result was proved by several and complementary techniques, such as ^{1}H NMR, AFM and viscosity studies. Interestingly, this approach was further improved by introducing redox sensible molecular recognition units for the control of supramolecular polymer network.[6]

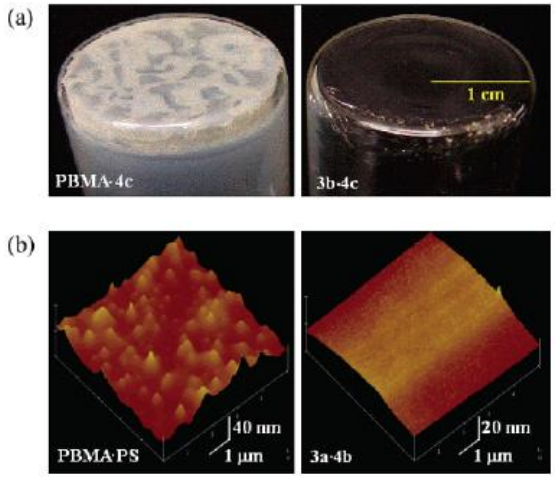

Figure 3.1 a) *Photographs of the PS-PBMA before and after functionalization; b) AFM images of PS-PBMA before and after functionalization.*

These noteworthy results inspired us to explore the potential of host-guest interactions to induce polymer blending, exploiting the molecular recognition properties of tetraphosphonate cavitand towards the *N*-methylpyridinium moiety. Our group already demonstrated that this interaction can lead to supramolecular polymers[7] or hybrid inorganic-organic materials.[8] In a recent paper Dalcanale *et al.*[9] modified the structure of polystyrene (PS) with tetraphosphonate cavitand host (PS-Host) and poly(butyl)methacrylate (PBMA) with *N*-methylpyridinium motif guest (PBMA-Py, Figure 3.2).

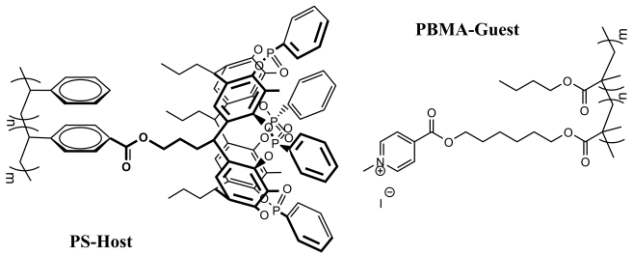

Figure 3.2 *PS-Host and PBMA-Py.*

The formation of a supramolecular polymer architecture was demonstrated in solution by ^{31}P NMR, and in solid state by atomic force microscopy (AFM) and differential scanning calorimetry (DSC). The AFM image of PS-Host:PBMA-Py 1:1 molar mixture showed no phase separation in accordance with the formation of a supramolecular network. A DSC study of the blend showed a single T_g (glass transition temperature) at temperature intermediate between the T_g of the two starting polymers. Moreover, segregation has been chemically induced by addition of a competitive guest (*N*-methylbutylammonium chloride) which replaced the *N*-methylpyridinium moiety in the cavitand binding.

3.2 Introduction

Compatibilization of an immiscible pair of polymers confirmed that host-guest interactions between **Tiiii** and *N*-methylpyridinium can be exploited to construct blends that are homogenous at the microscopic scale. In the first part of this work (paragraphs 3.3.1 and 3.3.2) we embedded the supramolecular complex studied in Chapter 2 (**Tiiii**@sarcosine) in real polymers (PS and PBMA) in order to form an homogenous blends (PS-Host/PBMA-Sarc, Figure 3.3) and further expand the scope of this host-guest counterpart in material science.

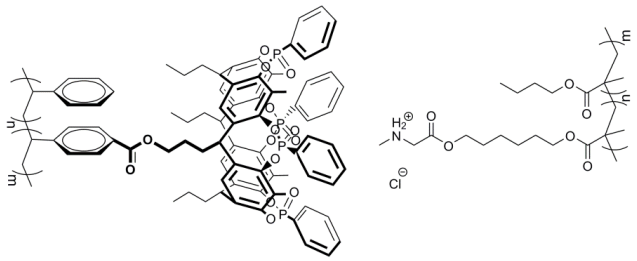

Figure 3.3 *PS-Host/PBMA-Sarc blend.*

Being connected by dynamic bonds, this materials is reversible because it can be segregated in solution by adding a competitive guest, as demonstrated for the PS-Host/PBMA-Py blend.[9] In this context, a special challenge is inducing the reversibility towards external stimuli directly in the solid state. In the second part of the chapter (paragraphs 3.3.3 and 3.3.4) we describe the responsiveness of the two supramolecular polymer blends (PS-Host/PBMA-Py, Figure 3.2 and PS-Host/PBMA-Sarc, Figure 3.3) towards external stimuli in the solid state.

As previously explained the supramolecular blends are held together by host-guest interactions. In fact the PS functionalized with tetraphosphonate cavitands can complex the methylpyridinium and methylammonium moieties embedded in the poly(butyl)methacrylate (PBMA-Py and PBMA-Sarc). These two blends are compatibilized and fully miscible in the solid state, hence a reduction of the methylpyridinium unit or a deprotonation of the methylammonium moiety can remove the interactions between the host-guest counterpart and in turn decompatibilize the blends causing a phase segregation. We investigated this process at the solid state studying through AFM the morphology of the two blends upon application of external stimuli.

To what concerns the PS-Host/PBMA-Py blend, the reversible compatibilization/decompatibilization processes can be induced at the solid-liquid interface through an electrochemical reduction of the *N*-methylpyridinium unit to a radical species (Figure 3.4), that being uncharged cannot be complexed by the tetraphosphonate cavitand.[10]

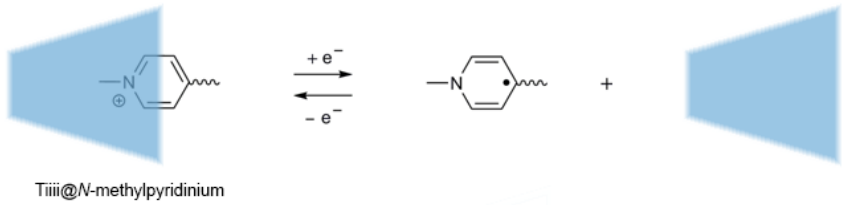

Figure 3.4 *Reversible decomplexation driven by electrochemical reduction of N-methyl pyridinium.*

Instead, for the PS-Host/PBMA-Sarc blend, the segregation can be performed using a simple acid-base reaction. At the solid-gas interface a proper base can permeate in the structure of the blend deprotonating the secondary amine thus decreasing the affinity of the guest towards the receptor (Figure 3.5).

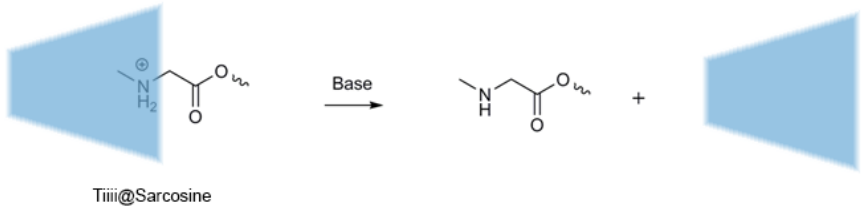

Figure 3.5 *Reversible decomplexation driven by deprotonation of sarcosine.*

3.3 Results and Discussion

3.3.1 Synthesis of PBMA-Sarc

The PS-Host and PBMA-Py were synthesized according to protocols outlined by Dalcanale *et al*.[9]

The PBMA-Sarc was synthesized by copolymerization of butyl methacrylate with the corresponding sarcosine-functionalized monomer: 6-((methylglycyl)oxy)hexyl methacrylate (**IV**). The monomer was easily prepared in three steps (Scheme 3.1). At first, monoesterification of 1,6-hexanediol with methacryloyl chloride introduced a single methacrylate group, then the monoester **II** was reacted with *N*-Boc-sarcosine using DCC/DMAP coupling procedure affording the diester **III**. Subsequently, the Boc protecting group was removed by treating **III** with trifluoroacetic acid, giving the monomer **IV** in 32% overall yield.

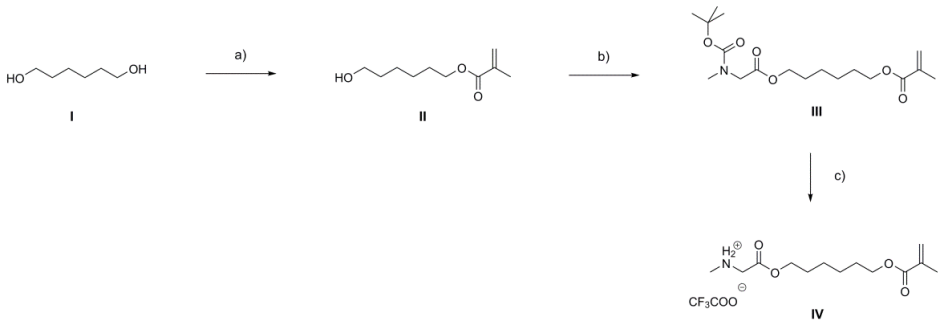

Scheme 3.1 *Synthesis of monomers **III** and **IV**: a) methacryloyl chloride, DMAP, Et3N, DCM, r.t., 12 h, 48%; b) N-Boc-sarcosine, DCC/DMAP, DCM, r.t., 12 h, 67%; c) TFA, DCM, r.t., 3 h, quantitative.*

The free radical copolymerization of **IV** with butyl methacrylate followed by treatment with hydrochloric acid afforded the copolymer **V** (Scheme 3.2).

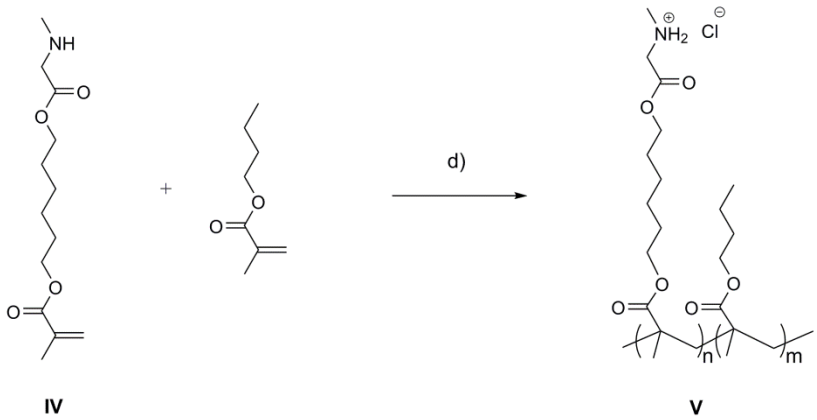

Scheme 3.2 *Synthesis of PBMA-Sarc **V**: d) 1) AIBN, toluene, 24 h, 70 °C, 70%; 2) HCl.*

The polymer was fully characterized by several techniques: elemental analysis, GPC, FT-IR and ^{1}H NMR. The ratio between **IV** and butyl methacrylate in the reaction was maintained 4:96 as in the PBMA-Py synthesis. We used this percentage of the guest because it assures a strong interaction with the host that will lead to the copolymer blending, without altering the main features of the pristine polymers. The percentage of the guest was estimated with elemental analysis and ^{1}H NMR integration. With the first technique a 2.8% of the guest was found in the copolymer. This data was confirmed from ^{1}H NMR

integration ratio of the methyl group of sarcosine (2.29 ppm) and OCH_2 groups (3.96 ppm).

3.3.2 Complexation Properties of PS-Host/PBMA-Sarc in Solution and at the Solid State

The ^{31}P NMR analysis demonstrated the association between the PS-Host and PBMA-Sarc, in fact a down-field shift of the phosphorous signal of the cavitand was observed (Figure 3.6).

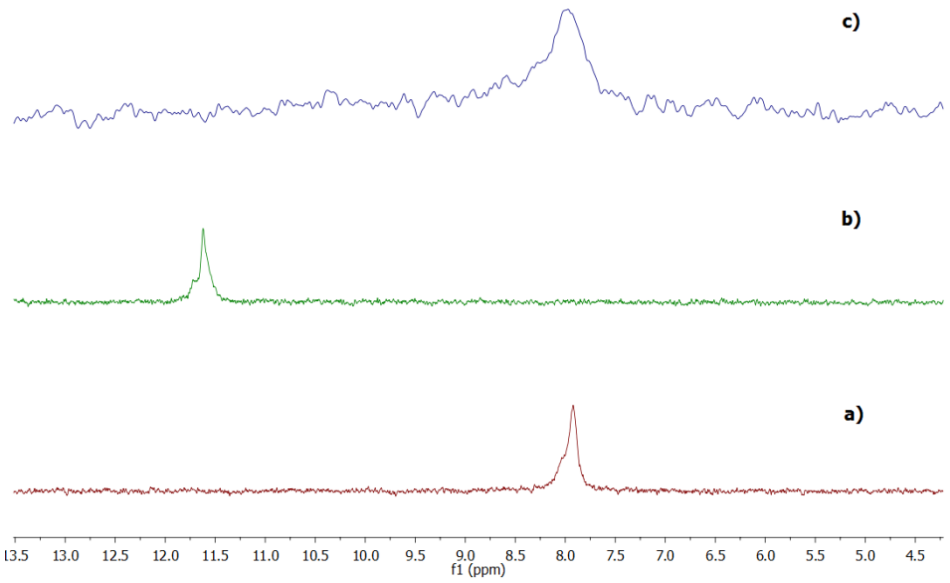

Figure 3.6 *^{31}P NMR spectra in $CDCl_3$ a) PS-Host (0.5 mM), b) PS-Host:PBMA-Sarc 1:1 (0.5 mM), c) PS-Host:PBMA-Sarc 1:1 + DBU.*

The signal at about 11.7 ppm is diagnostic of the 1:1 complex formed between the tetraphosphonate cavitand and the sarcosine moiety. Upon the addition of an excess of DBU the phosphorous signal returned to 8 ppm, proving the system reversibility in solution.

The miscibility of the blend between the two polymers was assessed with two different methods namely: differential scanning calorimetry (DSC) and atomic force microscopy (AFM).
Materials formed by a single phase structure exhibit only one glass transition temperature (T_g) that can be easily found by DSC.[11] The 1:1 molar mixture of

PS-Host and PBMA-Sarc shows one endothermic relaxation peak, in between the T_g of the two functionalized polymers, that correspond to an homogeneous blend (Table 3.1 and Figure 3.7).

Polymers	T_g
PS-Host	97.1 °C
PBMA-Sarc	14.6 °C
PS-Host + PBMA-Sarc	37.3 °C

Table 3.1 *Glass transition temperatures.*

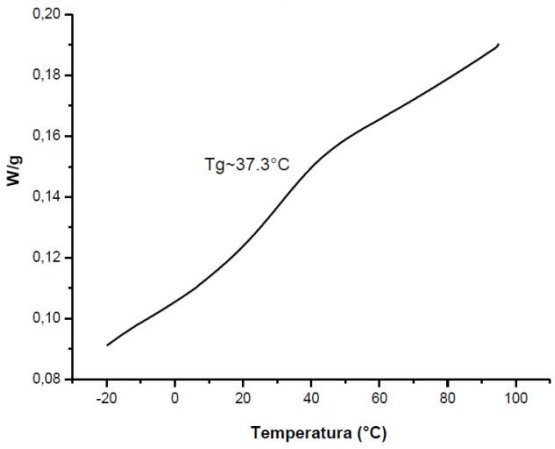

Figure 3.7 *DSC thermogram of 1:1 molar mixture PS-Host/PBMA-Sarc.*

In order to confirm the miscibility of the blend at the solid state an AFM experiment was performed. A thin film was prepared from a 0.5 mM solution of a 1:1 molar mixture of PS-Host and PBMA-Sarc which was deposited on silicon surface by spin coating (1500 rpm for 30 sec). The AFM topography shows a flat surface without phase separation (Figure 3.8).

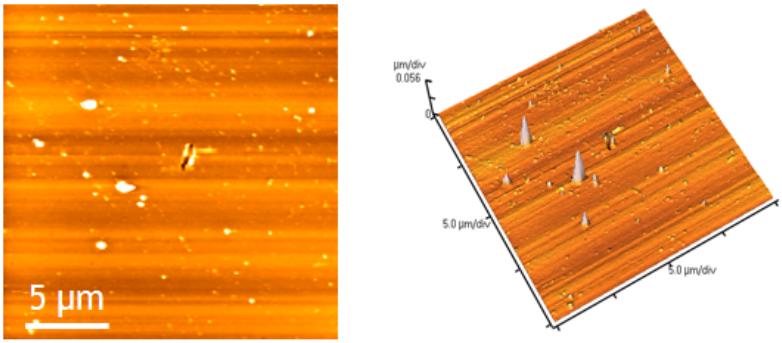

Figure 3.8 *AFM images of 1:1 molar mixture PS-Host/PBMA-Sarc.*

The studies of this material at the solid state indicated that the interactions between the cavitand and the sarcosine moiety drives the compatibilization of the two immiscible polymers and the formation of an homogenous blend.

3.3.3 Reversibility Studies of PS-Host/PBMA-Sarc Blend in the Solid State

In the case of the blend that contains the secondary amine, a series of segregation experiments with base vapors were carried out. The deprotonation of the amine although similar to the process that occur in solution, is more complicated in the solid state. The base has to permeate into the polymers in order to reach the reaction site, moreover the basicity of a substance changes at the solid-gas interface. To tackle these issues we expose the polymer blend to different base vapors.

Another problem is the mobility of the polymer chains. The decompatibilization of the blends have the purpose to induce a phase segregation in the polymeric films. Segregation requires mobility of the polymeric chains in the solid state. In order to enhance this parameter all the decompatibilization tests were carried out above the glass transition temperature of the blend. In fact at this temperature the polymer is in a rubber state and the polymer chains are more flexible and can rearrange in the solid state.

Polymer films were prepared by spin coating (1500 rpm for 30 sec.) 0.5 mM solution ($CHCl_3$) of the polymer blend onto a silicon slice.

Before starting the decompatibilization experiments, a control test without base was performed to study the annealing effect on the morphology of the blend surfaces. AFM images upon annealing at 110 °C show an homogeneous blend,

moreover the surface roughness decrease after being heated (before the treatment 3.42 nm, after the treatment 2.31 nm, Figure 3.9). This effect is due to the greater mobility of the polymer chains of the blend that homogenize the structure of the film.

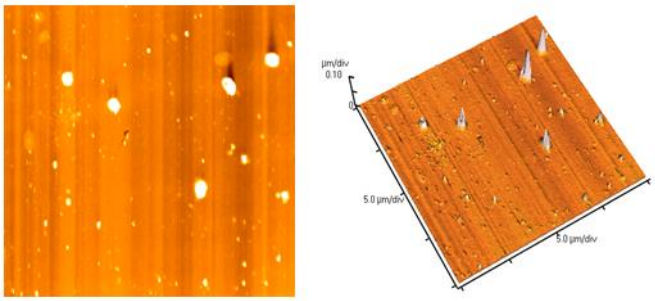

Figure 3.9 *AFM images 1:1 molar mixture PS-Host/PBMA-Sarc upon annealing at 110 °C.*

Then the films were exposed to vapors of different bases at various temperatures for 24 hours (see Experimental Section for procedure details and Table 3.2 for the segregation results).

Bases	Temperature of the polymer blend (°C)	Segregation
Control	110	NO
Ammonia	70 110	NO NO
Triethylamine	70 110	NO NO
DBU	110	NO
N-methyl pyrrolidine	110	NO

Table 3.2 *Segregation experiments.*

As summerized in Table 3.2 all the decompatibilization experiments carried out using four different bases did not induce surface segregation, or a significative change in the roughness of the surface. As an example, the treatment with triethylamine for 24 h at 110 °C is reported. The AFM images after the

decompatibilization process do not present the typical islands and depressions of a non-homogeneous blend (Figure 3.10).

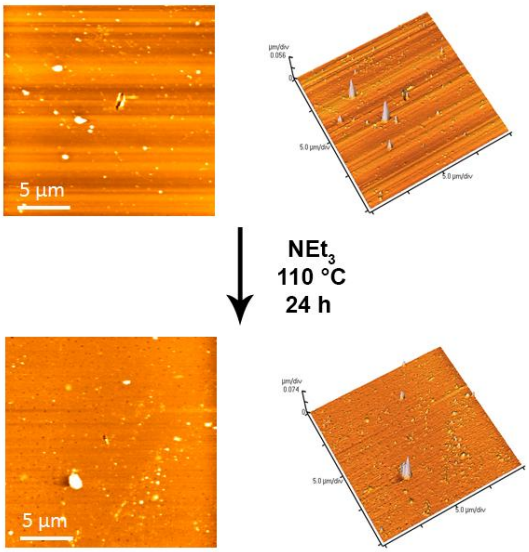

Figure 3.10 *AFM images of PS-Host/PBMA-Sarc before and after the basic treatment.*

The segregation experiments failure in the solid state can be due to different causes: i) the first one is probably the lack of permeability of the gaseous bases into the network structure of the blend; ii) another possible cause is that the deprotonating molecule is not basic enough (this is not the case for DBU) to remove the proton from the secondary amine embedded in the polymeric chain of the PBMA, because at the solid-gas interface the basicity of a substance can change dramatically; iii) the mobility of the polymer chains is not sufficient to trigger segregation.

3.3.4 Reversibility Studies of PS-Host/PBMA-Py Blend in the Solid State

The segregation of the PS-Host/PBMA-Py blend was studied through an electrochemical reduction of the methylpyridinium group at the solid-liquid interface. We reported earlier that in solution the pyridinium guest can be released from the cavity of the tetraphosphonate receptor after one-electron reduction of the pyridinium moiety.[10] The supramolecular complex can be restored upon removal of the extra electron of the guest, thanks to the reversibility of the redox process.

We investigated the voltammetric properties of the guest in the solid state using cyclic voltammetry (CV). The experiments were performed at room temperature and 60 °C in order to operate below and above the T_g of the blend in the electrochemical process.

The voltammetric measurements at room temperature showed the presence of cathodic peak between -0.7 and -0.8 V, this signal is attributable to the mono-electronic reduction of the *N*-methylpyridinium group (Figure 3.11). Interestingly, we observed a positive shift of the cathodic peak for repeated reduction cycles, whose magnitude is proportional to the scan rate of the cyclic voltammetry.

This behavior can be explained considering the host-guest properties of the supramolecular complex. In the first cycle of the CV the mono-electronic reduction of the *N*-methylpyridinium moiety affords a neutral species that has no affinity towards the host with resulting withdrawal from the cavity. At the beginning of the second cycle, if the scan rate is too high, the guest has not time enough to return into the cavity of the receptor, resulting in a positive shift of the cathodic peak (Figure 3.11b).

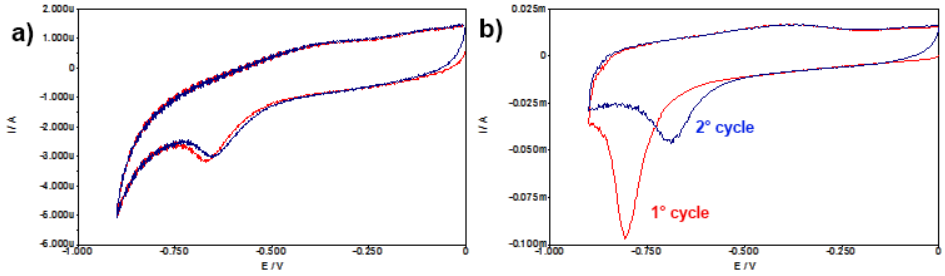

Figure 3.11 *Cyclic voltammogram at r.t.: a) scan rate 50 mV min^{-1}; b) scan rate 1 V min^{-1}.*

Furthermore the data collected indicated a linear relationship between the cathodic intensity values and the scan rates (Figure 3.12). This result proves that the electrochemical process is governed by electro-active immobilized species and it is not related to diffusion.

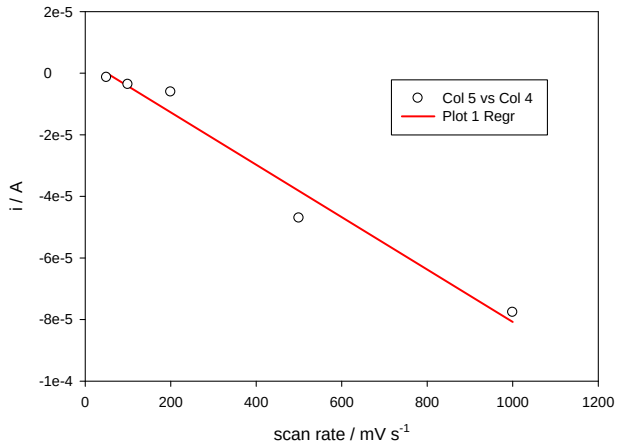

Figure 3.12 *Cathodic peak intensity vs. scan rate.*

Also the CV measurement performed at 60 °C shows the presence of a cathodic peak in the same regions of the previous experiment, and confirmed the presence of a reductive process (Figure 3.13).

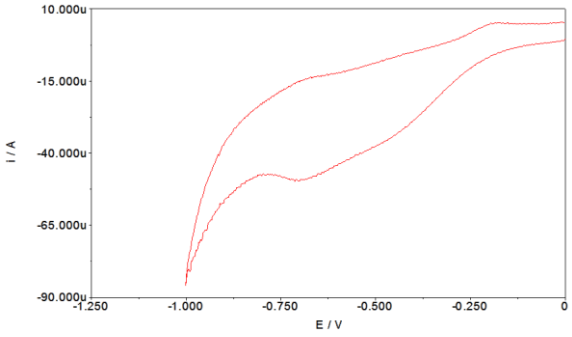

Figure 3.13 *Cyclic voltammogram at 60 °C, scan rate 200 mV min-1.*

The decompatibilization experiments were conducted applying a reduction potential of -0.8 V to the polymeric films dipped in the electrochemical cell. The electrolysis experiments were monitored through coulombometric measurements at 60 °C, above the T_g of the polymer blend (see Figure 3.14). At the beginning of the experiment, the charge follows an exponential behavior but after few second, rather than reach a stable value, it follows a linear relationship. This is probably due to the reduction of the proton ions of the water.

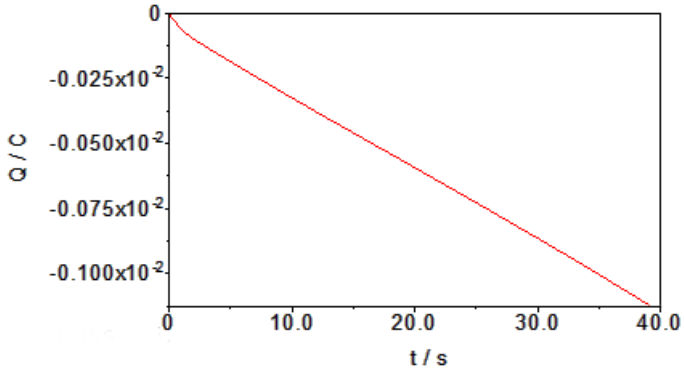

Figure 3.14 *Coulombometer experiment at 60 °C.*

The AFM images of the blend treated with an electrochemical stimulus show a change in the morphology surface, probably due to a phase segregation that occurred in the polymeric film in response to the immiscibility of the decompatibilized polymers. This alteration of the morphology can be appreciated observing an enlargement image of the film (Figure 3.15, 0.1 µm bar scale).

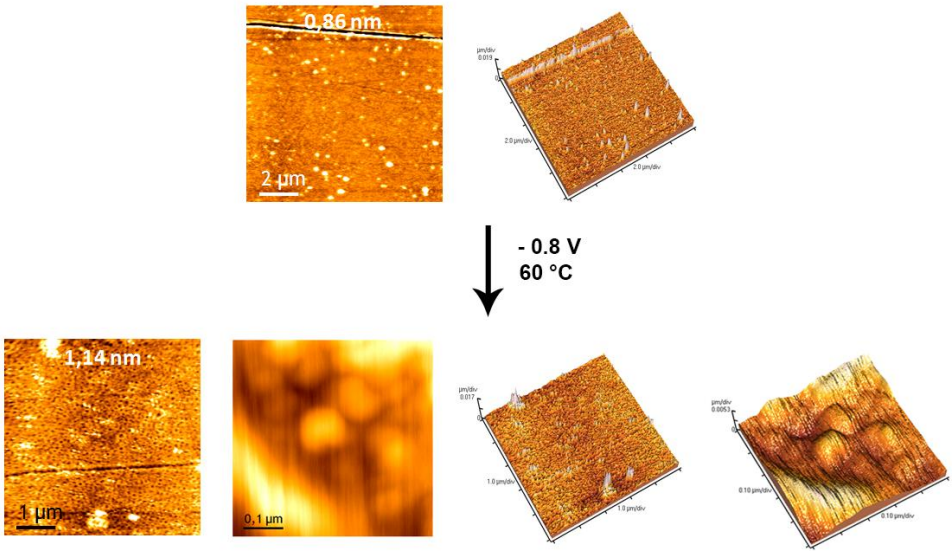

Figure 3.15 *AFM images (contact mode) of PS-Host/PBMA-Py before and after the electrochemical stimulus.*

However the study of the morphology with AFM in contact mode does not justify the presence of domains of different materials. To confirm our hypothesis of phase segregation we carried out an AFM experiment in non contact mode. In this technique the tip of the cantilever does not touch the surface of the sample, instead it oscillates close to its resonance frequency. An electronic feedback loop ensures that the oscillation amplitude remains constant, such that a constant tip-sample interaction is maintained during scanning. Forces that act between the sample and the tip will not only cause a change in the oscillation amplitude, but also change in the resonant frequency and phase of the cantilever. Different components of the sample which exhibit difference adhesive and mechanical properties will show a phase contrast and therefore allow a discrimination between different type of materials on the surface.
In Figure 3.16 are reported the topography and the phase lag images of the decompatibilized blend.

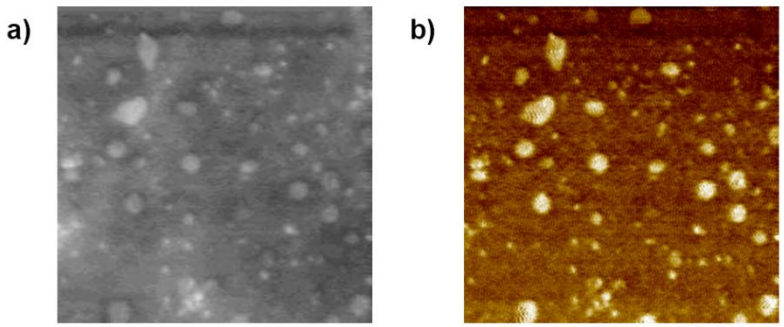

Figure 3.16 *AFM images (non contact mode) of PS-Host/PBMA-Py: a) topoghrapy, b) phase lag of the cantilever.*

A direct correlation between the two images can be observed, in other words all the domains detected on the morphology are composed to a material that has a different elasticity respect the rest of the sample, indicating a partial decompatibilization of the blend.

3.4 Conclusions

In this chapter we have successfully blended two immiscible polymers, namely PS and PBMA via **Tiiii**@sarcosine host-guest interactions. The formation of an homogeneous polymer blend was unambiguously confirmed by several and complementary analytical tools, namely NMR, DSC and AFM. Then we have investigated the responsiveness to external stimuli of two homogenous polymer blends at the solid state. The first blend composed by PS-Host/PBMA-Sarc has been treated with different gaseous bases at the solid-gas interface. All the experiments carried out have not shown a segregation of the two polymers, proving that the base does not permeate inside the tridimensional structure of the blend. A possible solution of this problem could be to transfer the deprotonation process from a solid-gas to a solid-liquid interface.
Regarding the second blend composed by PS-Host/PBMA-Py, we have gained new insights about the electrochemical behavior of the *N*-methylpyridinium moiety in the solid state. Moreover a change in the morphology of the blend has been found after the electrochemical experiment at the solid-liquid interface, our hypothesis was supported by an AFM non contact mode experiment. Although other experiments have to be performed in order to confirm the reversibility of this blend, we have demonstrated that a molecular modification of the host-guest interactions can promote a macroscopic modification of the properties of the materials such as the morphology.

3.5 Acknowledgments

Special thanks to Dr. Marco Dionisio, Dr. Federico Fanzini from Department of Chemistry and Dr. Tiziano Rimondi, Prof. Luigi Cristofolini from Department of Physics, University of Parma for AFM measurements. Thanks to Dr. Lucia Ricci and Prof. Giacomo Ruggeri from Department of Chemistry, University of Pisa for preparation of the polymers. Thanks to Prof. Alberto Credi and Dr. Monica Semeraro from Department of Chemistry, University of Bologna for electrochemical experiments.

3.6 Experimental Section

The PS-Host and PBMA-Py were synthesized following reported procedures.[9] *N*-Boc-sarcosine was prepared following procedure described in Chapter 2.

6-hydroxyhexyl methacrylate (II)
To a solution of 1,6-hexanediol **I** (5.6 g, 48 mmol) in dichloromethane, DMAP (0.46 g, 4 mmol) and triethylamine (3.96 ml, 29 mmol) were added. The mixture was cooled at 0 °C and methacryloyl chloride (1.85 ml, 20 mmol) was added dropwise. The solution was warmed at room temperature and stirred overnight. The reaction was quenched with water, the organic phase was separated and evaporated under reduced pressure. The crude was purified by silica gel column chromatography (hexane:dichloromethane 7:3) to give **II** as colorless oil (1.86 g, 9.7 mmol, 48 %).
^{1}H NMR ($CDCl_3$, 400 MHz): δ (ppm) = 6.05 (s, 1H, $\mathbf{H}_{TRANS}HC=C$), 5.51 (s, 1H, $\mathbf{H}_{CIS}HC=C$), 4.10 (t, 2H, J= 6.6 Hz, $(C=O)OC\mathbf{H_2}CH_2$), 3.58 (t, 2H, J= 6.6 Hz, $CH_2C\mathbf{H_2}OH$), 2.39 (s, 1H, $CH_2O\mathbf{H}$), 1.90 (s, 3H, $C\mathbf{H_3}$), 1.65 (m, 2H, $(C=O)OCH_2C\mathbf{H_2}$), 1.54 (m, 2H, $C\mathbf{H_2}CH_2OH$), 1.37 (m, 4H, $CH_2C\mathbf{H_2}C\mathbf{H_2}CH_2$); **ESI-MS**: *m\z* 209.2 $[M+Na]^+$.

6-((N-(tert-butoxycarbonyl)-N-methylglycyl)oxy)hexyl methacrylate (III)
To a solution of **II** (0.53 g, 2.80 mmol) in dichloromethane, DCC (0.58 g, 2.80 mmol) and DMAP (0.102 g, 0.841 mmol) were added. After 10 min. of stirring *N*-Boc-sarcosine (0.58 g, 3.08 mmol) was added. The reaction mixture was stirred for 12 h at room temperature and quenched adding saturated NH_4Cl solution. The organic phase was extracted twice with water, dried with $MgSO_4$ and evaporated under *vacuo*. Purification by silica gel column chromatography (hexane:ethyl acetate 8:2) yielded the desired product **III** as colorless oil (0.671 g, 1.88 mmol, 67%).
^{1}H NMR ($CDCl_3$, 400 MHz): δ (ppm) = 6.11 (bs, 1H, $\mathbf{H}_{CIS}HC=C$), 5.57 (bs, 1H, $\mathbf{H}_{TRANS}HC=C$), 4.17-4.13 (m, 4H, $C\mathbf{H_2}O$), 3.95 (d, 2H, J= 32 Hz, $NC\mathbf{H_2}C(O)$), 2.94 (d, J= 8 Hz, 3H, $NC\mathbf{H_3}$), 1.96 (s, 3H, $C\mathbf{H_3}$), 1.69-1.43 (m, 18H, alkyl chain, $C(C\mathbf{H_3})_3$); **ESI-MS**: *m/z* 380 $[M+Na]^+$.

2-((6-(methacryloyloxy)hexyl)oxy)-N-methyl-2-oxoethan-1-aminium2,2,2-trifluoroacetate (IV)
III (0.33 g, 0.92 mmol) was dissolved in dichloromethane and an excess of trifluoroacetic acid was added slowly. The solution was stirred at room temperature for 3 h. The reaction mixture was evaporated under reduced

pressure to give the product **IV** as colorless oil (0.246 g, 0.92 mmol, quantitative yield).
^{1}H NMR ($CDCl_3$, 400 MHz): δ (ppm) = 6.11 (s, 1H, **H_{CIS}**HC=C), 5.56 (s, 1H, **H_{TRANS}**HC=C), 4.17-4.13 (m, 4H, C**H_2**O), 3.41 (s, 2H, NC**H_2**C(O)), 2.48 (s, 3H, NC**H_3**), 1.96 (s, 3H, C**H_3**), 1.74-1.64 (m, 4H, C**H_2**CH_2O), 1.47-1.37 (m, 4H, C**H_2**CH_2CH_2O); **ESI-MS**: *m/z* 258 $[M+H]^+$.

Copolymerization between n-butyl methacrylate and 6-((methylglycyl)oxy)hexyl methacrylate (IV) (PBMA-Sarc) (V)
In a Schlenk with magnetic stirrer n-butyl methacrylate (3.9 mL, 24.84 mmol) and **IV** (0.266 g, 1.03 mmol) were dissolved in toluene under inert nitrogen atmosphere. The solution was purged with nitrogen for 30 minutes and heated to 70 °C, then AIBN was added (85 mg) and the polymerization mixture kept for 24 h in these conditions. At the end of the reaction, the copolymer was purified by twice precipitation in 500 mL of cold methanol and after filtration, copolymer was dried *under vacuum* at room temperature (70%).
^{1}H NMR ($CDCl_3$, 300 MHz): δ (ppm) = 3.96 (NC**H_2**C(O), C(O)OC**H_2**CH_2), 2.29 (NC**H_3**), 1.9-1.8 ($[CH_2C(CH_3)(C(O)OC_4H_9)]_n$), 1.63 ($C(O)OCH_2CH_2$), 1.43 ($CH_2CH_2CH_3$), 1.1-0.8 ($CH_2CH_2CH_3$, $[CH_2C(CH_3)(C(O)OC_4H_9)]_n$); **IR** (solution casting on KBr plate): 3410 (ν_{N-H}), 2960 (asym ν_{C-H} CH_3), 2936 (asym ν_{C-H} CH_2), 2875 (sym ν_{C-H} CH_3), 1728 ($\nu_{C=O}$), 1466 (asym δ_{CH3}), 1385 (sym δ_{CH3}), 1268, 1242, 1177, 1154 (ν_{C-O-C}), 750 (ρ_{CH2}), 666 (Wagging N-H) cm^{-1}; **Elemental analysis**: theoretical C 66.41, H 9.81, N 0.38 %; found C 68.32, H 10.09, N 0.27 %; **GPC** ($CHCl_3$): $\overline{Mn}$: = 23200 Da, $\overline{Mw}$ = 36600 Da, PDI = 1.58.

Film deposition
A 0.05 mM solution of 1:1 molar mixture of PS-Host and PBMA-Sarc/PBMA-Py in $CHCl_3$ was prepared. 100 µL of the resulting solution was filtered over 0.45 µm polypropylene filter and spin-coated on a silicon slice at 1500 rpm for 30 seconds.

Reversibility experiments of PS-Host/PBMA-Sarc blend in the solid state
The polymer blend films were positioned in Schlenk flasks, the base vapors were put into the flasks at room temperature. Then the flasks were heated with an oil bath for 24 hours at the temperature chosen for the experiment.

FT-IR

FT-IR spectra were recorded on a Perkin Elmer FT-IR Spectrum One Spectrometer on films obtained by solution casting onto KBr windows of polymers diluted $CHCl_3$ solution.

GPC measurements

GPC System apparatus equipped with Jasco PU-2089 Plus pump, Jasco RI 2031 Plus as Refractive Index Detector, Jasco CO_2063 Plus column oven (set at 30 °C) and 2 polymer laboratories PLgel MIXED D columns and PL gel guard column poly(styrene-co-divinylbenzene) (linear range 100 - 600000 Da), was used for determination of Molecular Weight of chloroform diluted solutions of samples (eluted at 1 ml/min). The calibration curve was made with polystyrene standards and calculations were carried out with software Borwin 1.21.61 (JMBS DEVELOPMENT).

AFM measurements

Surface topography was examined using an atomic force microscope Thermomicroscope Autoprobe CP Research. All measurements were performed either in contact mode or in tapping mode employing respectively Silicon Nitride probes (Veeco OTR4-35, typical spring constant 0.05 N/m) or silicon probes (Bruker, MPP-12100, typical spring constant 3 N/m). The collected images were analyzed using the proprietary software or Gwyddion, an Open Source software, covered by GNU General Public License. (Gwyddion.net)

DSC measurements

DSC thermograms were recorded by using a Mettler Toledo Stare System, model DSC 822e differential scanning calorimeter equipped with a Stare software.

Electrochemical experiments

Cyclic voltammetric (CV) experiments were carried out in argon-purged water (Romil Hi-Dry) at room temperature and 60 °C with an Autolab 30 multipurpose instrument interfaced to a PC. The working electrode was a 1:1 molar mixture of PS-Host/PBMA-Py blend deposited by spin coating on a Au surface, the counter electrode was a Pt wire, separated from the solution by a frit, and an Ag wire was employed as a quasi-reference electrode. Sodium chloride 0.1 M was added as supporting electrolyte.

3.1 References and Notes

[1] R. J. Wojtecki, M. A. Meador, S. J. Rowan, *Nat. Mat.* **2011**, *10*, 14-27.

[2] L. Brunsveld, J. B. Folmer, E. W. Meijer, R. P. Sijbesma, *Chem. Rev.* **2001**, *101*, 4071-4097.

[3] Y. S Lipatov, *Prog. Polym. Sci.* **2002**, *27*, 1721-1801.

[4] T. Park, S. C. Zimmerman, *J. Am. Chem. Soc.* **2006**, *128*, 11582-11590.

[5] C. Chunyan, W. Jie, S. E. Woodcock, Z. Chen, *Langmuir* **2002**, *18,* 1302-1309.

[6] Y. Li, T. Park, J. K. Quansah, S. C. Zimmerman, *J. Am. Chem. Soc.* **2011**, *133*, 17118-17121.

[7] R. M. Yebeutchou, F. Tancini, N. Demitri, S. Geremia, R. Mendichi, E. Dalcanale, *Angew. Chem. Int. Ed.* **2008**, *47*,4504-4508.

[8] M. Dionisio, F. Maffei, E. Rampazzo, L. Prodi, A. Pucci, G. Ruggeri, E. Dalcanale, *Chem. Commun.* **2011**, 6596-6598.

[9] M. Dionisio, L. Ricci, G. Pecchini, D. Masseroni, G. Ruggeri, L Cristofolini, E. Rampazzo, E. Dalcanale, *Macromolecules*, in press, DOI: 10.1021/ma401506t.

[10] B. Gadenne, M. Semeraro, R. M. Yebeutchou, F. Tancini, L. Pirondini, E. Dalcanale, A. Credi, *Chem. Eur. J.* **2008**, *14*, 8964-8971.

[11] M. Aubon, R. E. Prud'homme, *Macromolecules* **1988**, *21*, 2945-2949.

Chapter 4

Pyrene-Functionalized Fluorescent Cavitands for Illicit Drugs Sensing

4.1 State of the Art

The main stream in supramolecular chemistry is the design of artificial synthetic receptors that can recognize selectively a compound of interest. A significant application of these receptors is the development of chemical sensors, which can monitor different chemical environments, such as urban indoor and outdoor atmospheres, food aromas, explosives and so forth.[1]
Generally a chemical sensor is a device able to transform chemical information into an analytically useful signal.[2] In fact, a sensing effort requires not only the ability to bind the target analytes, but also the generation of a related readable signal. On this basis the chemical sensing process can be divided in two distinct steps: *recognition* and *transduction*. The sensing material responsible for recognition, interacts with the analytes, while the transducer produces a physical signal related to the binding process.
Molecular recognition impacts heavily the three main properties of a chemosensor indicated below: sensitivity, selectivity and reversibility.

- Sensitivity is defined as the slope of the analytical calibration curve, which is correlated with the magnitude of the change in the sensor signal upon a certain change in the analytical concentration.[3] Strongly complexing receptors are sensitive to analyties at very low concentration;
- selectivity is the ability of a sensor to respond to only one chemical species in the presence of other species (called interferents).[4] An highly selective receptor boosts selectivity;
- reversibility is the sensor's ability to return to its initial state after it has been exposed to chemical species. Weak interactions guarantee reversibility under normal operating conditions.

Supramolecular chemistry, the science that studies dynamic non covalent interactions, is best placed to maximize these three basic features of a chemical sensor. The exploitation of the guiding principles toolbox for receptor design, represented by the principle of *complementarity* and *preorganization*, allows the development of chemical sensors bearing high sensibility, selectivity and reversibility.
Complementarity encompasses the principle introduced by E. Fischer, the *Lock and Key Principle*, and according to Cram: "to complex, hosts must have binding sites which can simultaneously contact and attract the binding sites of the guests without generating internal strains or strong non-bonded repulsions."[5]

Although complementarity is necessary for structural recognition between molecules, it is in many cases not sufficient. Cram enounced another principle defined as follows: "the more highly hosts and guests are organized for binding and low solvation prior to their complexation, the more stable will be their complexes"(preorganization principle).[5] Consider two hosts, both of which present a single conformation that is complementary to a specific guest, but one host is rigid and can adopt a single low-energy conformation, while the second host is flexible and it has numerous conformations. In order to form a complex the flexible host must overcome the energetic costs associated with restricting itself to a single conformation which reduces the overall binding free energy.[6]

The principles of complementarity and preorganization operate in concert generating high-affinity and high-selectivity hosts that can be exploited in specific sensing.[7] This type of sensing aims to detect a class (or a single) analyte in a given environment. Usually, receptors design for specific sensing involves the identification of the correct recognition units that have to be incorporated into the host in order to bind each particular binding sites of the guest (Figure 4.1 top). Then these recognition units are pre-organized on the receptor scaffold (Figure 4.1 down), studying the best position and geometry exploiting other processes such as computer modeling and, trial and error testing in order to optimize the sensing ability of the receptor.[8]

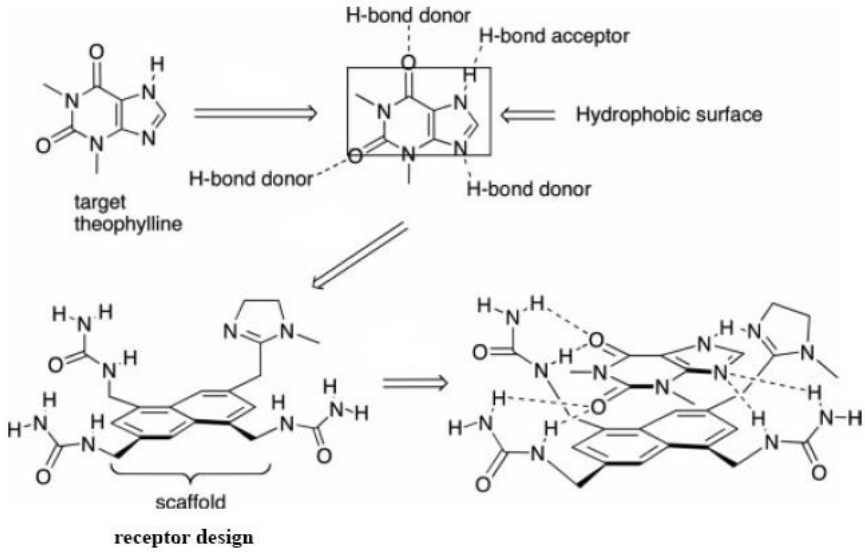

Figure 4.1 *Example of a selective synthetic receptor: design (top) and process (down).*

However the strict adherence of the basic principles of complementarity and preorganization can be detrimental for other types of chemical sensing such as differential sensing.[9] In this approach the procedure consists in the simultaneous detection of multiple analytes within a complex mixture. Inspired by the human sensory system (*e.g.* nose or tongue) researchers have built array of cross-reactive receptors that bind a variety of species with different affinity and selectivity profiles. These kind of synthetic receptors are cross-reactive because they may bind a number of analytes, but each of them binds the analytes differently than all other (Figure 4.2).[10] The use of these non-selective recognition sensor elements have promoted the growth of the so-called electronic noses,[11] tongues,[12] *etc.*

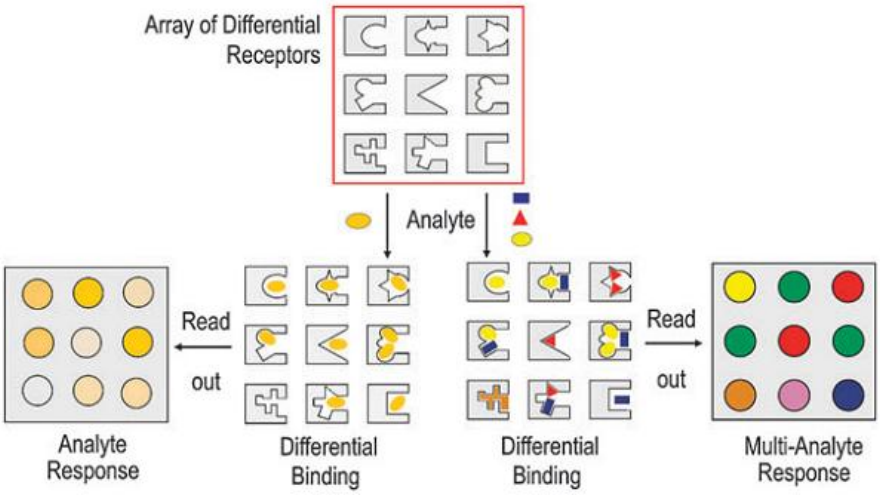

Figure 4.2 *Array-based sensor utilizing analyte binding by differential receptors. Regardless of whether the analyte is a single- or multicomponent analyte, receptors bind a number of analytes, but each receptor binds the analytes differently thus providing a differential response.*[9]

The other part of the sensors that must be carefully designed is the transducer element. This element transforms and amplifies the perturbation of the receptor unit, into an analytical useful signal. The selection of an high fidelity signal transduction mode is pivotal for the success of the sensing effort.

Commonly used detection methods are: fluorescence, colorimetry, electrochemistry, surface plasmon resonance (SPR) and quartz crystal microbalance (QCM). Each of them have many advantages, but fluorescence occupies a special role in chemical sensing because is an highly versatile and

low cost method that can be used in real time, at very low concentrations.[13] The versatility of fluorescence-based sensors originates from the wide number of parameters that can be tuned in order to optimize the convenient signal. Even very complex analytical problems can be solved by controlling the excitation and emission wavelengths, the time window of signal collection, and the polarization of the excitation beam or the emitted light. In most cases, luminescence intensity changes represent the most directly detectable response to target recognition; more recently, however, other properties such as excited state lifetime and fluorescent anisotropy have also been chosen as diagnostic parameters, since they are less affected by the environmental and experimental conditions.[14]

Mechanisms which control the response of a fluorophore to the substrate binding include: photoinduced electron transfer (PET),[15] photoinduced charge transfer (PCT),[16] fluorescence (Förster) resonance energy transfer (FRET),[16] and excimer/exciplex formation or extinction.[16] Obviously all these photophysical effects are dependent on the characteristics of the analyte and how the signaling unit (the fluorophore) is linked to the receptor moiety.

Fluorescent transducers of particular interest and widely employed are based on polyaromatic species such as those deriving from pyrene and naphthalene. These molecules are extensively used not only because they show a strong luminescence in the near UV, but they also own the unique property of excimer fluorescence.
Excimers are dimers in the excited state (the term excimer results from the contraction of 'excited dimer'). They are formed by collision between an excited molecule and an identical unexcited molecule.[17] The fluorescence band corresponding to an excimer is located at wavelengths higher than that of the monomer and does not show vibronic bands (Figure 4.3).[18]

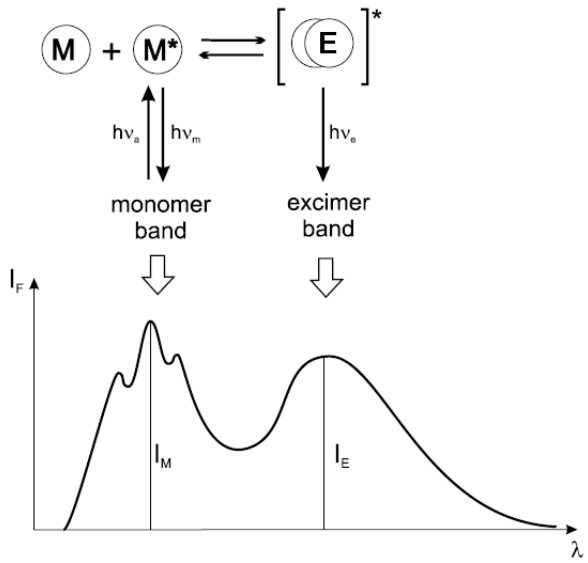

Figure 4.3 *Excimer formation, with the corresponding monomer and excimer bands.*

An excimer that has been extensively studied is that of pyrene (Figure 4.4).[19] The monomer band appears at 370-420 nm with well resolved vibronic features (M, M*), while the broad featureless excimer emission band is centered at about 450 nm (E). Another useful parameter is the intensity ratio of the excimer and the monomer (I_E/I_M), used to measure the efficiency of the excimer formation. In fact, contrary to the wavelength of the excimer λ_E, the ratio I_E/I_M is sensitive to the environmental factors that control excimer formation such as solvent polarity, viscosity or temperature.[20]

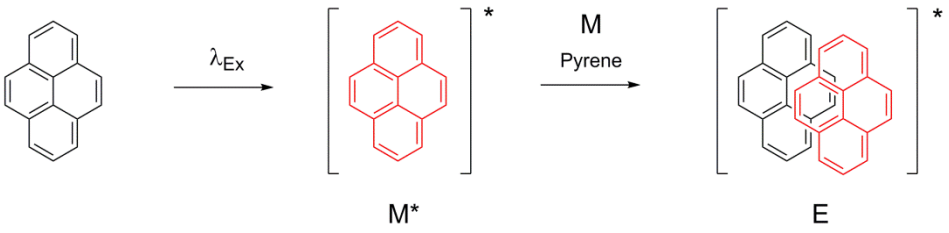

Figure 4.4 *Pyrene excimer formation.*

During the years a plethora of sensors based on the monomer-excimer dual luminescence of the pyrene unit have been prepared to detect cations, anions,[21] and biological target, such as oligonucleotides or ribonucleases.[20] The idea to exploit the excimer as transducer moiety is particularly interesting because one

can, using supramolecular interactions, bring the pair of fluorophores together or push them apart, modulating the I_E/I_M ratio. In the ideal situation, the sensor shows predominant monomer (or excimer) fluorescence in the absence of the analyte, and the opposite situation in the presence of the target molecule.[22]

4.2 Introduction

The need to develop a chemical sensor to detect small molecules bearing *N*-methylated moiety is a key topic because this functionality is present in many organic molecules that have a significant role in biology such as: drugs,[23] neurotransmitters[24] and cancer biomarkers.[25] In particular two classes of illicit drugs have drawn the attention of researchers in chemical sensing: amphetamine-type-stimulant (from now onward as ATS) and cocaine.

In the last decades the consumption of ATS has become a worldwide social problem, in fact the 2012 World Drugs Report[26] shows that after cannabinoids, the ATS (including MDMA also called ecstasy) is the second group of drugs most widely used globally, followed by opioids, opiates and cocaine.

Amphetamines, methamphetamines and their methylenedioxy-derivatives are a class of psychoactive synthetic drugs that belongs to the ATS group (Figure 4.5). Usually these substances are synthesized and sold not as free base but in the hydrochloride salt form, to enhance their bioavailability. They have a stimulant effect on the central nervous system, being able to increase the levels of neurotransmitters. Cocaine, a tropane alkaloid derived from the coca plant, is a powerful nervous system stimulant,[27] in 1970 this drug was declared illicit except for pharmaceutical purposes in the Controlled Substances Act.[28]

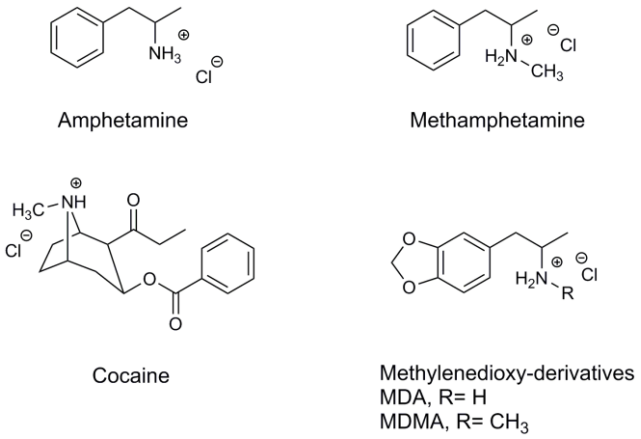

Figure 4.5 *Illicit drugs structures.*

So far a large variety of analytical methods have been developed to detect ATS including thin layer chromatography,[29] HPLC,[30] GC-MS,[31] immunoassay methods[32] and SERS.[33] For what concern cocaine detection the most valid methods are: HPLC,[34] GC-MS,[35] aptamers,[36] enzyme-based immunoassays like enzyme multiplied immunoassay technique (EMIT)[37] and enzyme-linked immunosorbent assay (ELISA).[38] The main drawbacks of these techniques are: long operation time, sosphisticated experimental procedures like sample pre-treatment and precautions from prior analysis.
Moreover, other two hurdles should be overcome to design a sensitive, selective and rapid on-site chemosensor for illicit drugs: the issue of the designer drugs and the problem of the interferents.
The first challenge is related to the identification of 'designer drugs' also called synthetic highs. A designer drug is the result of minor modifications in the chemical structure of an existing and controlled drug (Figure 4.6). They are produced in clandestine laboratories in an attempt to find loopholes in the chemical control regulations.

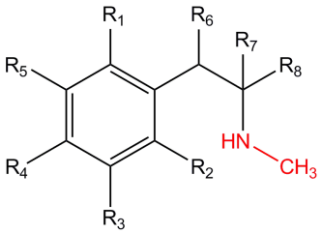

Figure 4.6 *Scheme of an ATS structure with all the possible structural modifications.*

These types of psychoactive molecules are alarming both authorities and health organizations because they show similar pharmacological effect with respect to its archetype, but they are sold openly since formally out of the 'black list' of illicit/controlled substances. Theoretically, the number of potential synthetic analogs that can be manufactured and distributed is very large. For this reason, ability to detect chemical similarity of the sample with controlled drugs is a fundamental asset for a chemosensor.

Another issue when trying to design a new drug detector device is that the "street samples", the real substances that are sold on the streets, are "cut" with excipients. The active principle content can vary from a minimum of 5% to a maximum of 60%. These auxiliary substances can act as interfering agents in the molecular recognition process, altering the response of the chemosensors. In the

case of the street samples in theory a large number of excipients can be chosen and the quantities can differ a lot depending also from the type of active principle. Despite this large option, the most common and used excipients are: glucose, lactose, paracetamol and caffeine. An effective drug sensor should not be affected by those interferents recording only the presence of the drug.

4.3 Results and Discussion

In this work we synthesized and tested a new fluorescent chemosensor based on tetraphosphonate cavitand able to detect not only illicit drugs like ATS and cocaine hydrochlorides but also their designer drugs, in the presence of interferents. The main properties of the chemosensor, molecular recognition unit and transducer element, were designed studying the binding site elements that characterize the target analytes.

4.3.1 Design of the Chemosensor

Bearing *N*-methyl ammonium moiety illicit drugs are well-suited to be recognized by tetraphosphonate cavitands (**Tiiii** from now onward). In solution, **Tiiii** has remarkable molecular recognition properties toward *N*-methylammonium salts, due to the presence of three interaction modes: (i) $N^{+}\bullet\bullet\bullet O{=}P$ cation–dipole interactions, (ii) CH_3–π interactions of the acidic $^{+}NH_2$–CH_3 group with the π basic cavity, (iii) two simultaneous hydrogen bonds between two adjacent P=O bridges and the two nitrogen protons (Figure 4.7).

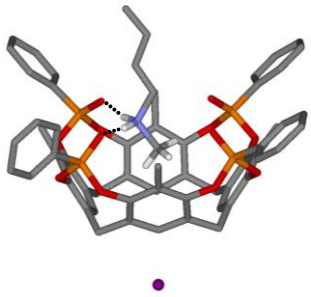

Figure 4.7 *X-Ray structure of the complex Tiiii@N-methylbutylammonium salt.*

The ability of the cavitand receptor **Tiiii** to recognize selectively the *N*-methylammonium hydrochloride group has been demonstrated in several works including the complexation of the series of *N*-alkylammonium salts[39] and

for molecules of biological interest like sarcosine[40] (see Chapter 1 for details) and antitumor drug procarbazine (PCZ) hydrochloride.[41] This property makes the cavitand able to detect ATS, cocaine and their designer drugs but also interferents such as *N*-methylammonium guest like sarcosine hydrochloride.
In order to differentiate molecules bearing the same functionality recognized by our cavitand receptor, we considered the bulky group that is present in the skeleton of ATS and cocaine molecules, but absent in other *N*-methylated ammonium molecules. To detect the presence of bulky substituents we turned the **Tiiii** cavitand into a fluorescent chemosensor tethering two pyrene moieties in distal position on the top of the cavity. As illustrated in Figure 4.8 the two pyrenes were connected to the two phosphonate groups by an alkyl spacer in a distal position. The pyrene moieties were attached on the phosphonate groups for synthetic reasons because the apical position of the cavity is difficult to functionalize. Distal functionalization guarantees the optimal overlap of pyrenes for excimer formation.

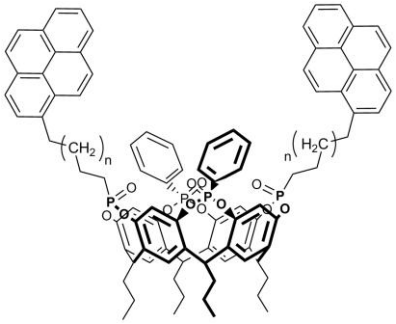

Figure 4.8 *The designed fluorescent chemosensor.*

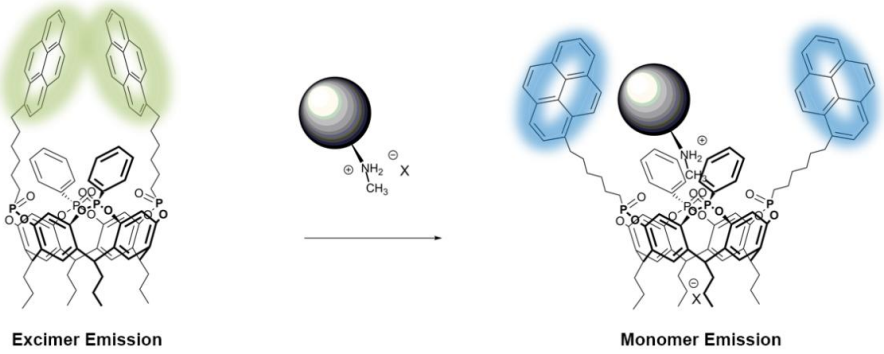

Figure 4.9 *Transduction mechanism.*

We envisaged that in the distal configuration the two pyrene moieties can act as transducer element forming an excimer. In absence of target analytes the molecule showed predominant excimer fluorescence while the presence of a proper bulky *N*-methyl ammonium guest can perturb the excimer formation causing the monomer emission (Figure 4.9).
The exploitation of the excimer-monomer dual luminescence allows to boost the selectivity of the chemosensor towards a specific class of molecules like ATS and cocaine guests that present a *N*-methylammonium group and a bulky part in their skeleton. By contrast the chemosensor is insensitive to interferents like sarcosine that are complexed by the cavitand but not reported by the transducer element.

4.3.2 Synthesis of the Fluorescent Tetraphosphonate Cavitands

The choice of the length of the tethers is pivotal for the selectivity of the chemosensor. With too long tethers the excimer cannot be perturbed by the guest and therefore the molecular recognition is not correctly translated into a signal. Instead too short tethers prevent the formation of the excimer.
Following molecular modeling, the first target molecule was designed with a butyl alkyl chain as tether (Figure 4.10).

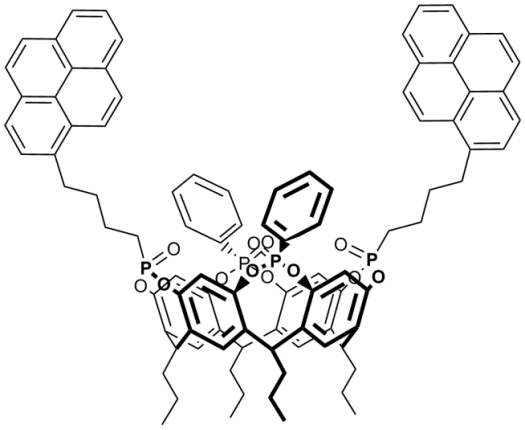

Figure 4.10 ***Tiiii [C_3H_7, H, (2 Ph, 2 butyl-pyrene)], IX.***

The preparation of the tetraphosphonate cavitand **Tiiii [C_3H_7, H, (2 Ph, 2 butyl-pyrene)]** (**IX**) required a convergent synthesis; in fact two fragments were synthesized, diphosphonate resorcinarene (**VIII**) and the phosphonic dichloride

bridging reagent (**VI**), that were joined together through a stereoselective reaction using as templating agent *N*-methyl pyrrolidine.[42]

The phosphonic dichloride (**VI**) was prepared in five steps and 85% overall yield (Scheme 4.1). The hydroxyl group of **I** was substituted with an iodine group (steps a and b), allowing an Arbuzov reaction with triethyl phosphite that led to diethyl (6-(pyren-1-yl)hexyl)phosphonate (**IV**). After hydrolysis under acidic conditions, chlorination of **V** with oxalyl chloride afforded the desired product (4-(pyren-1-yl)butyl)phosphonic dichloride **VI**. Due to its reactivity, the product was not isolated but used directly as bridging reagent with resorcinarene **VIII**.

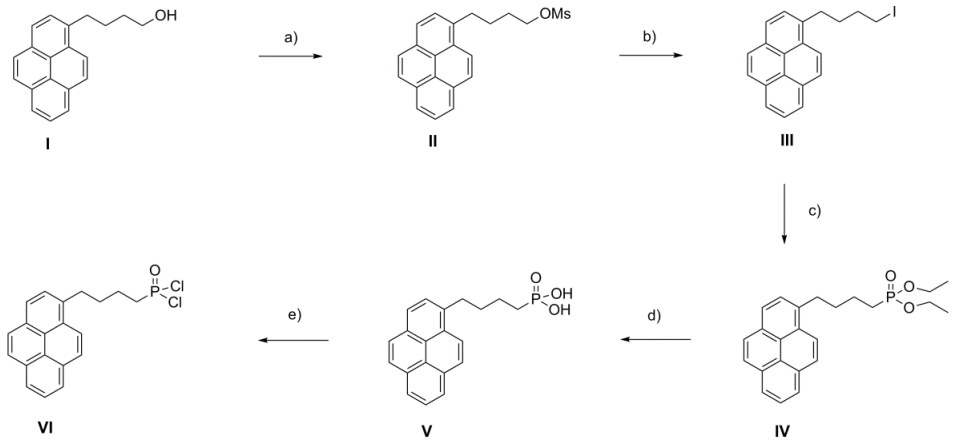

Scheme 4.1 *Synthesis of* ***(4-(pyren-1-yl)butyl)phosphonic dichloride, VI****: a) MsCl, NEt_3, DCM, r.t., 4 h; b) NaI, Acetone, reflux, 4 h, quantitative; c) $P(OEt)_3$, 2 h, microwave power 300 W, 200 °C , 90%; d) HCl 12 N, 2 h, microwave power 300 W, 95%; e) Oxalyl chloride/DMF, $CHCl_3$, 60 °C, 4 h.*

The diphosphonate resorcinarene **VIII** was synthesized from the tetraphosphonate cavitand **VII** by using an excision reaction with two equivalents of catechol and potassium carbonate in DMF (Scheme 4.2). The reaction afforded selectively the constitutional isomer with two phosphonate groups in distal position (AC isomer).[43]

The last step of the synthesis was the introduction of the phosphonate groups in the scaffold, bridging resorcinarene **VIII** with **VI** using *N*-methylpyrrolidine as both templating agent and base. The reaction gave mainly the cavitand **Tiiii [C_3H_7, H, (2 Ph, 2 butyl-pyrene)]** (**IX**) with a 10% yield. The low yield obtained is due to the limited reactivity of the phosphonic dichloride bridging reagent. Among characterization technique, ^{31}P NMR showed to be particularly

diagnostic. As expected the ^{31}P NMR spectra shows two singlet peaks at 25.1 and 10.5 ppm that confirm the presence of P=O groups linked to alkyl and phenyl groups respectively, both of them oriented inward with respect to the cavity.

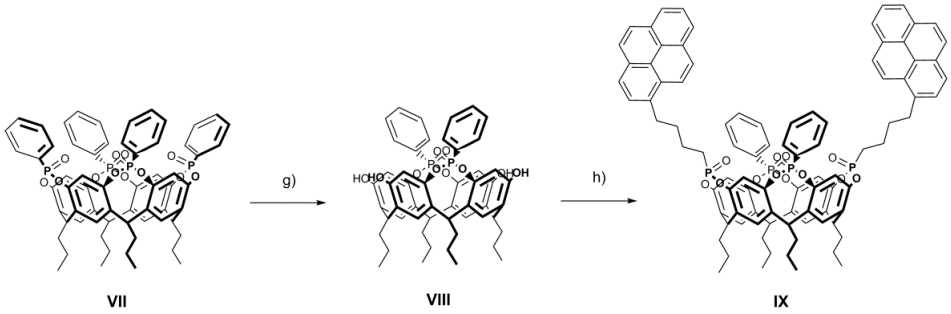

Scheme 4.2 *Synthesis of* ***Tiiii [C_3H_7, H, (2 Ph, 2 butyl-pyrene)]***, ***IX****: g) Catechol, K_2CO_3, DMF, 85 °C, 5 h,75%; h)* ***VII****, N-methylpyrrolidine, toluene/$CHCl_3$, 80 °C, 48 h, 10%.*

Cavitand **IX** was submitted to fluorescent measurements (λ_{exc} 330 nm) in various solvents to show the formation of the excimer as depicted in Figure 4.11. In all the solvents tested the fluorescent spectra show only the monomer emission band and total absence of the excimer band between 450 and 550 nm. We concluded that the tether length is not sufficient long to promote the π-stacking of the pyrene groups and the consequent formation of the excimer.

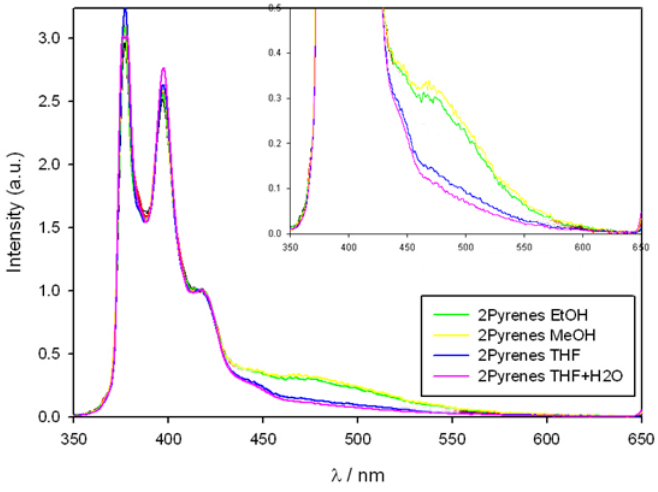

Figure 4.11 *Fluorescent spectra of* ***IX*** *($c = 2 \times 10^{-6}$ M).*

To solve the problem we decided to extent the length of the tethers to six carbon atoms (hexyl chain). Hence the new tetraphosphonate cavitand **Tiiii [C_3H_7, H, (2 Ph, 2 hexyl-pyrene)]** (**XVII**) target was synthesized (Figure 4.12).

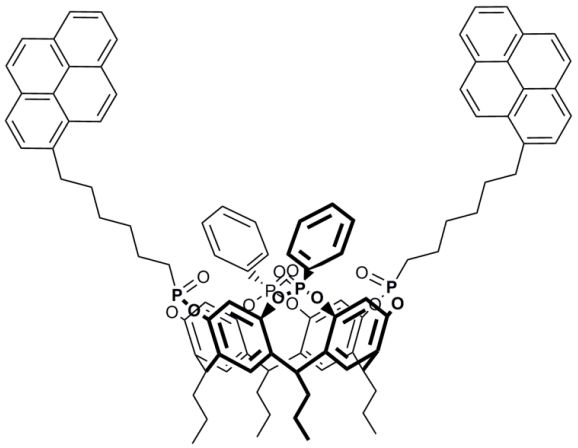

Figure 4.12 *Tiiii [C_3H_7, H, (2 Ph, 2 hexyl-pyrene)], XVII.*

The bridging reagent **XVI** was prepared in seven steps and 50% overall yield (Scheme 4.3). The multistep synthesis started from a Sonogashira cross-coupling reaction between the bromo-pyrene and 5-hexyn-1-ol. Then the alkyne group was reduced and the hydroxyl group was replaced with the phosphonate group as reported previously. The chlorination of the phosphonic acid **XV** was carried out with oxalyl chloride and the product (6-(pyren-1-yl)hexyl)phosphonic dichloride (**XVI**) was used directly without further purification.

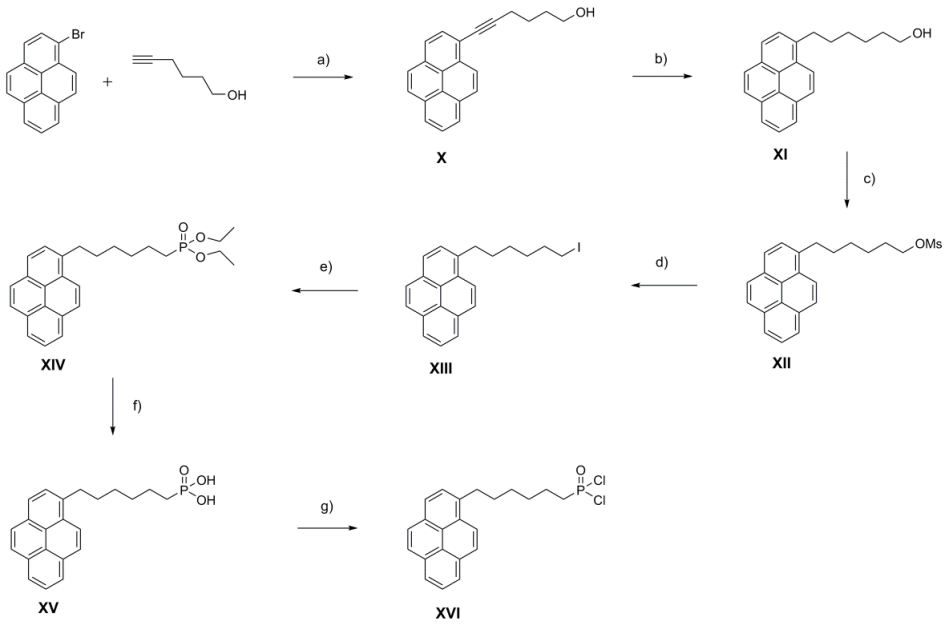

Scheme 4.3 *Synthesis of* ***(6-(pyren-1-yl)hexyl)phosphonic dichloride, XVI****: a) $Pd(PPh)_4$, CuI, THF/DIPEA, 50 °C, 12 h, 68%; b) H_2 (2 atm), Pd/C, AcOEt, r.t., 12 h, 94%; c) MsCl, NEt_3, DCM, r.t., 3 h; d) NaI, acetone, reflux, 4 h, quantitative; e) $P(OEt)_3$, 2 h, microwave power 300 W, 200 °C , 85%; f) HCl 12 N, 2 h, microwave power 300 W, 96%; g) Oxalyl chloride/DMF, $CHCl_3$, 60 °C, 4 h.*

The target product **XVII** was synthesized reacting the phosphonic dichloride **XVI** and the resorcinarene **VIII** under the same conditions described before in 4.5% overall yield (Scheme 4.4). Also in this case the ^{31}P NMR spectrum shows two diagnostic singlet resonances at 24.4 and 9.3 ppm, attributed to the phosphonate moieties linked to the alkyl and phenyl groups respectively. MALDI mass spectrometry confirms the presence of the molecular ion of the product **XVII** (calculated for: $C_{96}H_{92}O_{12}P_4$ 1560.5539 Da, found: 1560.5441 Da).

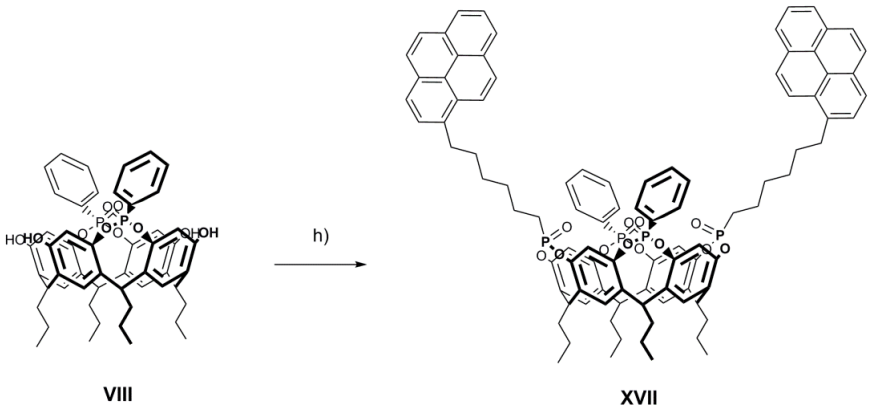

Scheme 4.4 *Synthesis of* ***Tiiii [C_3H_7, H, (2 Ph, 2 hexyl-pyrene)]***, ***XVII****: h)* ***VIII****, N-methylpyrrolidine, toluene/$CHCl_3$, 80 °C, 48 h, 12%.*

4.3.3 Fluorescence Spectroscopy Experiments

The fluorescence spectra in dichloromethane (λ_{exc} 330 nm, Figure 4.13) of compound **XVII** validated our new design, in fact an excimer emission band can be observed centered at about 480 nm.

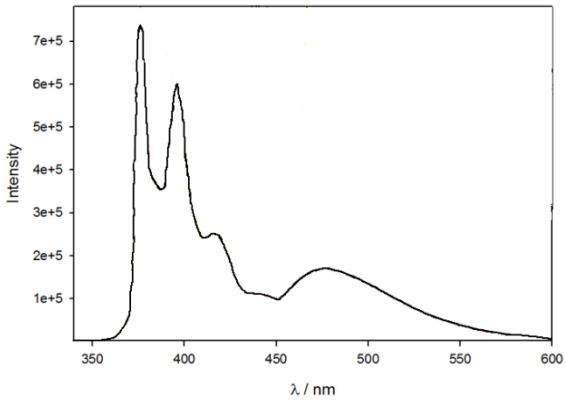

Figure 4.13 *Fluorescence spectrum of* ***XVII*** *in dichloromethane (c = 2 x 10^{-6} M).*

The sensor for illicit drugs sensing detection must operate at the solid-water interface. The multi-aromatic cavity of the tetraphosphonate receptor and the two pyrene moieties attached at the top of the molecule make our receptor extremely hydrophobic. In water **XVII** is thus not soluble, forming a dispersion of aggregates with a diameter of ca. 100 nm. To overcome this issue, we used

the strategy to load the cavitand molecules in silica nanoparticles having an outer PEG shell (Pluronic-Silica NanoParticles -PluS NPs), a strategy that was conveniently used with other chemical sensors.[44] In this case, we modified the synthesis of the NPs using a modified silica precursor (1,2-bis(triethoxysilyl)ethane, Figure 4.14b) in place of the commonly used tetraethoxysilane (TEOS, Figure 4.14a), in order to increase the loading ability of the NPs structure (L. Petrizza, unpublished results).

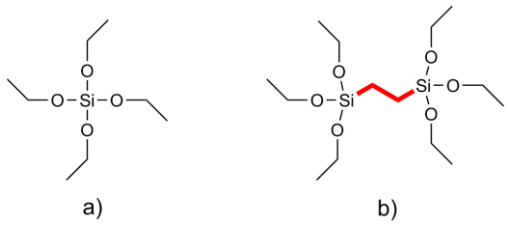

Figure 4.14 *a) TEOS; b) 1,2-Bis(triethoxysilyl)ethane.*

In addition, the use of a confined environment was conceived also to increase the formation of an intramolecular excimer as observed in other system like micelles,[45] bilayers,[46] zeolites,[47] sol-gel materials and glasses.[48]

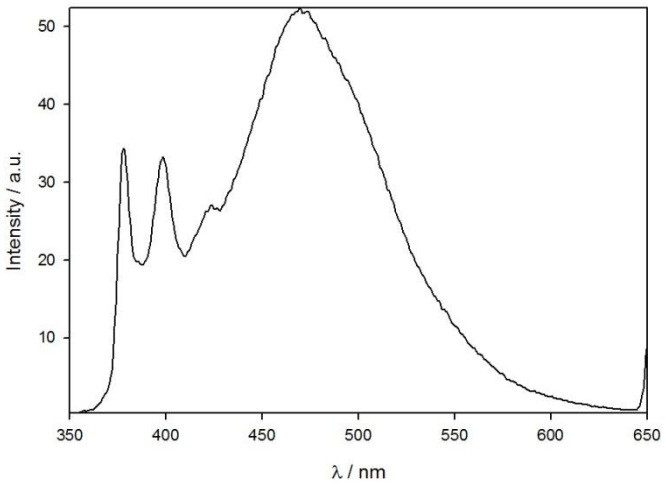

Figure 4.15 *Fluorescence spectrum (λ_{exc} 330 nm) of* ***XVII*** *+ nanoparticles in H_2O (c= 2 x 10^{-6} M).*

Interestingly, dynamic light scattering measurements of equimolar solutions of **XVII** and PluS NPs show only the typical, very narrow peak of the

nanoparticles, indicating the absence in these conditions of self-aggregation of **XVII** due to their loading into the structure of the nanoparticles. The fluorescence spectrum of the cavitand loaded nanoparticles in water (Figure 4.15) clearly shows, as expected, a large contribution from the excimeric emission, indicating that, by large, the major part of the excited states of pyrene decay to their ground state through the formation of excimers. NPs thus play here a major role in providing the best starting condition for fluorescence sensing: aggregation of the chemosensor is satisfactorily avoided, and we obtain stable and intense excimer emission.

We chose four different guests to test our chemosensor in aqueous solution: amphetamine, MDMA, cocaine and 3-fluoro-methamphetamine (FMA, a designer drug) all of them hydrochloride salts. Such guests were selected as representatives of the ATS and natural illicit drugs classes. FMA, in particular, is a representative of a so called "designer drugs". We then selected several control compounds in order to rule out possible interferences in the sensing procedures: glucose since it is commonly used as the excipient in street samples, glycine as an amine which is not hosted by the cavitand, and, sarcosine as control because, although it presents affinity towards the receptor, it does not have a bulky unit such as the illicit drugs, therefore it should not trigger any response.

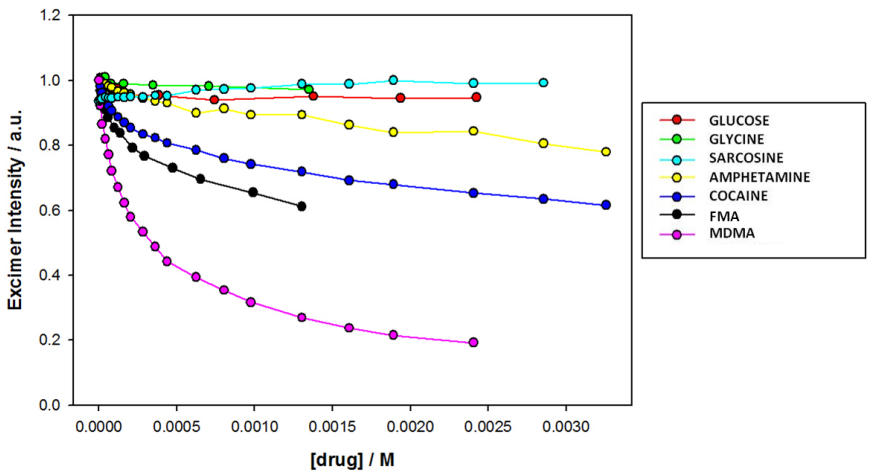

Figure 4.16 *Fluorescence intensity in the excimer band (λ_{exc} = 330 nm; λ_{em} = 475 nm) of* ***XVII*** *+ nanoparticles in H_2O (c = 2 x 10^{-6} M) upon addition of increasing amounts of guests.*

Interestingly, we observed large spectral changes upon addition of MDMA, amphetamine, cocaine, and FMA hydrochloride salts while control compounds sarcosine, glucose and glycine did not substantially affect the emission signal of the pyrene moieties, and in particular of the excimer (Figure 4.16).
The excimer emission of **XVII** loaded in NPs was indeed strongly depleted by the addition of MDMA, cocaine and FMA. This can be attributed to the sterical hindrance of these drugs which, hosted in the cavity, prevent the formation of excimers or, at least, significantly decrease the probability of their formation, as envisaged in designing this chemosensor.
Noteworthy, MDMA has a much stronger effect than any other guest in depleting the excimer emission (Figure 4.17).

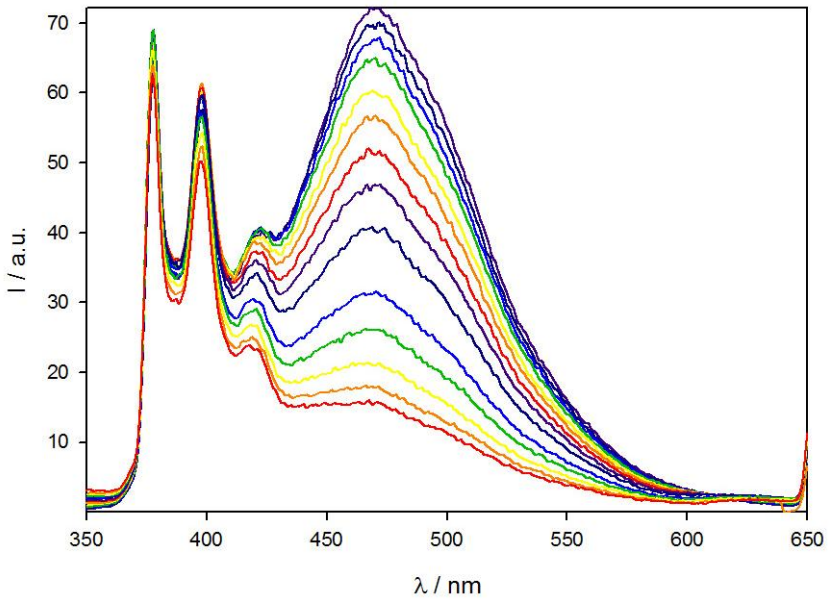

Figure 4.17 *Fluorescence spectrum (λ_{exc} = 330 nm) of **XVII** + nanoparticles in H_2O (c = 2 x 10^{-6} M) upon addition of increasing amounts of MDMA (0 – 0,0025 M).*

Furthermore, a dramatic decrease of the luminescence lifetime is observed both on the excimer and on the monomer emissions. Such observations prove the occurrence of an additional decay pathway that increases the rates of relaxation of both the excimer and monomer excited states. Such pathway can be attributed, since the energy transfer process from pyrene to MDMA is thermodynamically forbidden, to an efficient electron-transfer process involving the aromatic unit present in the MDMA molecule.

As far as the monomeric-type emission is concerned, we observed in all cases, as expected, an increase of the intensity of the monomeric emission, with a lower enhancement in case of sarcosine, and a subsequent decrease, after the initial steep increase, in case of MDMA (due to the onset of the electron-transfer quenching).
It is worth noticing that the presence of two different signals increase the possible information content that can be obtained from the analysis of fluorescence spectra, since the monomer-type emission responds to the presence in the analytic sample of this class of guests, while the decrease of the emission of the excimer-type emission can allow to discriminate the presence of MDMA among the other possible interferences.
Interestingly, the association constants that can be evaluated among the cavitand in the NPs (that can have, as previously described, a profound effect on the affinity for the analyte of a chemosensor) and the different species presents the following trend: MDMA > FMA > cocaine > amphetamine (Figure 4.18, sarcosine could not be evaluated due to the low signal variation). This trend is in agreement with the molecular recognition ability of the tetraphosphonate cavitand as demonstrated in a recent paper by isothermal titration calorimetry (ITC).[39] Most important, cavitand **XVII** does not respond to sarcosine, which is strongly bonded by tetraphosphonate cavitands.[40] These results strongly supports the proposed mechanism of detection, depicted in Figure 4.9.

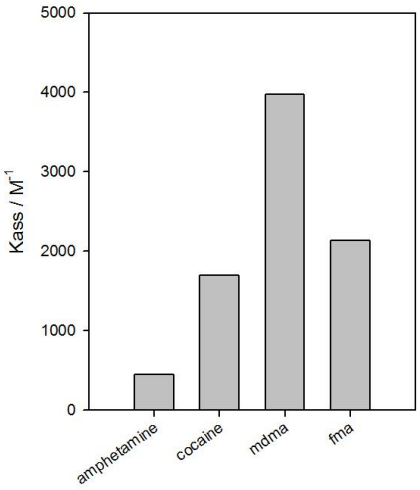

Figure 4.18 *Association constants in water solutions for the different analytes of* ***XVII****@NPs estimated from the titration curves reported in Figure 4.16.*

All the results presented so far indicate that **XVII** can be an efficient chemosensor for this family of analytes in aqueous solution. In particular, the presence of MDMA can be clearly identified by looking at the intensity of the excimeric emission and, as additional signal, by the analyses of the excited state lifetime. In all other cases the presence of the drug can be identified looking at the increase of the intensity of the monomeric band, with possibility to use the excimer band, through a ratiometric approach, to avoid any calibration needs.

4.3.4 Towards a Fluorescent Sensor Surface

In the last paragraphs we reported the molecular recognition properties of the fluorescent chemosensor towards a series of *N*-methylated illicit drug molecules. Furthermore we demonstrated that the transduction mode based on the monomer-excimer dual luminescence of pyrene is highly reliable in chemical sensing. In order to take full advantage of its particular features, the fluorescent receptor **XVII** should be grafted onto a surface, moving the binding properties from the solution to the surface.

Silicon is an attractive inorganic platform to deposited organic monolayers as it is possible to make robust and durable devices by forming stable Si-C covalent bonds. Recently, our research group has reported a protocol for the covalent assembly of cavitand molecules on silicon surface.[49] The process is the photochemical hydrosilylation[50] and it requires an hydrogenated silicon surface and at least one terminal alkene in the organic molecules to be attached. The extension of this procedure to the grafting of phosphonate cavitands on silicon has been reported, using **Tiiii** cavitands equipped with ω-decene feet (**Tiiii**[$C_{10}H_{19}$, H, Ph]).[51]

The next step in the illicit drug sensing will be the functionalization of a silicon surface with the fluorescent chemosensor previously tested. The fluorescent receptor (**XVII**) was derivatized with four terminal alkene at the lower rim in particular four decene feet. The target molecule **Tiiii [$C_{10}H_{19}$, H, (2 Ph, 2 hexyl-pyrene)]**, (**XX**) is illustrated in Figure 4.19.

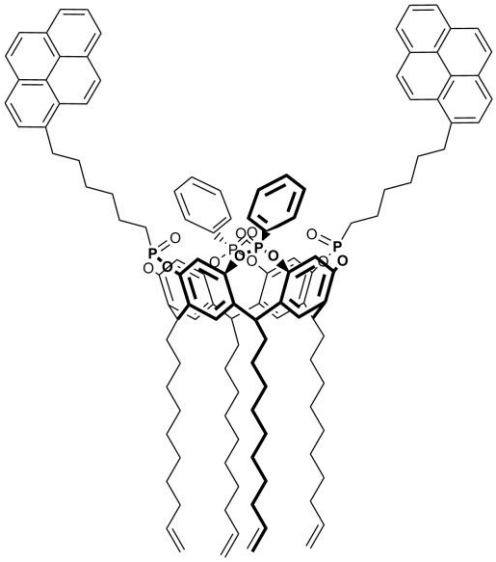

Figure 4.19 ***Tiiii [$C_{10}H_{19}$, H, (2 Ph, 2 hexyl-pyrene)], XX.***

The target cavitand **XX** was prepared using the same procedure previously explained for the cavitand **XVII**. The diphosphonate resorcinarene decene feet **XIX** was synthesized from tetraphosphonate cavitand **Tiiii [$C_{10}H_{19}$, H, Ph]** by an excision reaction with catechol and potassium carbonate in DMF (Scheme 4.5). Then the resorcinarene **XIX** was bridged with phosphonic dichloride **XVI** using *N*-methyl pyrrolidine as templating agent. The crude was purified by silica gel chromatography giving the cavitand **Tiiii [$C_{10}H_{19}$, H, (2 Ph, 2 hexyl-pyrene)]**, (**XX**) with a 3.5% overall yield. As expected the ^{31}P NMR spectrum shows two singlet resonances at 24.8 and 9.8 ppm that confirms the presence of phosphonate groups linked to alkyl and phenyl groups respectively, both of them oriented inward with respect to the cavity. The photochemical grafting of this cavitand on silicon is ongoing

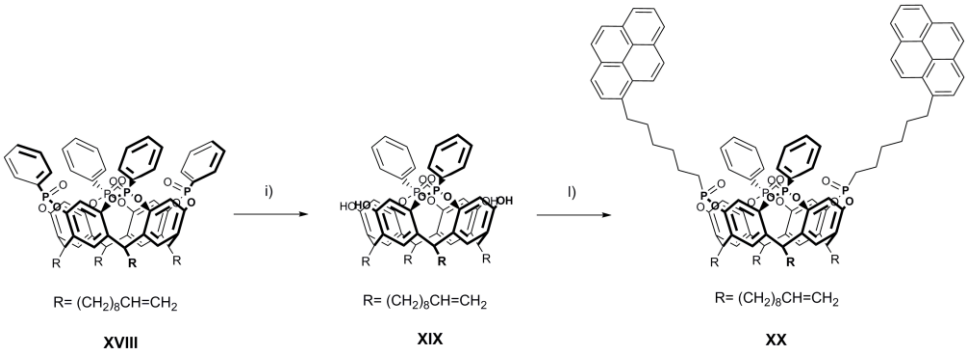

Scheme 4.5 *Synthesis of* ***Tiiii [$C_{10}H_{19}$, H, (2 Ph, 2 hexyl-pyrene)]***, ***XX****: i) Catechol, K_2CO_3, DMF, 85 °C, 5 h, 78%; l)* ***XVI****, N-methylpyrrolidine, toluene/$CHCl_3$, 80 °C, 48 h, 9%.*

4.4 Conclusions

In summary, a new pyrene-functionalized cavitand has been synthesized to detect illicit drugs. This chemosensor merges the complexation properties of the **Tiiii** cavitand with the unique luminescent properties of the pyrene excimer that acts as transducer element. As a consequence we boosted the selectivity of the cavitand introducing steric hindrance as an additional discrimination point. The sensor has been tested with four different illicit drugs containing *N*-methylated groups and three interferent molecules. The fluorescence experiments demonstrated that the drugs depleted the excimer emission due to their steric hindrance. Particularly appealing is the response towards MDMA. This molecule showed the stronger effect due to the combination of its steric hindrance and an efficient electron-transfer process involving the aromatic units of the pyrene groups and the MDMA molecule. By contrast the interferents like glycine, glucose and sarcosine did not change the emission of the excimer. Although sarcosine is complexed by the cavitand, it does not bring apart the pyrene groups since it does not possess a bulky group in its skeleton.

4.5 Acknowledgments

Special thanks to Dr. Damiano Genovese, Dr. Luca Petrizza, Dr. Enrico Rampazzo and Prof. Luca Prodi from Department of Chemistry "G. Ciamician", University of Bologna and Dr. Elisa Biavardi from Department of Chemistry, University of Parma for fluorescent measurements.

4.6 Experimental Section

Tiiii [$C_{10}H_{19}$, H, Ph] was synthesized according to a published procedure.[52]

4-(pyren-1-yl)butyl methanesulfonate (II)
A mixture of **I** (1 g, 3.64 mmol), triethylamine (10.1 mL, 72.8 mmol), mesyl chloride (2.81 m, 36.4 mmol) in dichloromethane was stirred at room temperature for 4 hours. The reaction mixture was quenched with saturated NH_4Cl solution and diluted with ethyl acetate. The organic layer was extracted twice with water, brine and dried over $MgSO_4$. The yellow solid was used without characterizations and further purification in the next step.

1-(6-iodobutyl)pyrene (III)
To a solution of **II** in acetone, NaI (5.4 g, 36.4 mmol) was added. After 4 hours of stirring at reflux the solution was allowed to cool at room temperature and the white solid was filtered off. The resulting solution was dried under reduced pressure and the crude was purified by silica gel column chromatography (hexane:ethyl acetate 95:5) to give pure **III** as white solid (1.38 g, 3.64 mmol, quantitative yield).
^{1}H NMR ($CDCl_3$, 400 MHz): δ (ppm) = 8.27 (d, J= 8 Hz, 1H, Ar**H**), 8.20-8.08 (m, 4H, Py**H**), 8.06-7.96 (m, 3H, Py**H**), 7.86 (d, J= 8 Hz, 1H, Py**H**) 3.40-3.34 (m, 2H, PyC**H$_2$**), 3.29-3.22 (m, 2H, C**H$_2$**I), 2.05-1.93 (m, 4H, $PyCH_2C\mathbf{H_2}C\mathbf{H_2}CH_2I$); **ESI-MS**: mass peak was not found.

Diethyl (6-(pyren-1-yl)butyl)phosphonate (IV)
III (1.38 g, 3.64 mmol) was suspended in triethyl phosphite (6.2 mL, 36.4 mmol). The reaction was conducted at the microwave reactor using the follow parameters: microwave power 300 W, 200 °C, stirring high, reaction time 2 h. The solution was allowed to cool at room temperature and dried under reduced pressure. The crude was purified by silica gel column chromatography (ethyl acetate:dichloromethane 1:9) to afford pure **IV** as white solid (1.29 g, 3.27 mmol, 90%).
^{1}H NMR ($CDCl_3$, 300 MHz): δ (ppm) = 8.15 (d, J=9 Hz 1H, Py**H**), 8.11-7.97 (m, 4H, Py**H**), 7.97-7.88 (m, 4H, Py**H**), 7.75 (d, J=3 Hz 1H, Py**H**), 4.17-3.97 (m, 4H, P(O)OC**H$_2$**CH3), 3.26 (t, 2H, J=6 Hz, PyC**H$_2$**CH_2), 1.95-1.68 (m, 6H, $PyCH_2C\mathbf{H_2}C\mathbf{H_2}C\mathbf{H_2}P(O)$), 1.29 (t, J=6 Hz, 6H, $P(O)OCH_2C\mathbf{H_3}$); **^{31}P{^{1}H}NMR** ($CDCl_3$, 161.9 MHz): δ (ppm) = 28.8 (s, P=O); **ESI-MS**: mass peak was not found.

(6-(pyren-1-yl)butyl)phosphonic acid (V)

IV (1.29 g, 3.27 mmol) was suspended in HCl 37% (5 mL). The reaction was conducted at the microwave reactor using the follow parameters: microwave power 300 W, 95 °C, stirring high, reaction time 2 h. The solution was allowed to cool at room temperature and the gray solid was recovered by suction filtration to give pure **V** (1.04 g, 3.1 mmol, 95%).

^{1}H NMR (DMSO-d_6, 400 MHz): δ (ppm) = 8.35 (d, J= 8 Hz, 1H, Py**H**), 8.30-7.99 (m, 7H, Py**H**), 7.93 (d, J= 8 Hz, 1H, Py**H**), 3.32 (t, 2H, J=8 Hz, PyC**H$_2$**CH$_2$), 1.90-1.77 (m, 2H, CH$_2$C**H$_2$**P(O)), 1.70-1.46 (m, 4H, PyCH$_2$C**H$_2$**C**H$_2$**CH$_2$P(O)); **^{31}P{^{1}H}NMR** (DMSO-d_6, 161.9 MHz): δ (ppm) = 26.3 (s, P=O); **ESI-MS**: m/z 361 $[M+Na]^+$.

(6-(pyren-1-yl)butyl)phosphonic dichloride (VI)

To a solution of **V** (0.281 g, 0.83 mmol) in dry DCM, oxalyl chloride (0.25 mL, 3 mmol) and two drops of dry DMF were added under nitrogen atmosphere. The green solution was stirred for 4 hours at room temperature then the solvent was removed under *vacuo* and the green solid was used without further purification in the next step.

^{1}H NMR ($CDCl_3$, 400 MHz): δ (ppm) = 8.27-7.78 (m, 9H, Py**H**), 3.40 (t, 2H, J=8 Hz, PyC**H$_2$**CH$_2$), 2.72-2.57 (m, 2H, CH$_2$C**H$_2$**P(O)), 2.11-1.91 (m, 4H, PyCH$_2$C**H$_2$**C**H$_2$**CH$_2$P(O)); **^{31}P{^{1}H}NMR** ($CDCl_3$, 161.9 MHz): δ (ppm) = 50.4 (s, P=O); **ESI-MS**: mass peak was not found.

Diphosphonate resorcinarene (VIII)

Tetraphosphonate cavitand **VII** (0.86 g, 0.75 mmol) was dissolved in dry DMF then cathecol (0.165 g, 1.5 mmol) and K_2CO_3 (1.03 g, 7.5 mmol) were added. The mixture was stirred at 80 °C for 5 hours and quenched by addition of an acidic solution (HCl 10%). The resulting solid was recovered by suction filtration. Purification by silica gel column chromatography (dichloromethane:ethanol 95:5) afforded the pure product **VIII** as white solid (0.5 g, 0.56 mmol, 75%).

^{1}H NMR ($CDCl_3$, 400 MHz): δ (ppm) = 9.55 (s, 4H, ArO**H**), 8.14-8.08 (m, 4H, Ar**H$_o$**), 7.70-7.68 (m, 2H, Ar**H$_p$**), 7.62-7.57 (m, 4H, Ar**H$_m$**), 7.11 (s, 4H, Ar**H**), 6.69 (s, 4H, Ar**H**), 4.80 (t, J=8 Hz 2H, ArC**H**), 4.28 (t, J=8 Hz, 2H, ArC**H**), 2.38-2.36 (m, 4H, C**H$_2$**CH$_2$CH$_3$), 2.05-2.03 (m, 4H, C**H$_2$**CH$_2$CH$_3$), 1.61-1.55 (m, 4H, CH$_2$C**H$_2$**CH$_3$), 1.24-1.13 (m, 10H, CH$_2$C**H$_2$**C**H$_3$**), 0.93-0.85 (m, 6H, CH$_2$CH$_2$C**H$_3$**); **^{31}P{^{1}H}NMR** ($CDCl_3$, 161.9 MHz): δ (ppm) = 6.28 (s, P=O); **ESI-MS**: m/z 902 $[M+H]^+$, 924 $[M+Na]^+$.

Tiiii [C_3H_7, H, (2 Ph, 2 butyl-pyrene)] (IX)

VIII (0.25 g, 0.27 mmol) was dissolved in dry toluene and *N*-methylpirrolidine (0.28 mL, 2.7 mmol). Then **VI** (0.311 g, 0.83 mmol) was dissolved in a mixture 1:1 of anhydrous toluene/chloroform and added dropwise to the resorcinarene solution. The dark green mixture was stirred at 80 °C for 48 hours. The reaction was allowed to cool at room temperature, the residual dark solid was filtered off and the solvent was removed under *vacuo*. The crude was purified by silica gel column chromatography (dichloromethane:ethanol 95:5) to give the pure product **IX** as yellowish solid (0.04 g, 0.027 mmol, 10%).

^{1}H NMR ($CDCl_3$, 400 MHz): δ (ppm) = 8.28 (d, J=12 Hz, 2H, Py**H**), 8.17-7.94 (m, 18H, Py**H,** P(O)Ar**H$_o$**), 7.89 (d, J=8 Hz, 2H, Py**H**), 7.72-7.64 (m, 2H, P(O)Ar**H$_p$**), 7.62-7.53 (m, 4H, P(O)Ar**H$_m$**), 7.42 (s, 4H, Ar**H**), 6.88 (s, 4H, Ar**H**), 4.80 (t, J=8 Hz, 2H, ArC**H**), 4.59 (t, J=8 Hz, 2H, ArC**H**), 3.49-3.35 (m, 4H, C**H$_2$**Py), 2.29-1.96 (m, 20H, PyCH$_2$C**H$_2$**C**H$_2$**C**H$_2$**P(O), ArCHC**H$_2$**CH$_2$CH$_3$), 1.53-1.31 (m, 8H, ArCHCH$_2$C**H$_2$**CH$_3$), 1.10 (t, J=8 Hz, ArCHCH$_2$CH$_2$C**H$_3$**), 1.03 (t, J=8 Hz, ArCHCH$_2$CH$_2$C**H$_3$**); **^{31}P{^{1}H}NMR** ($CDCl_3$, 161.9 MHz): δ (ppm) = 25.1 (s, P=O (buthyl-Py)), 10.5 (s, P=O(Ph)); **ESI-MS**: m/z 1528 $[M+Na]^+$; **MALDI TOF-TOF**: calcd. for $C_{92}H_{84}O_{12}P_4$ 1504.4913 Da, found: 1504.3596 Da.

6-(pyren-1-yl)hex-5-yn-1-ol (X)

A mixture of THF/DIPA (1/1) was degassed 3 times with freeze pump thaw technique followed by addition of bromo-pyrene (1 g, 3.55 mmol), 5-hexyn-1-ol (0.47 mL, 4.26 mmol), Pd tetrakis(triphenylphosphine) (0.205 g, 0.17 mmol) and CuI (0.067 g, 0.355 mmol). The reaction mixture was stirred for 12 hours at 50 °C and then filtered. Ethyl acetate was added into the solution and extracted twice with saturated NH_4Cl solution and brine, dried with anhydrous $MgSO_4$ and evaporated under reduced pressure to yield a brown oil. The crude was purified by silica gel column chromatography (hexane:ethyl acetate 6:4) to afford the desired product **X** as yellow oil (0.72 g, 2.41 mmol, 68%).

^{1}H NMR ($CDCl_3$, 300 MHz): δ (ppm) = 8.56 (d, J=8 Hz, 1H, Py**H**), 8.23-8.00 (m, 8H, Py**H**), 3.81 (t, J=6 Hz, 2H, C**H$_2$**OH), 2.73 (t, J=6 Hz, 2H, C**H$_2$**C≡C), 1.92-1.89 (m, 4H, C**H$_2$**C**H$_2$**OH); **^{13}C NMR** ($CDCl_3$, 100 MHz): δ (ppm) = 135.2, 131.8, 131.2, 131, 130.6, 129.6, 128, 127.7, 127.2, 126.1, 125.5, 125.34, 125.33, 124.4, 124.3, 118.6, 95.9, 80.1, 61.9, 31.7 16.5; **ESI-MS**: m/z 299.4 $[M+H]^+$, 321.4 $[M+Na]^+$, 337.4 $[M+K]^+$.

6-(pyren-1-yl)hexan-1-ol (XI)

X (0.72 g, 2.41 mmol) was dissolved in THF and Pd/C (catalytic amount) was added. The mixture was sealed in a Parr reaction bottle and mounted in a shaker hydrogenation apparatus. The air inside the bottle was removed by flushing with hydrogen and a 4 bar of hydrogen pressure was applied. The bottle was shaken for 12 hours at room temperature. The Pd/C was filtered off and the solvent removed in *vacuo* yielded the desired product **XI** as white solid (0.68 g, 2.27 mmol, 94%).

^{1}H NMR ($CDCl_3$, 400 MHz): δ (ppm) = 8.30 (d, J=8 Hz, 1H, Ar**H**), 8.15-7.99 (m, 7H, Py**H**), 7.88 (d, J=8 Hz, 1H, Py**H**), 3.66 (t, J=6 Hz, 2H, C**H$_2$**OH), 3.36 (t, J=6 Hz, 2H, C**H$_2$**Py), 1.90 (m, 4H, C**H$_2$**C**H$_2$**OH); **^{13}C NMR** ($CDCl_3$, 100 MHz): δ (ppm) = 137.1, 131.4, 130.9, 129.7, 128.6, 127.5, 127.2, 127.1, 126.5, 125.7, 125, 124.8, 124.7, 124.6, 123.4, 62.9, 33.5, 32.7, 31.8, 29.5, 25.7; **ESI-MS**: m/z 303.5 $[M+H]^+$, 325.2 $[M+Na]^+$, 341.2 $[M+K]^+$.

6-(pyren-1-yl)hexyl 4-methylbenzenesulfonate (XII)

The synthesis was carried out as compound **II** and used in the next step without characterization and further purification.

1-(6-iodohexyl)pyrene (XIII)

The synthesis and purification were carried out as compound **III** (0.93 g, 2.25 mmol, quantitative).

^{1}H NMR ($CDCl_3$, 400 MHz): δ (ppm) = 8.30 (d, J=12 Hz, 1H, Py**H**), 8.21-8.19 (m, 4H, Py**H**), 8.06-7.97 (m, 3H, Py**H**), 7.89 (d, J=8 Hz, 1H, Py**H**), 3.67 (t, J=8 Hz, 2H, C**H$_2$**Py), 3.37 (t, J=8 Hz, 2H, C**H$_2$**I), 1.96-1.84 (m, 2H, C**H$_2$**CH_2I), 1.67-1.39 (m, 6H, PyCH_2C**H$_2$**C**H$_2$**C**H$_2$**CH_2CH_2I); **ESI-MS**: mass peak was not found.

Diethyl (6-(pyren-1-yl)hexyl)phosphonate (XIV)

The synthesis and purification were carried out as compound **IV** (0.8 g, 1.91 mmol, 85%).

^{1}H NMR ($CDCl_3$, 400 MHz): δ (ppm) = 8.26 (d, J=8 Hz, 1H, Py**H**), 8.18-7.93 (m, 7H, Py**H**), 7.85 (d, J=8 Hz, 1H, Py**H**), 4.15-3.99 (m, 4H, C**H$_2$**O), 3.33 (t, J=6 Hz, 2H, CH_2C**H$_2$**Py), 1.92-1.79 (m, 2H, CH_2C**H$_2$**P(O)), 1.79-1.53 (m, 4H, PyCH_2C**H$_2$**CH_2CH_2C**H$_2$**CH_2P(O)), 1.53-1.42 (m, 4H, PyCH_2CH_2C**H$_2$**C**H$_2$**CH_2CH_2P(O)), 1.36-1.24 (m, 6H, C**H$_3$**CH_2O); **^{31}P{^{1}H}NMR** ($CDCl_3$, 161.9 MHz): δ (ppm) = 27.9 (s, P=O); **ESI-MS**: m/z 423.3 $[M+H]^+$, 445.3 $[M+Na]^+$, 461.2 $[M+K]^+$.

(6-(pyren-1-yl)hexyl)phosphonic acid (XV)

The synthesis and purification were carried out as compound **V** (0.67 g, 1.83 mmol, 96%).

^{1}H NMR ($CDCl_3$, 400 MHz): δ (ppm) = 8.35 (d, J=8 Hz 1H, Py**H**), 8.30-8.00 (m, 7H, Py**H**), 7.95 (d, J=8 Hz, 1H, Py**H**), 3.33 (t, J=6 Hz, 2H, $CH_2C\mathbf{H_2}Py$), 1.83-1.69 (m, 2H, $CH_2C\mathbf{H_2}P(O)$), 1.60-1.33 (m, 8H, $PyCH_2C\mathbf{H_2}C\mathbf{H_2}C\mathbf{H_2}C\mathbf{H_2}CH_2P(O)$); **^{31}P{^{1}H}NMR** ($CDCl_3$, 161.9 MHz): δ (ppm) = 26.9 (s, P=O); **ESI-MS**: m/z 389.4 $[M+Na]^+$, 405.2 $[M+K]^+$.

(6-(pyren-1-yl)hexyl)phosphonic dichloride (XVI)

The synthesis and purification were carried out as compound **VI** and used without further purification.

^{31}P{^{1}H}NMR ($CDCl_3$, 161.9 MHz): δ (ppm) = 51 (s, P=O).

Tiiii [C_3H_7, H, (2 Ph, 2 hexyl-pyrene)] (XVII)

The synthesis and purification were carried out as compound **VII** (0.045 g, 0.028 mmol, 12%).

^{1}H NMR ($CDCl_3$, 400 MHz): δ (ppm) = 8.17 (d, J=12 Hz, 2H, Py**H**), 8.08-7.81 (m, 18H, Py**H,** P(O)Ar$\mathbf{H_o}$), 7.76 (d, J=8 Hz, 2H, Py**H**), 7.59-7.51 (m, 2H, P(O)Ar$\mathbf{H_p}$), 7.49-7.37 (m, 4H, P(O)Ar$\mathbf{H_m}$), 7.18 (s, 4H, Ar**H**), 6.74 (s, 4H, Ar**H**), 4.67 (m, 2H, Ar**CH**), 4.50 (t, J=8 Hz, 2H, Ar**CH**), 3.30-3.18 (m, 4H, $C\mathbf{H_2}Py$), 2.11-1.95 (m, 4H, $C\mathbf{H_2}P(O)$), 2.53-2.18 (m, 8H, $ArCHC\mathbf{H_2}CH_2CH_3$), 1.86-1.69 (m, 8H, $PyCH_2C\mathbf{H_2}CH_2CH_2C\mathbf{H_2}CH_2P(O)$), 1.51-1.40 (m, 8H, $PyCH_2CH_2C\mathbf{H_2}C\mathbf{H_2}CH_2CH_2P(O)$), 1.40-1.22 (m, 8H, $ArCHCH_2C\mathbf{H_2}CH_3$), 1.06-0.86 (m, $ArCHCH_2CH_2C\mathbf{H_3}$); **^{31}P{^{1}H}NMR** ($CDCl_3$, 161.9 MHz): δ (ppm) = 24.4 (s, P=O(hexyl-Py)), 9.3 (s, P=O(Ph)); **ESI-MS**: m/z 803.5 $[M+Na]^{2+}$, 1584 $[M+Na]^+$, 1600 $[M+K]^+$; **MALDI TOF-TOF**: calcd. for $C_{96}H_{92}O_{12}P_4$ 1560.5539 Da, found: 1560.5441 Da.

Diphosphonate resorcinarene decene feet (XIX)

Tetraphosphonate cavitand **XVIII** (0.7 g, 0.44 mmol) was dissolved in dry DMF then cathecol (0.1 g, 0.88 mmol) and K_2CO_3 (0.3 g, 2.21 mmol) were added. The mixture was stirred at 80 °C for 5 hours and quenched by addition of an acidic solution (HCl 10%). The resulting solid was recovered by suction filtration. Purification by silica gel column chromatography (dichloromethane:ethanol 95:5) afforded the pure product **XIX** as white solid (0.44 g, 0.34 mmol, 78%).

^{1}H NMR ($CDCl_3$, 300 MHz): δ (ppm) = 9.49 (s, 4H, ArO**H**), 8.15-7.99 (dd, 4H, Ar$\mathbf{H_o}$), 7.71-7.62 (m, 2H, Ar$\mathbf{H_p}$), 7.61-7.50 (m, 4H, Ar$\mathbf{H_m}$), 7.05 (s, 4H, Ar**H**), 6.64

(s, 4H, Ar**H**), 5.90-5.69 (m, 4H, C**H**=CH_2), 5.04-4.85 (m, 8H, CH=C**H_2**), 4.72 (t, J=8 Hz, 2H, ArC**H**), 4.28 (t, J=8 Hz, 2H, ArC**H**), 2.40-2.23 (m, 4H, C**H_2**$(CH_2)_7CH=CH_2$), 2.09-1.92 (m, 12H, C**H_2**$(CH_2)_7CH=CH_2$, C**H_2**$CH=CH_2$), 1.65-1.05 (m, 56H, CH_2(C**H_2**$)_7CH=CH_2$); **$^{31}P\{^1H\}$NMR** ($CDCl_3$, 161.9 MHz): δ (ppm) = 6.32 (s, P=O); **ESI-MS**: m/z 1286 $[M+H]^+$, 1308 $[M+Na]^+$.

Tiiii [$C_{10}H_{19}$, H, (2 Ph, 2 hexyl-pyrene)] (XX)

XIX (0.21 g, 0.16 mmol) was dissolved in dry toluene and *N*-methylpirrolidine (0.16 mL, 1.5 mmol). Then **XVI** (0.15 g, 0.41 mmol) was dissolved in a mixture 1:1 of anhydrous toluene/chloroform and added dropwise to the resorcinarene solution. The dark green mixture was stirred at 80 °C for 48 hours. The reaction was allowed to cool at room temperature, the residual dark solid was filtered off and the solvent was removed under *vacuo*. The crude was purified by silica gel column chromatography (dichloromethane:ethanol 93:7) to give the pure product **XX** as yellowish solid (0.03 g, 0.015 mmol, 9%).

^1H NMR ($CDCl_3$, 400 MHz): δ (ppm) = 8.28 (d, J=12 Hz, 2H, Py**H**), 8.21-7.93 (m, 18H, Py**H,** P(O)Ar**H_o**), 7.87 (d, J=8 Hz, 2H, Py**H**), 7.70-7.62 (m, 2H, P(O)Ar**H_p**), 7.60-7.49 (m, 4H, P(O)Ar**H_m**), 7.44 (s, 4H, Ar**H**), 6.87 (s, 4H, Ar**H**), 5.90-5.75 (m, 4H, C**H**=CH_2), 5.07-4.88 (m, 8H, CH=C**H_2**), 4.80-4.68 (m, 2H, ArC**H**), 4.64-4.50 (m, 2H, ArC**H**), 3.41-3.27 (m, 4H, C**H_2**Py), 2.51-2.27 (m, 8H, C**H_2**$(CH_2)_7CH=CH_2$), 2.22-1.94 (m, 20H, C**H_2**P(O), $PyCH_2C$**H_2**CH_2CH_2C**H_2**$CH_2P(O)$), C**H_2**$CH=CH_2$), 1.95-1.76 (m, 8H, $PyCH_2C$**H_2**CH_2CH_2C**H_2**$CH_2P(O)$, 1,64-1.09 (m, 56H, CH_2(C**H_2**$)_7CH=CH_2$); **$^{31}P\{^1H\}$NMR** ($CDCl_3$, 161.9 MHz): δ (ppm) = 24.8 (s, P=O(hexyl-Py)), 9.8 (s, P=O(Ph)); **MALDI TOF-TOF**: calcd. for $C_{124}H_{140}O_{12}P_4Na$ 1967,9193 Da, found: 1967,9193 Da.

Fluorescence measurements

1) Preparation of the suspension: 0.5 mL of a 0.03 mM acetonitrile solution of cavitand were added to 25 mL of an aqueous suspension of NPs (6×10^{-7} M) under vigorous stirring. The pH is moderately acidic (HCl 10^{-4}M) to ensure the protonated state of guest analytes. The suspension was the stirred for few minutes and sonicated, and found to be stable for at least two days under standard conditions. The signal obtained, particularly in terms of monomer to excimer ratio, was quite reproducible (~10% variations) among different preparations.

2) Photophysical measurements: absorption spectra and fluorescence spectra were taken with a Perkin Elmer Lambda 45 spectrophotometer and a Perkin Elmer Lambda 60 spectrofluorimeter respectively. Lifetimes were measured with an Edinburgh FLS920 equipped with a photomultiplier Hamamatsu R928P and connected to a PCS900 PC card used for the TCSPC. Absorption spectra allowed to quantify the number of cavitands per NP, assuming the molar extinction coefficient of pyrene does not change (ε= 54000 at λ=330 nm). This assumption is supported by the structured shape of the absorption spectrum, analogous to what is observed for diluted pyrene solutions.

4.7 References and Notes

[1] a) J. Janata, *Principles of Chemical Sensors*, Second edition, Springer, **2009**; b) *Artificial Receptors for Chemical Sensors*, Editors: V. M. Mirsky, A. K. Yatsimirsky, WILEY-VCH Verlag & Co., **2011**.

[2] A. Hulanicki, S. Glab, F. Ingman, *Pure Appl. Chem.* **1991**, *63*, 1247-1250.

[3] A. D'Amico, C. Di Natale, *IEEE Sensors J.* **2001**, *1*, 183-190.

[4] J. Janata, M. Josowicz, *Anal. Chem.* **1998**, *70*, 179-208.

[5] D. J. Cram, J. M. Cram, *Container Molecules and their Guests*, The Royal Society of Chemistry, Cambridge, **1994**.

[6] J. B. Wittenberg, L. Isaacs, *Supramolecular Chemistry: From Molecules to Nanomaterials*, John Wiley & Sons, **2012**, DOI: 10.1002/9780470661345.smc004.

[7] a) L. Pirondini, E. Dalcanale, *Chem. Soc. Rev.* **2007**, *36*, 695-706; b) R. Pinalli, E. Dalcanale, *Acc. Chem. Res.* **2013**, *46*, 399-411.

[8] B. Wang, E. V. Anslyn, *Chemosensors: Principles, Strategies, and Applications (Wiley Series in Drug Discovery and Development)*, **2011**.

[9] A. T. Wright, E. V. Anslyn, *Chem. Soc. Rev.* **2006**, *35*, 14-28.

[10] P. Anzenbacher, P. Lubal, P. Bucek, M. A. Palacios, M. E. Kozelkova, *Chem. Soc. Rev*. **2010**, *39*, 3954-3979.

[11] E. Llobet, J. Rubio, X. Vilanova, J. Brezmes, X. Correig, J. W. Gardner, E. L. Hines, *Sens. Act. B* **2001**, *76*, 419-429.

[12] J. J. Lavigne, S. Savoy, M. B. Clevenger, J. E. Ritchie, B. McDoniel, S. J. Yoo, E. V. Anslyn, J. T. McDevitt, J. B. Shear, D. Neikirk, *J. Am. Chem. Soc.* **1998**, *120*, 6429-6430.

[13] L. Prodi, *New J. Chem.* **2005**, *29,* 20-31.

[14] J. R. Lakowicz, *Principles of Fluorescent Spectroscopy*, 2nd Eds, Kluwer Academic/Plenum Publisher, New York, **1999.**

[15] A. Prasanna de Silva, T. S. Moody, G. D. Wright, *Analyst* **2009**, *134*, 2385-2393.

[16] J. S. Kim, D. T. Quang, *Chem. Rev.* **2007**, *107*, 3780-3799.

[17] J. B. Birks, *Rep. Prog. Phys.* **1975**, *38*, 903-974.

[18] B Valeur, *Molecular Fluorescence: Principles and Applications*, Wiley-VCH, **2001**.

[19] F. M. Winnik, *Chem. Rev.* **1993**, *93*, 587-614.

[20] S Karuppannan, J. C. Chambron, *Chem. Asian J.* **2011**, *6*, 964-984.

[21] E. Manandhar, K. J. Wallace, *Inorg. Chim. Acta* **2012**, *381,*15-43.

[22] A. P. de Silva, H. Q. N. Gunaratne, T. Gunnlaugsson, A. J. M. Huxley, C. P. McCoy, J. T. Rademacher, T. E. Rice, *Chem. Rev.* **1997**, *97*, 1515-1566.

[23] ATLAS on Substance Use (**2010**), *Resources for the prevention and treatment of substance use disorders*, World Health Organisation, **2011**.

[24] O. Von Bohlen und Halbach, R. Dermietzel, *Neurotransmitters and Neuromodulators: Handbook of receptors and Biological Effects*; Wiley-VCH, Weinheim **2006**.

[25] A. Sreekumar, L. M. Poisson, T. M. Rajendiran, A. P. Khan, Q. Cao, J. Yu, B. Laxman, R. Mehra, R. J. Lonigro, Y. Li, M. K. Nyati, A. Ahsan, S. Kalyana-Sundaram, B. Han, X. Cao, J. Byun, G. S. Omenn, D. Ghosh, S. Pennathur, D. C. Alexander, A. Berger, J. R. Shuster, J. T. Wei, S. Varambally, C. Beecher, A. M. Chinnaiyan, *Nature* **2009**, *457*, 910-914.

[26] UNODC: 2012 World Drug Report. June **2012**. Vienna, Austria: United Nations Office on Drugs and Crime. Available at: http://www.unodc.org/documents/data-and analysis/WDR2012/WDR_2012_web_small.pdf

[27] World Health Organization (**2004**). *Neuroscience of psychoactive substance use and dependence.*

[28] Warner, E. A. *Annals of Internal Medicine* **1993**, *119,* 233-235.

[29] N. Kato, S. Fujita, H. Ohta, M. Fukuba, A. Toriba, K. Hayakawa, *J. Forensic Sci.* **2008**, *53*, 1367-1371.

[30] a) T. Kraemer, L. D. Paul, *Anal Bioanal Chem* **2007**, *388*, 1415-1435; b) R. Herraez-Hernandez, P. Campins-Falco, J. V. Andres, *Analyst* **2001**, *126*, 581-586; c) F. Sadeghipour, J. L. Veuthey, *J. Chromatogr. A* **1997**, *787*, 137-143.

[31] L. W. Chung, K. L. Lin, T. C. Yang, M. R. Lee, *J. Chromatogr. A* **2009**, *1216*, 4083-4089.

[32] W. Matapatara, P. Thongnopnuaa, V. Lipipun, *Asian Biomedicine* **2007**, *1*, 167-179.

[33] C. Andreou, M. R. Hoonejani, M. R. Barmi, M. Moskovits, C. D. Meinhart, *ACS Nano* **2013**, *7*, 7157-7164.

[34] a) S. S. Johansen, H. M. Bhatia, *J. Chromatogr. B* **2007**, *852*, 338-344; b) K. Nesmerak, M. Sticha, M. Cvancarova, *Anal. Lett.* **2010**, *43*, 2572-2581.

[35] a) M. Barroso, M. Dias, D. N. Vieira, J. A. Queiroz, M. Lopez-Rivadulla, *Rapid Commun. Mass Spectrom.* **2008**, *22*, 3320-3326; b) S. Cristoni, E. Basso, P. Gerthoux, P. Mocarelli, E. Gonella, *Rapid Commun. Mass Spectrom.* **2007**, *21*, 2515-2523; c) S. Valente-Campos, M. Yonamine, R. Moreau, O. A. Silva, *Forensic Science International* **2006**, *159*, 218-222.

[36] a) M. N. Stojanovic, P. de Prada, D. W. Landry, *J. Am. Chem. Soc.* **2001**, *123,* 4928-4931; b) B. R. Baker, R. Y. Lai, M. S. Wood, E. H. Doctor, A. J. Heeger, K. W. Plaxco, *J. Am. Chem. Soc.* **2006**, *128*, 3138-3139; c) Y. Shi, H. Dai, Y. Sun, J. Hu, P. Ni, Z. Li, *Analyst* **2013**, *138*, 7152-7156.

[37] a) J. E. Baker, A. Jenkins, *Am. J. Forensic Med. Pathol.* **2008**, *29*, 141-144; b) M. T. Contreras, A. E. Hernandez, M. Gonzalez, S. Gonzalez, R. Ventura, A. Pla, J. L. Valverde, J. Segura, R. de la Torre, *Forensic Science International* **2006**, *164*, 168-171; c) J. A. Mead, J. Niekro, M. Staples, *Clin. Chem.* **2003**, *49*, A122-A122.

[38] a) P. Lopez, S. Martello, A. M. Bermejo, E. De Vincenzi, M. J. Tabernero, M. Chiarotti, *Anal. Bioanal. Chem.* **2010**, *397*, 1539-1548; b) V. Spiehler, D. S. Isenschmid, P. Matthews, P. Kemp, T. J. Kupiec, *Anal. Toxicol.* **2003**, *27*, 587-591; c) S. Kerrigan, W. H. Phillips, *Clin. Chem.* **2001**, *47*, 540-547.

[39] M. Dionisio, G. Oliviero, D. Menozzi, S. Federici, R. M. Yebeutchou, F. P. Schmidtchen, E. Dalcanale, P. Bergese, *J. Am. Chem. Soc.* **2012**, *134*, 2392-2398.

[40] E. Biavardi, C. Tudisco, F. Maffei, A. Motta, C. Massera, G. G. Condorelli, E. Dalcanale, *Proc. Natl. Acad. Sci. USA* **2012**, *109*, 2263-2268.

[41] C. Tudisco, F. Bertani, M. T. Cambria, F. Sinatra, E. Fantechi, C. Innocenti, C. Sangregorio, E. Dalcanale, G. G. Condorelli, *Nanoscale* **2013**, 5, 11438-11446.

[42] P. Delangle, J. P. Dutasta, *Tetrahedron Lett.* **1995**, *36*, 9325-9328.

[43] B. Cantadori, P. Betti, F. Boccini, C. Massera, E. Dalcanale, *Supramol. Chem.* **2008**, *20*, 29-34.

[44] M. Montalti, E. Rampazzo, N. Zaccheroni, L. Prodi, *New J. Chem.,* **2013**, *37*, 28-34; b) M. Helle, E. Rampazzo, M. Monchanin, F. Marchal, F. Guillemin, S. Bonacchi, F. Salis, L. Prodi, L. Bezdetnaya, *ACS Nano* **2013**, *7*, 8645-8657; c) E. Rampazzo, R. Voltan, L. Petrizza, N. Zaccheroni, L. Prodi, F. Casciano, G. Zaulic, P. Secchiero, *Nanoscale* **2013**, *5*, 7897-7905.

[45] K. Kalyanasundaram, J. K. Thomas, *J. Am. Chem. Soc.* **1977**, *99,* 2039-2044.

[46] L. Mohanambe, S. Vasudevan, *J. Phys. Chem. B* **2006**, *110*, 14345-14354.

[47] X. Liu, K. K. Iu, J. K. Thomas, *J. Phys. Chem.* **1989**, *93*, 4120-4128.

[48] a) V. R. Kaufman, D. Avnir, *Langmuir* **1986**, *2*, 717-722; b) B. Dunn, J. I. Zink, *Acc. Chem. Res.* **2007**, *40*, 747-755.

[49] G. G. Condorelli, A. Motta, M. Favazza, I. L. Fragalà, M. Busi, E. Menozzi, E. Dalcanale, *Langmuir* **2006**, *22*, 11126-11133.

[50] Q. Y. Sun, L. C. P. M. de Smet, B. van Lagen, M. Giesbers, P. C. Thune, J. van Engelenburg, F. A. de Wolf, H. Zuilhof, E. J. R. Sudholter, *J. Am. Chem. Soc.* **2005**, *127*, 2514-2523.

[51] E. Biavardi, M. Favazza, A. Motta, I. L. Fragalà, C. Massera, L. Prodi, M. Montalti, M. Melegari, G. G. Condorelli, E. Dalcanale, *J. Am. Chem. Soc.* **2009**, *131*, 7447-7455.

[52] B. Bibal, B. Tinant, J. P. Declercq, J. P. Dutasta, *Supramol. Chem.* **2003**, *15*, 25-32.

Chapter 5

Supramolecular Host-Guest Vesicles Based on Cucurbit[*8*]uril*

* This work has been carried out in the group of Dr. Oren A. Scherman at Cambridge University.

5.1 State of the Art

Vesicles are enclosed structures dispersed into and filled with a liquid solvent, typically water.[1] These hollow aggregates are usually composed of a flexible bilayer membrane of natural or synthetic amphiphiles. Vesicles assume in general a spherical shape but, due to their flexibility, they can be unilamellar, multilamellar or oligovesicular.[2]
During the years these objects have gained the interest of scientists as they represent the simplest model of a living cell with a membrane wall. Furthermore, they can have appealing and promising applications in drug/gene delivery systems,[3] nanoreactors[4] and in the field of delivery vehicles since these materials can easily trap hydrophilic molecules in their cavity full of water, such as therapeutics. Moreover the bilayer membrane (called vesicle wall) can sequester hydrophobic guests like dye molecules in order to assist the imaging of these structures. In addition, the hydrophilic corona could be modified with particular functionalities to conjugate biologically active macromolecules, thereby altering the vesicle's interaction with the surrounding environment.

Conventionally, vesicles are constructed by self-assembly of amphiphiles, molecules that contains a hydrophobic tail and a hydrophilic head connected by covalent bonds. When amphiphiles are dissolved in water, the hydrophobic parts tend to aggregate while the hydrophilic units favor to stay in water, generating aggregates with various nanostructures, such as vesicles.
In contrast to common amphiphiles, supramphiphiles refers to molecules that are linked by non covalent dynamic interactions.[5] It should be pointed out that there are two order of self-assembly in this approach: the first one is the formation of the supramphiphiles, followed by the second order assembly in which these aggregates function as building blocks for constructing highly order aggregates. Both types of self-assembly should be careful studied in order to develop functional materials that present appealing properties.[6] Fabrication of vesicles using supramolecular approach presents several advantages, for example the time consuming covalent synthesis and the purification processes can be avoided to some extent and the amphiphilicity of the building block can be easily tuned.
Until now numerous kinds of weak interactions have been used to build supramolecular amphiphiles including hydrogen bondings, charge transfer and

π-π interactions.[7] However there are only few reports on the formation of supramolecular vesicles from amphiphiles based on host-guest interactions.[8]
With this strategy a fine tuning of the functionalities and of the stimuli-responsiveness behavior of the soft materials would be possible, resulting from the facile introduction of different chemical moieties on host or guest molecules. Thanks to their ability to form water soluble architectures, receptors like cucurbiturils, cyclodextrins and sulfonatocalixarenes are the most used host molecules for the formation of vesicles. In addition, such macrocycles have been shown to be very biocompatible,[9] which is essential for application in the fields of biotechnology and medicine.[10]

Cucurbit[*n*]urils are a family of macrocyclic receptors that presents a hydrophobic cavity similar to cyclodextrins which can be used to incorporate guest molecules with high binding affinities in aqueous media.[11]
Kim *et al*.[12] firstly explored cucurbit[*8*]uril (from now on referred to as CB[*8*]) as building block for supramolecular amphiphiles by harnessing its capability to act as "supramolecular handcuff" to join two molecules together. As shown in Figure 5.1 in the presence of CB[*8*] the electron poor viologen (substituted with different alkyl chains) and the electron rich 2,6-dihydroxynaphtalene can form a charge transfer complex inside the cavity of the host. This supramolecular amphiphile, composed by a large polar head group and a hydrophobic tail, displays new aggregation behavior in water because it assemblies in vesicle-like aggregates, as observed by dynamic light scattering (DLS), transmission electron microscopy (TEM) and scanning electron microscopy (SEM). Since the ternary complex is stabilized by an electron donor-acceptor pair, they demonstrated that the vesicle could be collapsed by using redox chemistry, upon addition of cerium (IV) ammonium nitrate.

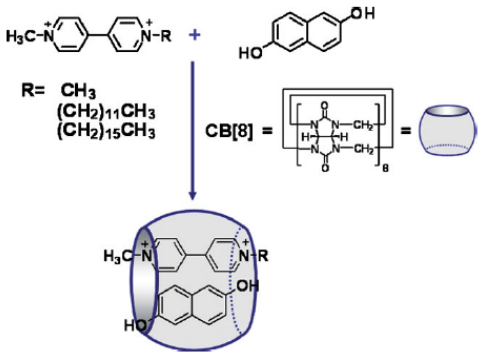

Figure 5.1 *Supramolecular amphiphile assembly based on charge-transfer interaction.*

A natural step forward in the fabrication of smart vesicles would be embedding these materials with multiple functional sites with the purpose of enable biocompatible and responsive properties. As above mentioned, these tasks could be solved using host-guest chemistry.

The system of Kim *et al.* has been boosted by Scherman *et al.*,[13] reporting the preparation of supramolecular peptide amphiphiles by host-guest complexation of a pyrene-functionalized peptide and a viologen lipid with CB[*8*] (Figure 5.2). The formation of the supramolecular ternary complex was observed by fluorescence spectroscopy since the pyrene experienced a fluorescence quenching upon the inclusion in the cavity of the CB[*8*]. The assembly of supramolecular vesicles from the non-covalent amphiphiles was also demonstrated by several techniques like DLS and TEM. Being covered by three lysine molecules, a well known cell penetrating peptides (CPP),[14] the vesicles were easily taken up by HeLa cells and responded to multiple external trigger that modulated the citotoxicity of the supramolecular system.

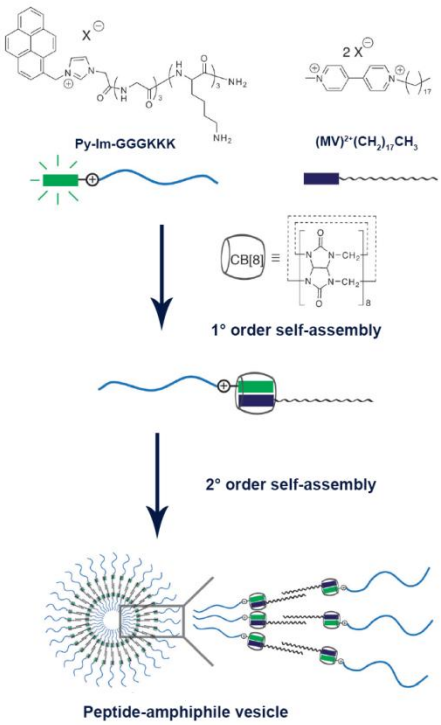

Figure 5.2 *First and second order self-assembly of supramolecular peptide amphiphile vesicle.*

5.2 Introduction

The results reported by Scherman's group have opened a new avenue toward the formation of multifunctional vesicles through hierarchical self-assembly in aqueous media. The derivatization of the two guests of the ternary complex has allowed to decorate the surface of the supramolecular aggregates with new specific functionalities.

Herein we describe the self-assembly of differently charged supramolecular vesicles driven by the formation of a ternary complex that acted as a supramolecular amphiphile. The building blocks used in this work were: CB[*8*], an hydrophilic block and an hydrophobic moiety. The cucurbituril receptor (Figure 5.3b) guided the organization of the other two components into an amphiphilic ternary complex (see Figure 5.2). The hydrophobic block is composed by a n-heptadecane alkyl chain attached to the first guest of the CB[*8*], the methyl-viologen group (Figure 5.3a). The hydrophilic unit is formed by two different peptide sequences, both of them containing three molecules of

glycine linked to three molecules of lysine (K) and three molecules of glutamic acid (E), these two sequences are linked to a pyrene group that acted as second guest in the ternary complex (Figure 5.3c).

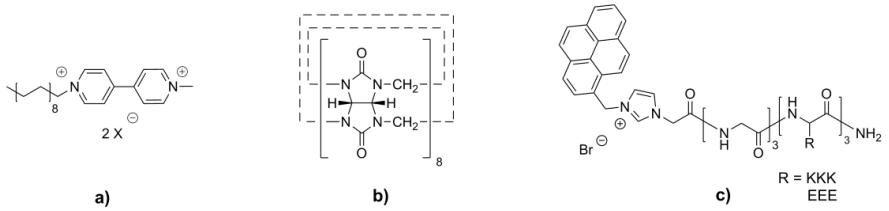

Figure 5.3 *Building blocks of the supramolecular amphiphiles: a) MV-lipid; b) CB[8]; c) Pyrene-imidazole-peptides.*

The three molecules of K and E, being positively and negatively charged at pH 7 in water, impart different charges on the inner core and on the surface of the vesicles. The role of the charges in the self-assembly process was investigated in an effort to understand whether they can affect either the morphology or the size of the supramolecular vesicles. The hierarchical self-assembly was followed by different complementary techniques namely: fluorescence spectroscopy, DLS, TEM and environmental scanning electron microscopy (ESEM).

5.3 Results and Discussion

5.3.1 Synthesis of the Hydrophilic and Hydrophobic Blocks

The hydrophilic blocks, as previously explained, are composed by the pyrene imidazolium group connected to a peptide sequence through an amide bond.

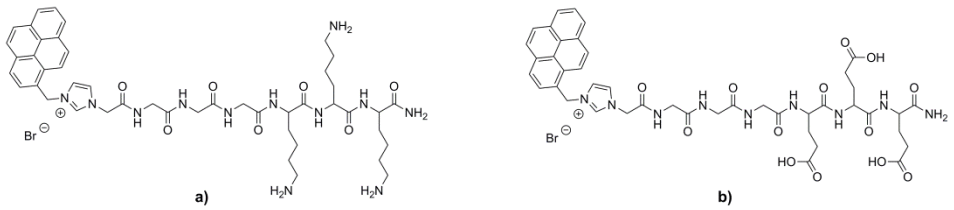

Figure 5.4 *a) Py-Im-GGGKKK; b) Py-Im-GGGEEE.*

The sequences of amino acids were designed in order to place a spacer between the guest of the CB[*8*] and the fraction of the peptide that contains the information to be introduced on the surface of the vesicles (Figure 5.4).

These two molecules were synthesized connecting covalently two different building blocks: the carboxylic acid containing the pyrene group and the hexapeptide sequences.
The two peptides were easily prepared by Solid Phase Peptide Synthesis (SPPS) using standard Fmoc protocols and they were both characterized by RP-HPLC and ESI-MS to ensure their purity (see Experimental Section).
The other part of the target molecule, the 1-(carboxymethyl)-3-(pyren-1-ylmethyl)-1H-imidazol-3-ium bromide (**V**), was synthesized in five steps and with a 49% overall yield (Scheme 5.1). The imidazole group was inserted on the 1-(bromomethyl)pyrene (**II**) through a nucleophilic substitution. Then the imidazole was functionalized with a methyl acetate group which was hydrolyzed straightforwardly in the next step with sodium hydroxide. The salt was treated with hydrochloridric acid recovering the carboxylic acid (**V**) quantitatively.

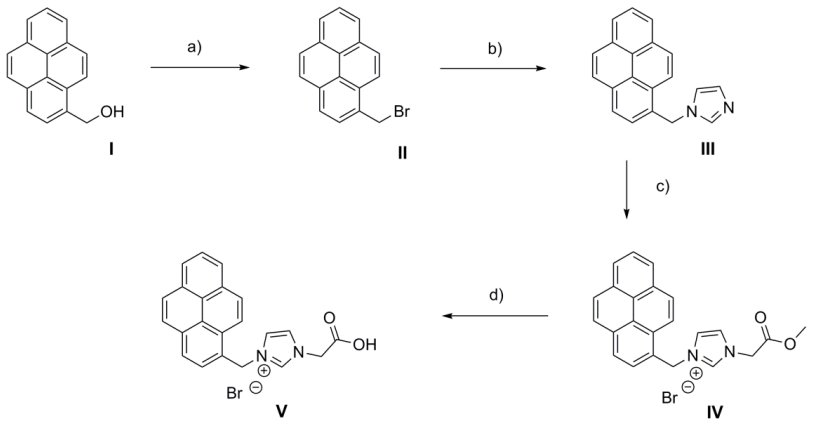

Scheme 5.1 *Synthesis of **1-(carboxymethyl)-3-(pyren-1-ylmethyl)-1H-imidazol-3-ium bromide (V)**: a) PBr_3, Toluene, r.t., 3 h, 90%; b) Imidazole/K_2CO_3, THF, reflux, 24 h, 60%; c) Methyl-bromo-acetate, toluene, reflux, 12 h; 92%; d) 1) NaOH 10%, reflux, 2 h, 2) HCl 37%, quantitative (over two steps).*

Subsequently, the two target molecules Py-Im-GGGKKK and Py-Im-GGGEEE were prepared using solid phase synthesis. As illustrated in Scheme 5.2, while the peptide was still kept on the resin, the Fmoc group was removed with a solution of piperidine in DMF (20% v/v). Then the amine group was reacted twice for 24 h with the carboxylic acid **V** using the HATU/DIPEA catalytic system, monitoring the consumption of the amine group with the Kaiser test.[15] Afterwards, the target molecule was cleaved from the resin using a proper

cleavage cocktail and the crude peptide was purified by RP-HPLC (the same procedure was used to synthesize Py-Im-GGGEEE, see Experimental Section).

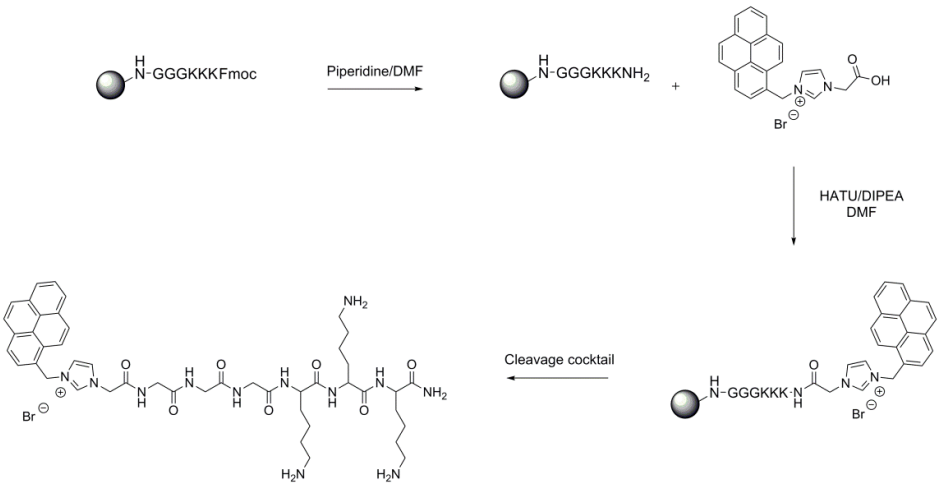

Scheme 5.2 *Synthesis of* ***Py-Im-GGGKKK****.*

The hydrophobic part of the ternary complex was easily synthesized in two steps in a 31% overall yield (Scheme 5.3). The starting material 4,4′-bipyridine was methylated in the first step with methyl iodide. Afterwards the mono-cationic 4,4′-bipyridinium was treated with octadecyl bromide affording the methyl-octadecyl viologen di-cationic first guest **VIII** with a 32% overall yield.

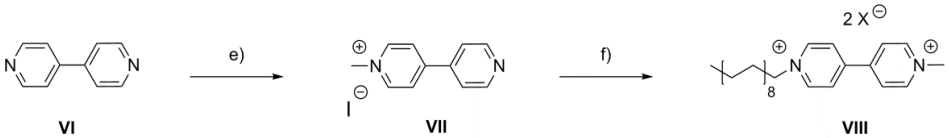

Scheme 5.3 *Synthesis of* ***1-methyl-1'-octadecyl-[4,4'-bipyridine]-1,1'-diium (VIII)****: e) MeI, DCM, reflux, 2 h, 45%; f) 1-bromo-octadecane, ACN, reflux, 48 h, 70%.*

5.3.2 Fluorescence Spectroscopy Measurements

The pyrene part of the hydrophilic block represents not only a guest for the CB[*8*] receptor but also a fluorescent probe for the formation proof of the ternary complex. In fact the emission spectra show (Figures 5.5 and 5.6) a fluorescence quenching of the pyrene group as a result of the formation of an electron donor-acceptor complex between pyrene and viologen moieties, inside the cavity of CB[*8*] (red line). As a control experiment CB[*7*] was used instead of

CB[*8*]. Its smaller cavity does not allow the formation of the ternary complex as witnessed by the slight change of the fluorescence emission of the pyrene moiety (blue line).

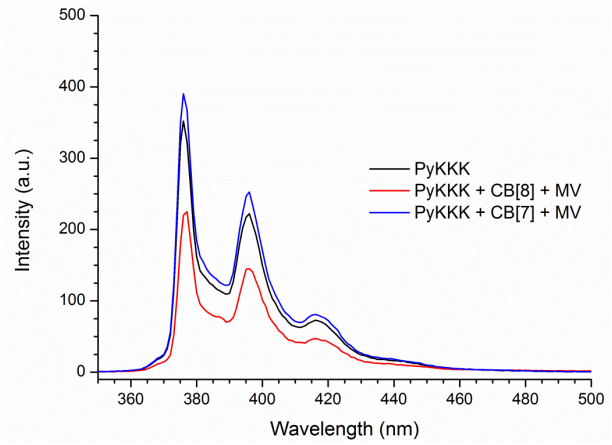

Figure 5.5 *Emission spectra of: black line) Py-Im-GGGKKK (25 μM, H_2O); red line) ternary complex; blue line) Py-Im-GGGKKK, MV with CB[7].*

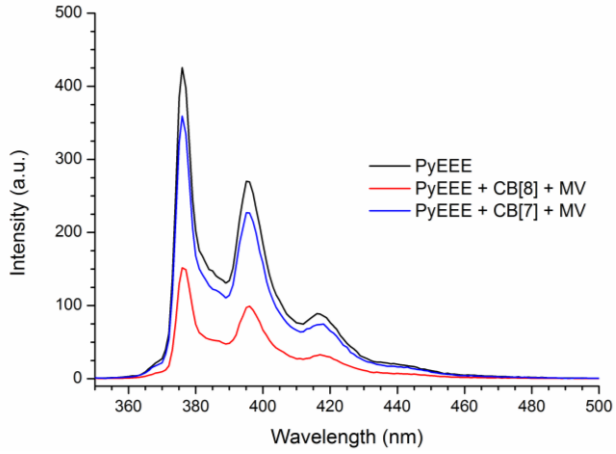

Figure 5.6 *Emission spectra of: black line) Py-Im-GGGEEE (25 μM, H_2O); red line) ternary complex; blue line) Py-Im-GGGEEE, MV with CB[7].*

As illustrated in Figure 5.5 and 5.6, we observed for both the peptide sequences a quenching of the pyrene emission, proving the formation of a ternary complex inside the CB[*8*] cavity.

5.3.3 Light Scattering Measurements

In order to study the size of the vesicles in water we performed a series of DLS experiments. The spectra in Figure 5.7 shows that both vesicles present a monodisperse system and they revealed an average size of (180 ± 80) nm for the positively charged vesicles (Figure 5.7a) and (492 ± 120) nm for the negatively charged vesicles (Figure 5.7b). These data confirm our hypothesis that the different charges located on the core and on surface of the vesicles have an influence on the size of the supramolecular aggregates.

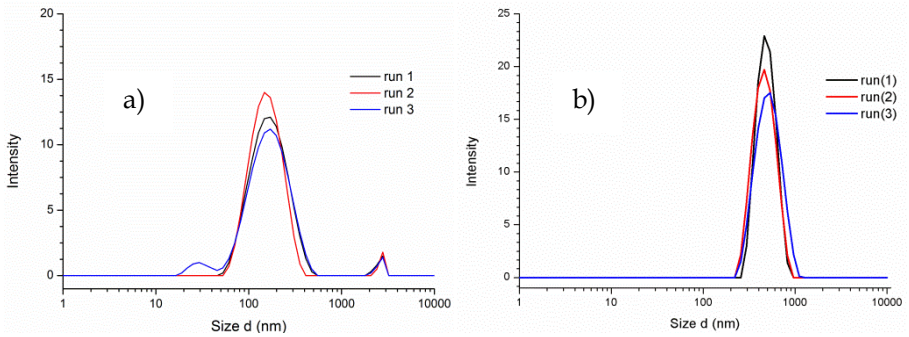

Figure 5.7 *DLS measurements (three separate measurements were taken for the same sample), 25 µM, H_2O, 25 °C): a) Py-Im-GGGKKK +MV + CB[8]; b) Py-Im-GGGEEE +MV + CB[8].*

To validate our assumption that the vesicles are charged on the surface, a series of zeta-potential (ζ) measurements were performed. The zeta-potential analysis is a technique for determining the surface charge of nanoparticles in solution. Nanoparticles that have a surface charge attract a thin layer of ions of opposite charge to the nanoparticle surface. This double layer of ions travels with the nanoparticles as it diffuses throughout the solution. The electric potential at the boundary of the double layer is known as the zeta-potential.[16]

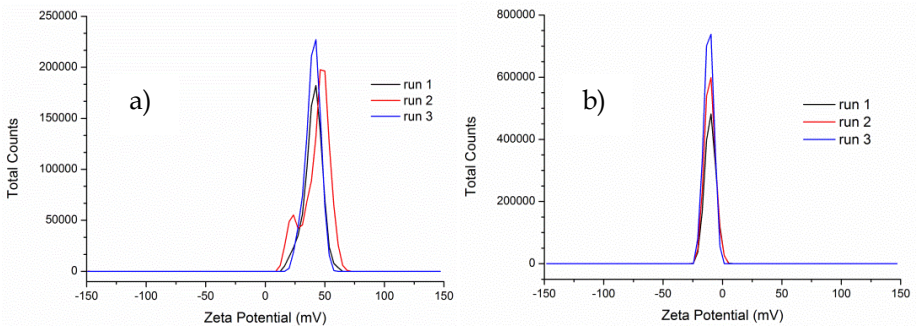

Figure 5.8 *Zeta-potential measurements (three separate measurements were taken for the same sample), 25 μM, H_2O, 25 °C): a) Py-Im-GGGKKK +MV + CB[8]; b) Py-Im-GGGEEE +MV + CB[8].*

The spectra in Figure 5.8a and 5.8b evidence the formation of positively and negatively charged species, in fact values of (39 ± 6) mV and (-10 ± 4) mV were found according to the polarity of the hydrophobic block used in the ternary complex. From the two potentials data it appears that the charge density on the cationic vesicles is higher with respect to the anionic one.

5.3.4 Transmission Electron Microscopy Measurements

To demonstrate that the hierarchical self-assembly process led to the formation of supramolecular vesicles a series of electron microscopy experiments were carried out.

The TEM images in Figure 5.9 and 5.10 highlight the formation of vesicles with a size that is in agreement with the average diameter obtained from DLS. To what concern the positively charged vesicles aggregates of about 100 nm was observed, while for the negatively charged vesicles larger aggregates were observed ranging from 200 to 400 nm.

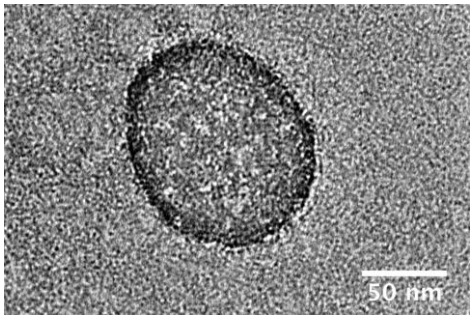

Figure 5.9 *TEM image of vesicle formed by Py-Im-GGGKKK, MV, CB[8] obtained on copper/carbon grid, staining effectuated with uranyl acetate 2% (w/w) in water.*

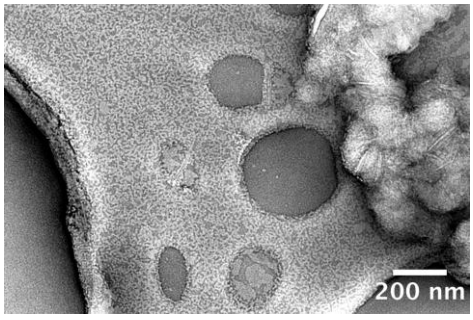

Figure 5.10 *TEM image of vesicle formed by Py-Im-GGGEEE, MV, CB[8] obtained on copper/carbon grid, staining effectuated with uranyl acetate 2% (w/w) in water.*

5.3.5 Environmental Scanning Electron Microscopy (ESEM) Measurements

To further help elucidating the morphology of the supramolecular aggregates ESEM images were collected. This technique allows the imaging of wet specimens in their natural state as a results of the gaseous environment in the specimen chamber, hence, in contrast of SEM, high *vacuum*, electrical conductivity and sample preparation are unnecessary. The most commonly used gas in the specimen chamber is water vapor, thus ESEM has the ability to obtain high quality images of hydrated samples and it is particular attractive for supramolecular aqueous soft materials.
Both ESEM images reported in Figure 5.11 and 5.12 show spherical aggregates providing more evidence of the formation of the vesicle structure. From the first image (Figure 5.11, negatively charged vesicles) we observed spheres, whose size is in agreement with the data found with DLS and TEM. Moreover larger

vesicles of about 1-2 µm were detected. This behavior could be explained by the association of the vesicles with each other, which is similar to the process of cell fusion in biology. In the second ESEM image (Figure 5.12 positively charged vesicles) smaller vesicles ranging from 100 to 300 nm were observed that are in agreement with DLS and TEM results.

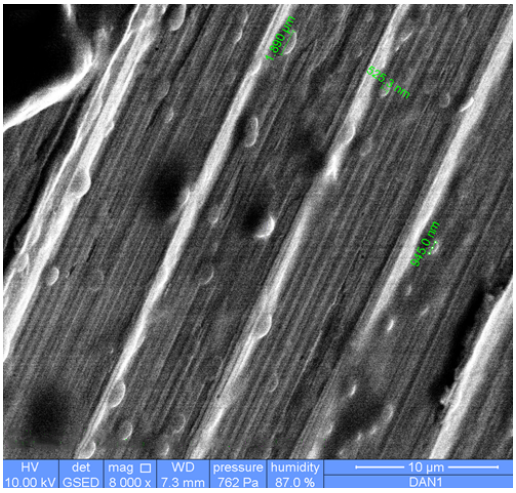

Figure 5.11 *ESEM image of vesicles (25 µM) formed by Py-Im-GGGEEE, MV, CB[8].*

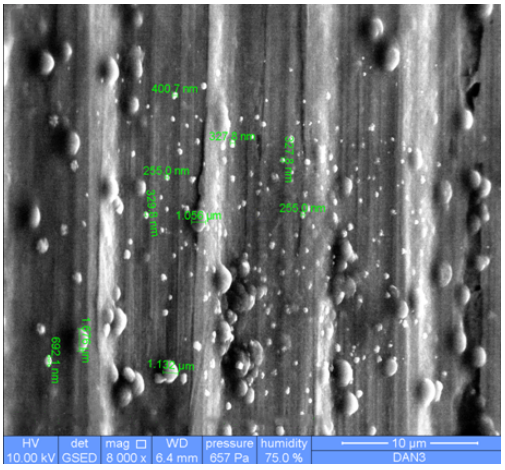

Figure 5.12 *ESEM image of vesicles (25 µM) formed by Py-Im-GGGKKK, MV, CB[8].*

5.3.6 Catanionic Vesicles Self-Assembly

From the previous results we inferred that the self-assembly process between the three building blocks generated supramolecular vesicles and the different charges located on the hydrophilic block can alter the size of these aggregates. Having synthesized two hydrophobic blocks positively and negatively charged, we decided to study whether mixing together these two blocks with CB[*8*] and MV, we could assemble a particular type of aggregates called catanionic vesicles.[17] These types of vesicles result from the mixture of cationic and anionic surfactants and were inspired by mimicking phospholipids, amphiphilic molecules that are the major components of the membrane cell as they can form lipid bilayers and vesicles (Figure 5.13).

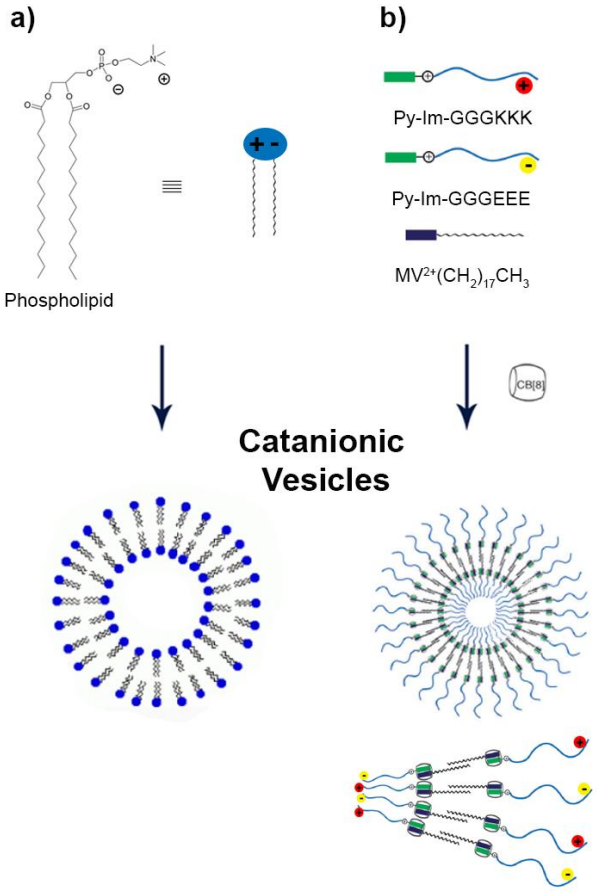

Figure 5.13 *Catanionic vesicles self-assembly: a) phosholipid based vesicles; b) cucurbit[8]uril based vesicles*

In this perspective, we investigated whether mixing different ratio of hydrophilic blocks we can control the charge of the vesicles and, as consequence, their size. In particular, we chosen three different Py-Im-GGGKKK/Py-Im-GGGEEE molar ratios and specifically: 1/1, 75/25, 25/75.
Figure 5.14 shows the DLS measurement of the various aggregates. Interestingly, by changing the ratio of the hydrophilic molecules we obtained supramolecular aggregates with different sizes.

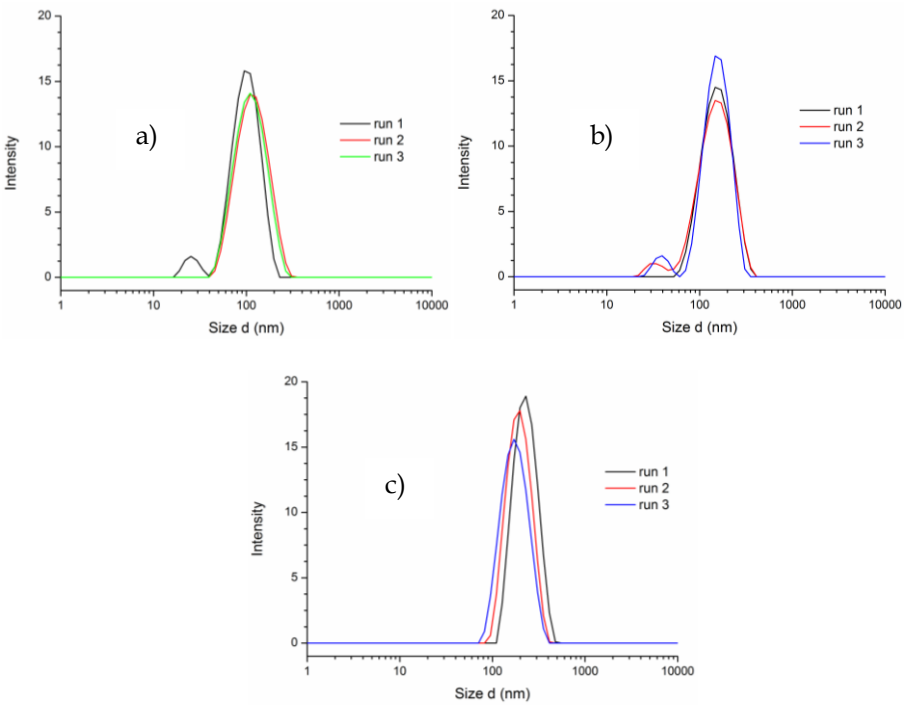

Figure 5.14 *DLS measurements (three separate measurements were taken for the same sample), 25 µM, water, 25 °C) of PyEEE+PyKKK (X,Y), MV, CB[8]: a) X= 1, Y= 1 (181 ± 67) nm; b) X= 75, Y= 25 (248 ± 73) nm; c) X= 25, Y= 75 (280 ± 89) nm.*

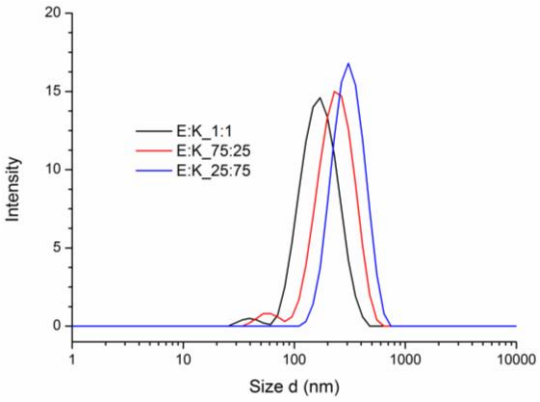

Figure 5.15 *Average diameters from DLS measurements PyEEE+PyKKK (X,Y), MV, CB[8].*

The vesicles containing a 1/1 ratio (Figure 5.14a) of the hydrophilic block present the smaller size (181 ± 67) nm, behavior that could be explained invoking the strong electrostatic interactions between the anionic and cationic hydrophilic blocks. These strong interactions could reduce the head-group area promoting a dense packing of surfactant molecules in the aggregates. For the 75/25 and 25/75 ratio the diameters of the aggregates are (248 ± 73) nm and (280 ± 89) nm respectively (Figure 5.14b,c).

In addition to DLS measurements we reported the zeta-potential experiments of the three supramolecular aggregates. The results depicted in Figure 5.16 are in agreement with the polarity of the aggregates. In detail, the vesicle with 1:1 molar ratio of hydrophilic blocks has no overall charge, while a small positive and negative charge was observed for the other two vesicles.

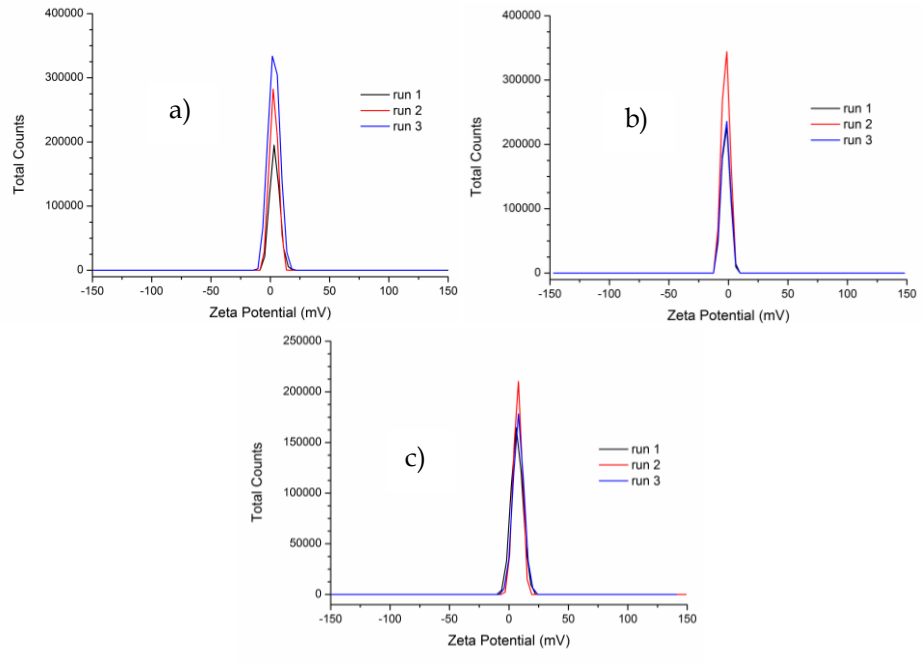

Figure 5.16 *Zeta-potential measurements (three separate measurements were taken for the same sample), 25 μM, water, 25 °C) of PyEEE+PyKKK (X,Y), MV, CB[8] (25 μM, water, 25 °C): a) X= 1, Y= 1 (3 ± 4.8) mV; b) X= 75, Y= 25 (-1.8 ± 3.5) mV; c) X= 25, Y= 75 (7.9 ± 4.5) mV.*

5.4 Conclusions

In summary we have reported the self-assembly of supramolecular vesicles positively and negatively charged driven by the formation of a ternary complex based on CB[*8*]. The two types of vesicles present the same spherical morphology but different size as demonstrated with several technique like DLS, TEM and ESEM. These data underscore the influence of the types of charges on the size of the vesicles. In addition the two peptides have been used to assemble catanionic aggregates. Although microscopy experiment should be performed to proof the presence of spherical vesicles, DLS data confirmed the formation of aggregates with different sizes.

5.5 Acknowledgments

Special thanks to Dr. Oren A. Scherman, Silvia Sonzini, Dr. Jesus del Barrio and Yang Lan from Department of Chemistry, University of Cambridge (UK). Thanks to Dr. Monica Mattarozzi from Department of Chemistry, University of Parma for ESEM measurements.

5.6 Experimental Section

Cucurbit[*8*]uril and cucurbit[*7*]uril (CB[*8*] and CB[*7*]) were synthesized according to a published procedure.[18] The following compounds were bought from AGTC Bioproducts at peptide synthesis purity grade: (L)-Fmoc-Gly-OH, (L)-Fmoc-Lys-(Pbf)-OH, (L)-Fmoc-Glu(OtBu)-OH and O-(benzotriazol- 1-yl)-N,N,N′,N′-tetramethyluronium hexafluorophosphate (HBTU), dichloromethane (DCM), dimethyl formamide (DMF). Water was obtained from a Synergy UV Ultrapure water system (18.2 MΩ cm at 25 °C).

1-(bromomethyl)pyrene (II)
A suspension of 1-pyrenemethanol **I** (4 g, 17.2 mmol) in toluene was cooled to 0 °C followed by addition of phosphorous tribromide (2 mL, 22.3 mmol). The mixture was stirred at 0 °C for 1 hour and then warmed to room temperature. Saturated Na_2CO_3 solution was added slowly and the organic phase was washed with water, brine and dried over Mg_2SO_4. The filtrate was concentrated to minimum volume and the yellow needle like solid **II** was collected and dried by suction filtration (4.5 g, 15.3 mmol, 90%).
^{1}H NMR ($CDCl_3$, 400 MHz): δ (ppm) = 8.36 (d, 1H, J=8, Ar**H**), 8.25-8.18 (m, 3H, Ar**H**), 8.11-7.97 (m, 5H, Ar**H**), 5.24 (s, 2H, BrC**H$_2$**); **ESI-MS**: mass peak was not found.

1-(pyren-1-ylmethyl)-1H-imidazole (III)
Imidazole (1.15 g, 17 mmol) and K_2CO_3 (1.7 g, 12.7 mmol) were mixed in 100 mL of THF with stirring for 10 minutes. Then **II** (2.5 g, 8.5 mmol) was added into the reaction mixture and heated to reflux for 24 hours. The insoluble was filtered off and the solvent removed *under vacuum*. The residual was dissolved in DCM and washed with water and treated with HCl 2N. The precipitate was filtered and washed with NaOH/$NaHCO_3$ solution to give pure **III** as white solid (1.4 g, 4.96 mmol, 60%).
^{1}H NMR (DMSO-d_6, 400 MHz): δ (ppm) = 8.43 (d, 1H, J=8, Ar**H**), 8.32-8.20 (m, 4H, Ar**H**), 8.12 (q, J=8 Hz, 2H, Ar**H**), 8.04 (t, J=8 Hz, 1H, Ar**H**), 7.88 (s, 1H, C**H$_{Imid}$**), 7.81 (d, J=8 Hz, 1H, Ar**H**), 7.19 (s, 1H, C**H$_{Imid}$**), 6.88 (s, 1H, C**H$_{Imid}$**), 5.94 (s, 2H, C**H$_2$**); **ESI-MS**: m/z 283 $[M+H]^+$.

1-(2-methoxy-2-oxoethyl)-3-(pyren-1-ylmethyl)-1H-imidazol-3-ium bromide (IV)

III (1.4 g, 5 mmol) was suspended in 180 mL of toluene, followed by addition of methyl bromo acetate (1.5 g, 10 mmol) slowly. The reaction mixture was refluxed overnight. After cooling to room temperature the precipitate was filtered and washed with toluene. The compound **IV** was obtained as white solid (2.09 g, 4.6 mmol, 92%).

^{1}H NMR (CD_3CN, 400 MHz): δ (ppm) = 8.82 (s, 1H, C**H**$_{Imid}$), 8.28-7.98 (m, 9H, Ar**H**), 7.46 (s, 1H, C**H**$_{Imid}$), 7.39 (s, 1H, C**H**$_{Imid}$), 6.08 (s, 2H, C**H**$_2$), 4.93 (s, 2H, C**H**$_2$), 3.63 (s, 3H, OC**H**$_3$); **ESI-MS**: m/z 355 $[M\text{-}Br]^+$.

1-(carboxymethyl)-3-(pyren-1-ylmethyl)-1H-imidazol-3-ium bromide (V)

IV (2 g, 4.6 mmol) was suspended in 150 mL of NaOH 1M, the solution was refluxed for 2 hours. The reaction mixture was allowed to cool at room temperature and HCl 37% was added slowly. The precipitate was filtered and washed with water to give **V** as white solid (1.9 g, 4.6 mmol, quantitative yield).

^{1}H NMR (DMSO-d_6, 400 MHz): δ (ppm) = 9.15 (s, 1H, C**H**$_{Imid}$), 8.42 (d, J=8 Hz, 1H, Ar**H**), 8.36-8.23 (m, 4H, Ar**H**), 8.18 (q, J=8 Hz, 2H, Ar**H**), 8.10-8.00 (m, 2H, Ar**H**), 7.78 (s, 1H, C**H**$_{Imid}$), 7.65 (s, 1H, C**H**$_{Imid}$), 6.21 (s, 2H, C**H**$_2$), 4.80 (s, 2H, C**H**$_2$); **ESI-MS**: mass peak was not found.

1-methyl-[4,4'-bipyridin]-1-ium iodide (VII)

A solution of 4,4'-bipyridine (3 g, 19.2 mmol) and iodomethane (1.55 g, 25 mmol) in DCM was stirred at reflux for 2 hours. After cooling to room temperature the precipitate was filtered and washed with ethyl acetate. The crude product was crystallized from methanol affording **VII** as yellow solid (2.6 g, 8.7 mmol, 45%).

^{1}H NMR (D_2O, 400 MHz): δ (ppm) = 8.84 (d, J=8 Hz, 2H, Ar**H**), 8.71 (d, J=4 Hz, 2H, Ar**H**), 8.32 (d, J=8 Hz, 2H, Ar**H**), 7.85 (d, J=4 Hz, 2H, Ar**H**), 4.38 (s, 3H, C**H**$_3$); **ESI-MS**: mass peak was not found.

1-methyl-1'-octadecyl-[4,4'-bipyridine]-1,1'-diium (VIII)

A solution of methyl bipyridyl (1 g, 3.35 mmol) and 1-bromo-octadecane (5 g, 15 mmol) in ACN was refluxed for 48 hours. The precipitate was filtered and washed with DCM. The crude product was crystallized from methanol affording **VIII** as orange solid (1.47 g, 2.34 mmol, 70%).

^{1}H NMR (DMSO-d_6, 400 MHz): δ (ppm) = 9.39 (d, J=8 Hz, 2H, Ar**H**), 9.29 (d, J=8 Hz, 2H, Ar**H**), 8.77 (dd, 4H, Ar**H**), 8.18 (q, J=8 Hz, 2H, Ar**H**), 4.69 (t, J=8 Hz, 2H,

Ar**H**), 4.45 (s, 3H, C**H**$_3$), 2.03-1.90 (m, 2H, C**H**$_2$), 1.27 (s, 28H, (C**H**$_2$)$_{14}$), 0.85 (t, J=8 Hz, 3H, C**H**$_3$); **ESI-MS**: mass peak was not found

Peptide synthesis

Solid phase peptide synthesis was performed on a Liberty Microwave Peptide Synthesizer (CEM Corporation) using Fmoc-strategy and Nova Rink amide resin 0.59 mM/g as solid support for 0.1 mmol scale. The Fmoc group was removed in each step with 20% (v/v) piperidine in DMF for 3 min using a microwave power of 45W. The maximum temperature was set to 75°C. The coupling step was performed with 5 equiv. of Fmoc protected amino acid in DMF (0.2 M), 4.5 equiv. of HBTU in DMF (0.45 M) and 10 equiv. of DIPEA in NMP (2 M). All couplings were performed for 10 min at 25 W at a maximum temperature of 75°C. Following completion of the sequence a small amount of the peptide was released from the resin for checking its purity by treatment with TFA/thioanisole/phenol/water/1,2-ethanedithiol (EDT) (82.5/5/5/5/2.5, v/v/v/v/v) at room temperature for 3 h. The crude peptide was precipitated in cold Et_2O and centrifuged for 4 times at 4 °C, using 4000 rpm over 5 min before being lyophilized and stored as a white powder. Peptide purity was verified by HPLC analysis on a Varian 940-LC and ESI-MS. The analytical column used was a reversed phase Agilent Eclipse plus C18 5 µm 4.6x150 mm column. The gradient applied was from A:B 95:5 to 100% B in 30 min, where A was water (0.1% TFA) and B was acetonitrile (0.1% TFA). The UV-Vis trace was followed at 220 nm. **HPLC** eluition time: Fmoc-GGGKKK 13.2 min, Fmoc-GGGEEE 14.5 min (Figure 5.17 and 5.18); **ESI-MS**: Fmoc-GGGKKK m/z 398.3 $[M+H]^{2+}$, 795.5 $[M+H]^+$, 818.5 $[M+Na]^+$; Fmoc-GGGEEE m/z 797.5 $[M+H]^+$, 820.5 $[M+Na]^+$.

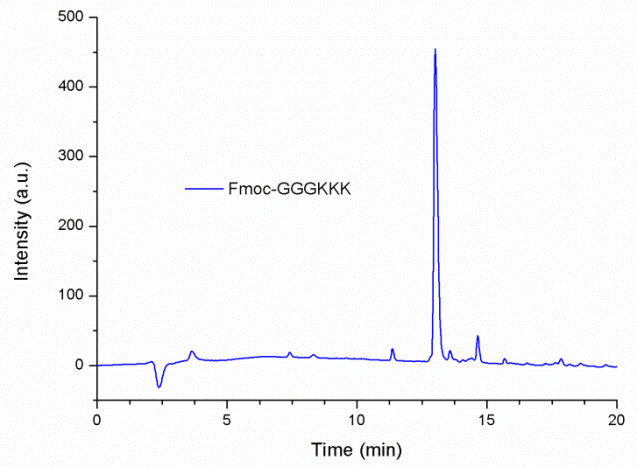

Figure 5.17 *HPLC trace Fmoc-GGGKKK.*

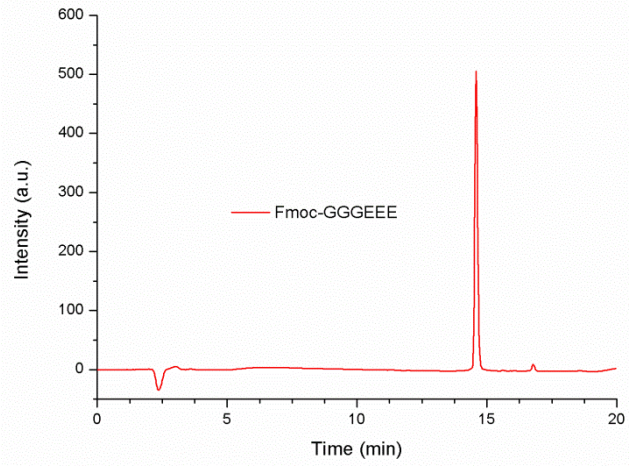

Figure 5.18 *HPLC trace Fmoc-GGGEEE.*

Synthesis of Py-Im-GGGKKK and Py-Im-GGGEEE

The Fmoc group of the peptides was removed with 20% (v/v) piperidine in DMF for 2 times for 3 min. The peptides were coupled twice with **V** using HATU/DIPEA catalyst system for 24 hours. Finally, the peptides were cleaved from the resin using TFA/phenol/water/thioanisole/EDT (82.5/5/5/5/2.5, v/v/v/v/v) at room temperature for 3 hours. The crude peptides were precipitated in cold Et_2O and centrifuged for 4 up to 6 times at 4 °C, using 4000 rpm over 5 min before being lyophilized. Afterwards they were purified on a

Varian 940-LC using a reversed phase semipreparative Zorbax C18 5 µm 9.4x250 mm column. The gradient applied was from A:B 95:5 to 100% B in 30 min, where A was water (0.1% TFA) and B was acetonitrile (0.1% TFA). **HPLC** eluition time: Fmoc-GGGKKK 13.2 min, Fmoc-GGGEEE 14.5 min (Figure 5.19 and 5.20); **MALDI**: Py-Im-GGGKKK calcd. for $C_{46}H_{63}N_{12}O_7$ 895,4937 Da found 895,3568 Da; Py-Im-GGGEEE calcd. for $C_{43}H_{48}N_9O_{13}$ 898,3366 Da found 898,0761 Da.

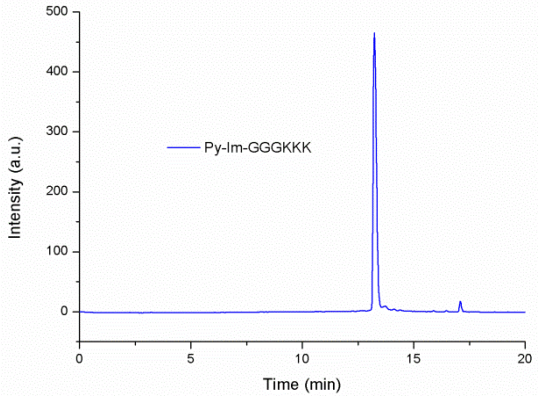

Figure 5.19 *HPLC trace Py-Im-GGGKKK.*

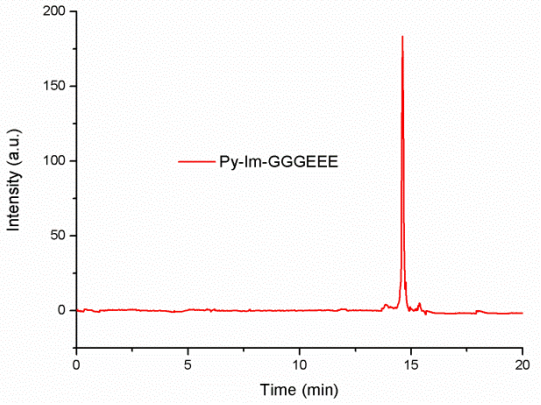

Figure 5.20 *HPLC trace Py-Im-GGGEEEE.*

Light scattering measurements

Electrophoretic mobilities and size distribution were determined at 25 °C with a Zetasizer Nano ZS (Malvern Instruments) operating with a 4 mW HeNe laser (632.8 nm), a detector positioned at the scattering angle of 173° and a temperature-control jacket for the cuvette. For the zetapotential measurements,

the samples with volume 0.75 ml were loaded in folded capillary zeta-potential cells with integral gold electrodes. Three measurements consisting of 100 runs with duration 10 s were performed for every sample. The mobility was converted to zeta-potential (ζ) using the Helmholtz–Smoluchowski relation.

TEM measurements

Transmission electron microscopy (TEM) characterization was carried out by a JEOL 2000FX TEM under an accelerating voltage of 200 kV. Samples were prepared by applying one drop of the vesicles solution onto a carbon coated copper TEM grid and incubated for 5 minutes. This solution was wicked off and the vesicles were stained with 10 µL of 2% (w/v) uranyl acetate water solution. The solution was air dried overnight.

ESEM measurements

ESEM experiments were performed on a Environmental Scanning Electron Microscope Quanta™ 250 FEG (FEI Company).

5.7 References and Notes

[1] V. Guida, *Adv. Colloid Interface Sci.* **2010**, *161*, 77-88.

[2] S. Segota, D. Tezak, *Adv. Colloid Interface Sci.* **2006**, *121*, 51-75.

[3] T. M. Allen, P. R. Cullis, *Science* **2004**, *303*, 1818-1822.

[4] S. M. Christensen, D. Stamou, *Soft Matter* **2007**, *3*, 828-836.

[5] X. Zhang, C. Wang, *Chem. Soc. Rev.* **2011**, *40*, 94-101.

[6] a) Y. Wang, H. Xu, X. Zhang, *Adv. Mater.* **2009**, *21*, 2849-2864; b) C. Wang, Z. Wang, X. Zhang, *Small* **2011**, *7*, 1379-1383.

[7] a) N. Kimizuka, T. Kawasaki, K. Hirata, T. Kunitake, *J. Am.Chem. Soc.* **1998**, *120*, 4094-4104; b) X. Zhang, Z. Chen, F. Würthner, *J. Am. Chem. Soc.* **2007**, *129*, 4886-4887; c) Y. Wang, N. Ma, Z. Wang, X. Zhang, *Angew. Chem. Int. Ed.* **2007**, *46*, 2823-2826; d) C. Wang, S. Yin, S. Chen, H. Xu, Z. Wang, X. Zhang, *Angew. Chem. Int. Ed.* **2008**, *47*, 9049-9052; e) Y. H. Ko, E. Kim, I. Hwang, K. Kim, *Chem. Commun.* **2007**, 1305-1315; f) C. Bize, J. C. Garrigues, M. Blanzat, I. Rico-Lattes, O. Bistri, B. Colasson, O. Reinaud, *Chem. Commun.* **2010**, *46*, 586-588.

[8] a) Q. Zhou, H. Wang, T. Gao, Y. Yu, B. Ling, L. Mao, H. Zhang, X. Meng, X. Zhou, *Chem. Commun.* **2011**, *47*, 11315-11317; b) K. Wang, D. Guo, X. Wang, Y. Liu, *ACS Nano* **2011**, *5*, 2880-2894; c) D. Guo, K. Wang, Y. Wang, Y. Liu, *J. Am. Chem. Soc.* **2012**, *134*, 10244-10250; d) D. Jiao, J. Geng, X. J. Loh, D. Das, T.-C. Lee, O. A. Scherman, *Angew. Chem. Int. Ed.* **2012**, *51*, 9633-9637; e) G. Yu, X. Zhou, Z. Zhang, C. Han, Z. Mao, C. Gao, F. Huang, *J. Am. Chem. Soc.* **2012**, *134*, 19489-19497; f) Q. Duan, Y. Cao, Y. Li, X. Hu, T. Xiao, C. Lin, Y. Pan, L. Wang, *J. Am. Chem. Soc.* **2013**, *135*, 10542-10549; g) L. Yang, H. Yang, F. Li, X. Zhang, *Langmuir* **2013**, *29*, 12375-12379; h) O. Roling, C. Wendeln, U. Kauscher, P. Seelheim, H. J. Galla, B. J. Ravoo, *Langmuir* **2013**, *29*, 10174-10182.

[9] a) F. Perret, A. N. Lazar, A. W. Coleman, *Chem. Commun.* **2006**, 2425-2438; b) K. Uekama, F. Hirayama, T. Irie, *Chem. Rev.* **1998**, *98*, 2045-2076; c) V. D. Uzunova,

C. Cullinane, K. Brix, W. M. Nau, A. I. Day, *Org. Biomol. Chem.* **2010**, *8*, 2037-2042.

[10] D. S. Guo, K. Wang, Y. X. Wang, Y. Liu, J. *Am. Chem. Soc.* **2012**, *134*, 10244-10250.

[11] a) J. Lee, S. Samal,N. Selvapalam, H. Kim, K. Kim, *Acc. Chem. Res.* **2003**, *36*, 621-630; b) J. Lagona, P. Mukhopadhyay, S. Chakrabarti, L. Isaacs, *Angew. Chem. Int. Ed.* **2005**, *44*, 4844-4870.

[12] Y. J. Jeon, P. K. Bharadwaj, S. W. Choi, J. W. Lee, K. Kim, *Angew. Chem. Int. Ed.* **2002**, *41*, 4474-4476.

[13] D. Jiao, J. Geng, X. J. Loh, D. Das, T. C. Lee, O. A. Scherman, *Angew. Chem. Int. Ed.* **2012**, *51*, 9633-9637.

[14] Y. Su, T. Doherty, A. J. Waring, P. Ruchala, M. Hong, *Biochemistry* **2009**, *48,* 4587-4595.

[15] E. Kaiser, R. L. Colescott, C. D. Bossinger, P. I. Cook, *Analytical Biochemistry* **1970**, *34*, 595.

[16] R. J. Hunter, *Zeta Potential In Colloid Science: Principles And Applications*, **1988**, Academic Press, UK.

[17] a) E. W. Kaler, K. A. Murthy, B. E. Rodriguez, J. A. N. Zasadzinski, *Science* **1989**, *245*, 1371-1374; b) E. Marques, A. Khan, M. G. Miguel, B. Lindman, *J. Phys. Chem.* **1993**, *97*, 4729-4736; c) V. Francisco, N. Basilio, L. Garcia-Rio, J. R. Leis, E. F. Maques, C. Vazquez-Vazquez, *Chem. Commun.* **2010**, *46*, 6551-6553.

[18] J. W. Lee, S. Samal, N. Selvapalam, H. J. Kim, K. Kim, *Acc. Chem. Res.* **2003**, *36*, 621-630.

Chapter 6

Synthetic Approaches Towards Water Soluble Tetraphosphonate Cavitands

6.1 State of the Art

One of the main challenges in supramolecular chemistry is gaining better insights on the mechanism of molecular recognition in water. This is a key step to achieve advanced applications of supramolecular chemistry in biology.
Natural receptors such as enzymes and antibodies show strong and selective host-guest complexation in water through weak intermolecular bonds towards the binding partners. These natural systems provide the inspiration for the design of artificial receptors that can be used as modern tools to investigate biological processes. Although several different water soluble macrocyclic receptors have been synthesized, good hosts for many organic guests and biological macromolecules have not yet been found.[1] In fact a common problem that must be faced is solubility in water, hence limiting the type of building blocks that can be used for the synthesis of good receptors. Moreover special attention has to be paid to avoid, minimize or exploit the strong involvement of water in non-covalent processes.[2]
In general, applications of synthetic supramolecular receptors in biology have to fulfill particular requirements:[3]

a) supramolecular interactions in biological systems typically occur in the μM to pM regime, analogously synthetic hosts should feature similar interactions strength;

b) complexes based only on a single type of interaction such as hydrophobic or ionic bonds would lead to unselective interactions with biological matter. In order to guarantee an high selectivity, recognition motifs are preferably based on two or more weak intermolecular forces;

c) supramolecular systems should incorporate biomarkers for bioconjugation, which is crucial for applications in biological systems.

Among biological macromolecules, proteins are the most studied because they are virtually involved in all biological processes. In particular protein surface recognition by small molecules represents a big challenge in life sciences as this would allow many types of applications, namely: controlling protein-protein interactions,[4] biosensors[5] and protein crystallization.[6] Supramolecular host-guest systems constitute a new molecular strategy for selective and reversible control of proteins and their interactions. Several water soluble receptors have been employed to recognize protein elements such as cucurbiturils,[7] cyclodextrins,[8] calixarenes[9] and crown ethers.[10]

A recent breakthrough in protein surface recognition has been done by Urbach *et al.*,[11] reporting the binding of human insulin by a cucurbit[*7*]uril (CB[*7*]) receptor. Isothermal titration calorimetry (ITC) and fluorescence spectroscopy experiments demonstrated that CB[*7*] binds insulin, through *N*-terminal Phe residue, with an association constant of 1.5×10^6 M^{-1}. The crystal structure of the CB[*7*] insulin complex confirmed that binding occurs at *N*-Phe residue and that the *N*-terminus unfolds to enable the binding process (Figure 6.1).

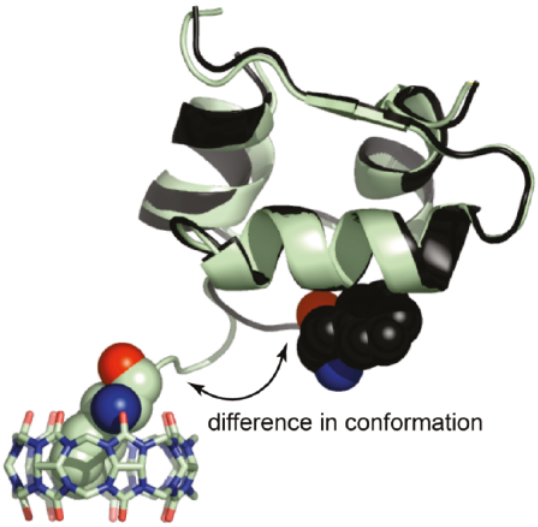

Figure 6.1 *Molecular recognition of insulin by CB[7].*

Another interesting paper in the field of bio-supramolecular chemistry has been the work of Crowley *et al.*,[12] in which they presented high resolution crystal structure of the complex between the tetra-sulfonato-calix[*4*]arene and the cytocrome *c* protein. The crystal structure reveals that the host binds multiple sites of the protein surface and in particular only the lysine moieties. All the lysine residues are complexed in the same way, with their methylene chain deeply inserted into the calixarene cavity and the ammonium functionality placed between two sulfonate anions (Figure 6.2). The crystallographic information is strongly supported by NMR data in solution. Knowing which are the interactions involved in the recognition process is extremely important for designing new calixarenes that have specific affinity towards a target protein.

A further appealing aspect observed by the Authors is that the calixarene mediates protein-protein interactions by virtue of its apolar surface. In fact,

interactions of the calixarene benzene rings with non polar residues on the protein surface coupled to the hydrophobic effect improved the interaction among proteins, facilitating crystallization.
This study must be considered a milestone in the field of bio-supramolecular chemistry, because for the first time a crystal structure that clarifies how a small synthetic complexing agent interacts with the proteins domain, and which aminoacids are involved in the process has been obtained. Although there are no direct application of this complex, it represent a valuable model for future design of artificial receptors targeting proteins surface. Moreover it has been proven that small molecules host can disguise the surface of proteins, having profound consequences in protein-protein interactions, and thus potential applications in drug discovery and medicinal diagnostic.[13]

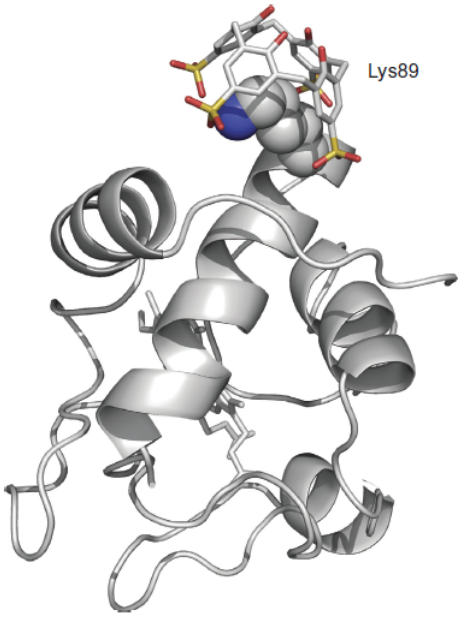

Figure 6.2 *One of the crystal structures of the supramolecular bio-complex.*

This work underlies the fact that cationic groups play a critical role in protein-protein interactions, and molecular recognition of this group by synthetic scaffold could provide new insights in the chemical investigations of biological macromolecules.
Lysine in particular is involved in the process of gene regulation through hystone methylation. Hystones are the proteins around which DNA coils and its chemical modifications[14] (acetylation, methylation, phosphorylation)

regulate DNA-based events such as gene transcription and DNA repair. Histones are methylated on lysine or arginine residues by histone methyltransferases (Figure 6.3). Nature has evolved a special motif for recognizing the methylation state of lysine, called the "aromatic cage". It is a preorganized collection of aromatic amino acids residues that coordinate to create a desolvated π-electronic rich pocket, occasionally containing an adjacent anionic residue. Taking inspiration from nature, researchers have explored the possibility to use chemical approaches to recognize methylated lysine using a synthetic pocket.[15]

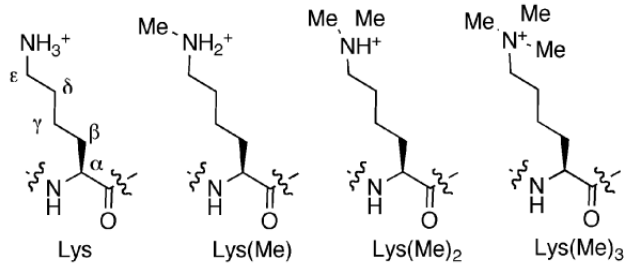

Figure 6.3 *Methylation states of lysine.*

6.2 Introduction

So far the most employed synthetic host for cationic groups recognition, has been the tetranionic p-sulfonatocalix[4]arene. This receptor, featuring a multiaromatic cavity, presents high affinity toward trimethyl-lysine moiety,[16] hence it is a promising tool to study the histone methylation. However the other two methylation states of the lysine group are complexed with a low association constant, therefore other macrocycles should be used to perform the detection of the mono- and di- methylated lysine.

Recently, the Dalcanale's group developed a molecular receptor based on a resorcinarene bridged with phosphonate groups (see Chapter 1). The resulting tetraphosphonate cavitand (**Tiiii**) offers remarkable complexation capabilities toward charged *N*-methylammonium species,[17] exhibiting a high K_a value, about 4 x 10^5 M^{-1} in methanol.[18] This property makes tetraphosphonate cavitands an interesting candidate for the detection of different methylation states of lysine. However, an extensive study of the complexation properties of the tetraphosphonate cavitand in water have never been carried out because of its inherent hydrophobicity.

The presence of a multi-aromatic cavity and four phenyl groups at the upper rim renders very challenging to induce water solubility in tetraphosphonate cavitands. We envisioned that a water soluble cavitand could be obtained in the following way:

I. introducing water soluble functionalities at the lower rim;

II. reducing the hydrophobicity at the upper rim, substituting the phenyl groups with small alkyl chain.

A common approach to enhance solubility in water consists in attaching ionizable functional groups. This solution is inappropriate for work spanning a wide range of pH and can prevent binding of charged guests.[19] Alternatively water solubility can be achieved with neutral hydrophilic functional groups such as oligoethyleneglycols[20] or carbohydrates.[21]

Herein we describe a series of synthetic approaches towards water soluble tetraphosphonate cavitands, using the two aforementioned methods: reducing the lipophilicity at the upper rim and functionalize the lower rim with four carbohydrate moieties through azide-alkyne click reaction (Figure 6.4).

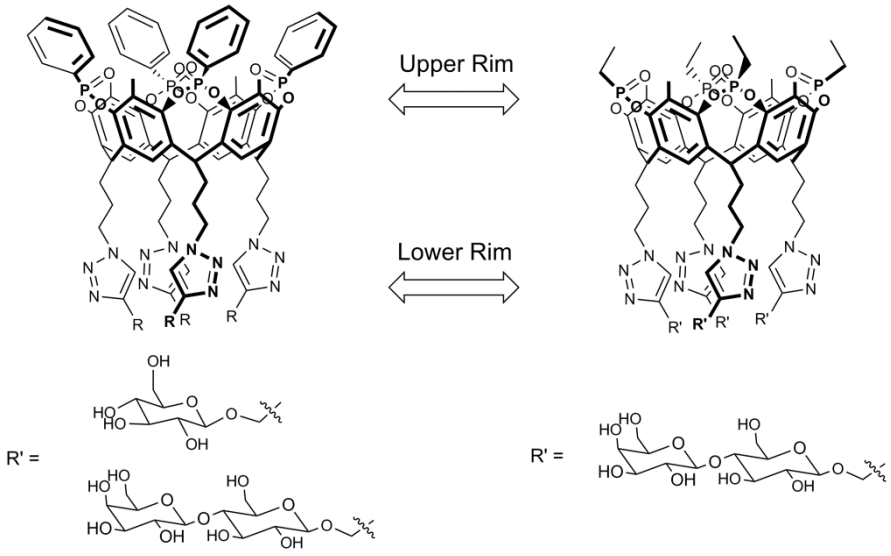

Figure 6.4 *Target molecules.*

We decided to link the four carbohydrate groups with the triazole unit through the Cu(I)-catalyzed Huisgen 1,3-dipolar reaction.[22] This reaction requires simple conditions, readily available starting materials and reagents, the use of benign

or easily removable solvents, and simple product isolation. In order to explore the feasibility of the CuAAC reaction, the **Tiiii** cavitand that bears four phenyl groups at the upper rim was functionalized at the lower rim with glucose and lactose. In a second attempt, the hydrophobicity of the upper rim was reduced by using a cavitand with four ethyl substituents on the P=O bridges. With this two different chemical derivations we surmised the formation of a water soluble tetraphosphonate cavitand.

6.3 Results and Discussion

With the purpose of investigate the practicability of the click reaction on the cavitand scaffold, we first synthesized the **TSiiii** bearing four glucose groups at the lower rim (**VII**, Scheme 6.1). This route was chosen because the P=S group is more manageable during the synthesis by virtue of its low polar nature, moreover it can be easily oxidized to P=O group afterwards.
The **TSiiii** cavitand **VII** was prepared in six steps with a 46% overall yield, starting from the hydroxyl footed silyl cavitand (**I**). The key steps in the synthesis were: the introduction of the azide moiety at the lower rim of the cavitand after the bridging reaction and the click reaction of **V** with propargyl glucose peracetate.[24] In the first step of the synthesis the hydroxyl groups of the silyl cavitand were replaced with chloride groups in a quantitative way. After removal of the silyl protecting groups by HF, the resulting resorcinarene **III** was bridged with dichlorophenylphosphine. The tetraphosphonite intermediate was oxidized *in situ* with sulfur, which proceeded with retention of configuration at the phosphorous centre, leading to **IV**. The tetra-azide, which was readily synthesized in high yield from **IV** and sodium azide, was then subjected to the CuAAC reaction with propargyl glucose peracetate using toluene/chloroform as solvent and $[(EtO)_3PCuI]$ as catalyst.[23]
The ^1H NMR of **VI** shows the singlet at about 7.68 ppm diagnostic for the formation of the triazole linker, and the characteristic pattern of the glucose group from 5.5 and 3.5 ppm (Figure 6.5). Finally, the product **VI** was treated with sodium methoxide for 2 hours and quenched with amberlite proton exchange resin to give the desired tetrakis(β-D-glucopyranosyl) tetraphosphotionate cavitand **VII** quantitatively. The compound **VII** resulted not soluble in water, but only in methanol as confirmed by ^1H NMR spectrum. The P=S group, as above mentioned, can be interconverted into a P=O group by a mixture of H_2O_2/acetone which forms acetone peroxide, a strong oxidizing agent. In our case the overnight oxidation of compound **VI** at 75 °C gave the

tetraphosphonate cavitand **VIII**, as confirmed by the ^{31}P NMR shift from 78.8 ppm to 11.6 ppm and by MALDI spectrometry although the ^{1}H NMR spectra was not perfectly pure. Attempts to purify the compound failed due to the presence of large amount of by-products.

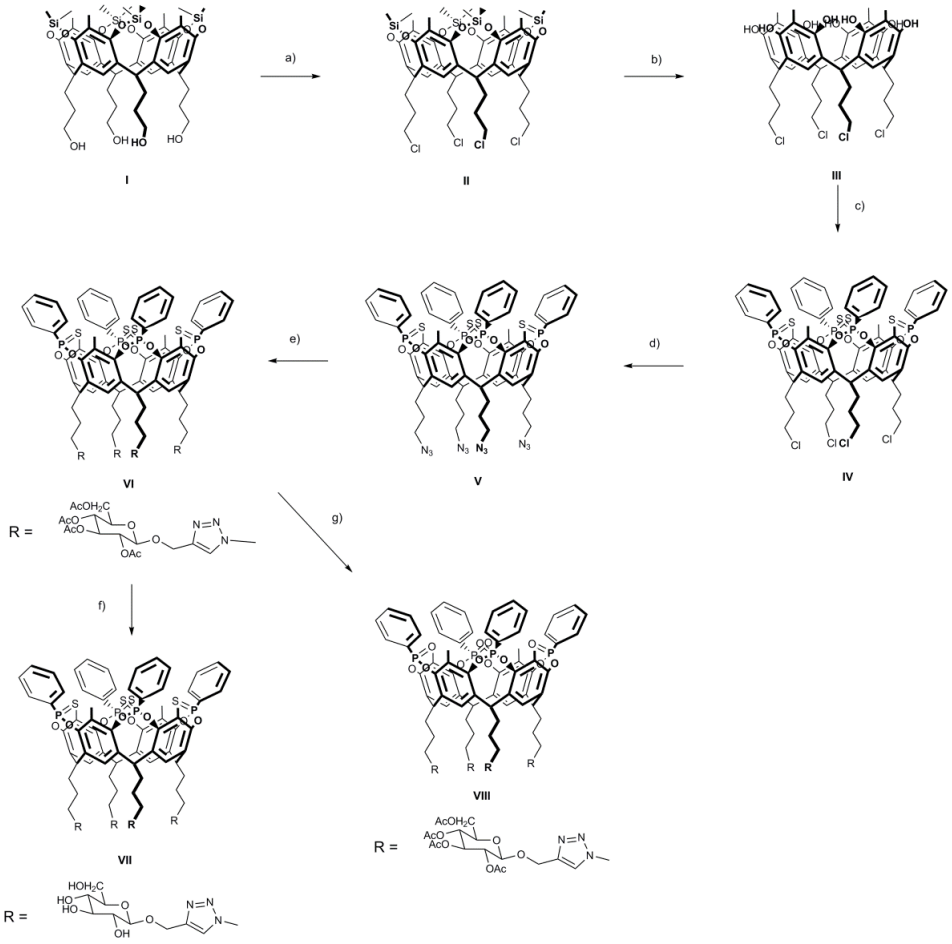

Scheme 6.1 *Synthesis of* ***Tiiii [glucose peracetate, CH_3, Ph]***, ***VIII*** *and* ***TSiiii [glucose, CH_3, Ph]***, ***VII***: *a) $SOCl_2$, 1,1,2,2-tetrachloroethane, 90 °C, 12 h, 93%; b) HF, DMF, 55 °C, 12 h, quantitative; c) 1) $PhPCl_2$, Py, 75 °C, 3 h; 2) S_8, 2 h, 70% (over two steps); d) NaN_3, DMF, 50 °C, 16 h, 86%; e) Glucose propargyl peracetate, $[(EtO)_3PCuI]$, DIPEA, toluene/$CHCl_3$, 80 °C, 70%; f) 1) MeOH/Na, 2 h, r.t.; 2) Dowex IR-120, r.t., 1 h, quantitative (over two steps); g) Acetone/H_2O_2, toluene, 75 °C, 24 h.*

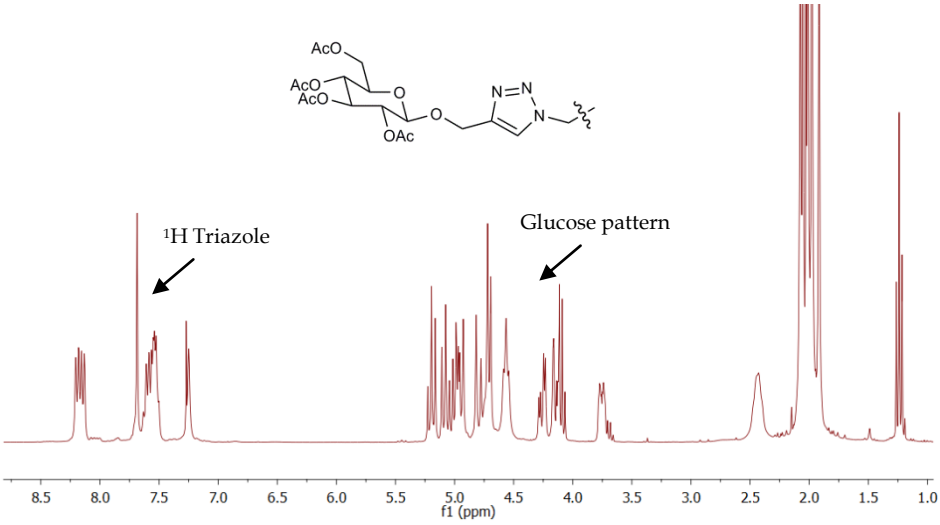

Figure 6.5 *^{1}H NMR spectra of **VI** in $CDCl_3$.*

Taking into account the lack of water solubility of compound **VII,** the amount of hydroxyl groups were increased attaching four lactose moieties using the same click procedure (Scheme 6.2). For this purpose the tetra-azide cavitand **V** was reacted with propargyl lactose peracetate[24] to give the corresponding cavitand **X**. Also in this case the acetyl protecting groups of compound **X** were removed with sodium metoxide, unfortunately product **XI** resulted not soluble in water but only in DMSO.

The oxidation of the P=S group to P=O was tested using the mixture hydrogen peroxide/acetone, but the MALDI-TOF spectra showed only the peak of the starting material proving that in this case the reaction does not work. The reaction was already problematic for **VIII**, increasing the number of sugar moieties from four to eight, makes the P=S oxidation ineffective.

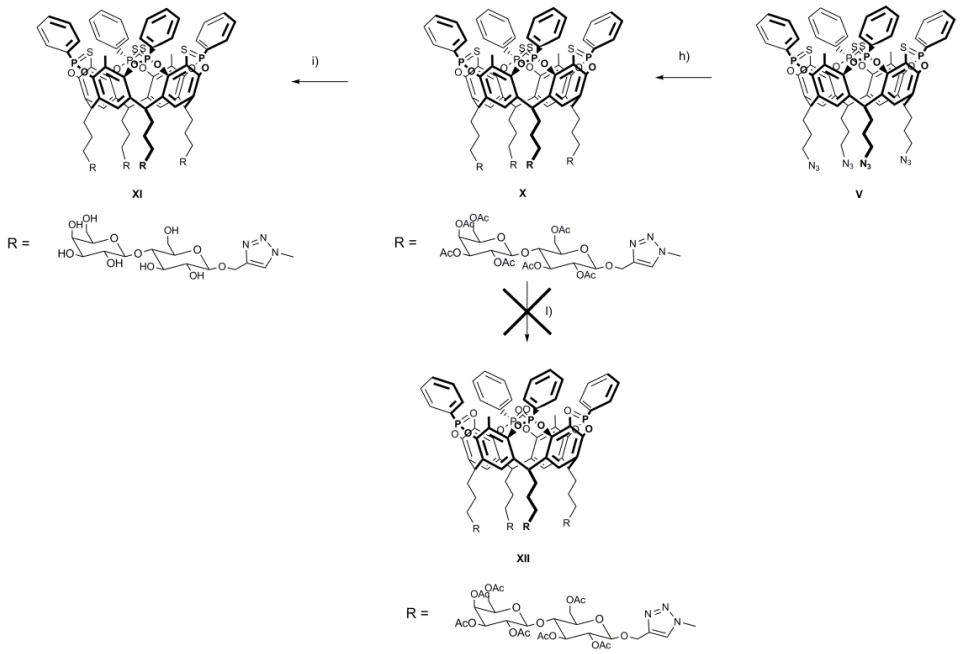

Scheme 6.2 *Synthesis of* ***TSiiii [lactose, CH_3, Ph]***, ***XI*** *and* ***Tiiii [lactose peracetate, CH_3, Ph]***, ***XII****: h) Lactose propargyl peracetate, [$(EtO)_3PCuI$], DIPEA, toluene/$CHCl_3$, 80 °C, 65%; i) 1) MeOH/Na, 2 h, r.t.; 2) Dowex IR-120, r.t., 1 h, quantitative (over two steps); l) Acetone/H_2O_2, toluene, 75 °C, 24 h, the reaction does not work.*

The hydrophobicity of the cavitand can be decreased also by changing the bridging groups at the upper rim of the resorcinarene. For this purpose a tetraphosphonate cavitand functionalized with four ethyl groups at the upper rim and that bears four lactose groups at the lower rim was synthesized (Scheme 6.3). We hypothesized that the combination of a lower lipophilicity at the top of the cavitand and the presence of four lactose groups at the lower rim could increase the water solubility of the receptor.

The pathway is similar to the previous one: after removal of the silyl protecting groups by HF, the resulting resorcinarene **III** was bridged with the commercially available dichloroethylphosphine. The tetraphosphonite intermediate was oxidized *in situ* with sulfur, which proceeded with retention of configuration at phosphorous centre leading to **XIII**. The ^{31}P NMR spectra showed a singlet resonance at 92.2 ppm that is correlated to the presence of four phosphonate groups at the upper rim functionalized with ethyl moieties. Afterward, the tetra-chloride cavitand was reacted with sodium azide to give the tetra-azide cavitand **XIV** which was subjected to the CuAAC click reaction

with propargyl lactose peracetate using toluene as solvent and $[(EtO)_3PCuI]$ as catalyst. The cavitand **XV** was characterized with ^1H and ^{31}P NMR. The acetyl protecting groups were removed as previously seen. The ^{31}P NMR of the cavitand **XVI** showed a peak at about 92.3 ppm while the ^1H NMR showed a confused and broad spectra without the presence of the signal of the cavitand. Moreover the MALDI spectra did not show either the peak of the target molecule or the starting material, indicating that the reaction does not lead to the desired product.

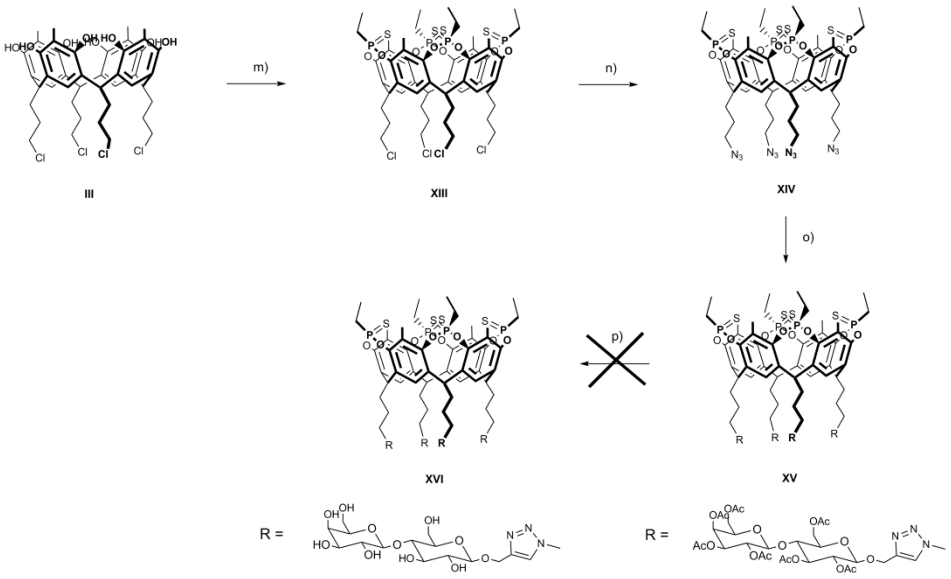

Scheme 6.3 *Synthesis of Tiiii [lactose, CH_3, CH_2CH_3], **XVI**: m) 1) $CH_3CH_2PCl_2$, Py, 75 °C, 3 h; 2) H_2O_2, 1 h, 51% (over two steps); n) NaN_3, DMF, 50 °C, 16 h, 79%;o) lactose propargyl peracetate X, $[(EtO)_3PCuI]$, DIPEA, Toluene/$CHCl_3$, 80 °C, 93%; p) 1) MeOH/Na, 2 h, r.t.; 2) Dowex IR-120, r.t., 1 h, the reaction does not work.*

6.4 Conclusions

Mimicry of biological process involves the study of recognition properties of synthetic receptors in water. In this chapter we have reported different attempts to make neutral water soluble tetraphosphonate cavitands. They comprise the introduction of hydrophilic moieties such as carbohydrates groups and the functionalization of the upper rim of the receptor with a less hydrophobic functional groups. The presence of four glucose or lactose groups at lower rim is not sufficient to solubilize the **Tiiii** cavitand (with four phenyl groups at the

upper rim). To tackle this problem we have functionalized the cavitand with four lactose group at the upper rim. Unfortunately the oxidation of the four P=S groups to P=O as last step is not compatible with the sugars at the lower rim. The P=O introduction must be moved at the beginning of the synthetic scheme. As a general comment, the introduction of neutral hydrophilic substituents only at the lower rim is not sufficient to impart water solubility to the whole cavitand. Therefore, in the design of a neutral water soluble cavitand also the introduction of hydrophilic groups at the upper rim must be planned.

6.5 Acknowledgments

Special thanks to Dr. Roberta Pinalli and Dr. Daniela Menozzi from Department of Chemistry, University of Parma for help in the synthesis.

6.6 Experimental Section

The propargyl glucose peracetate and propargyl lactose peracetate were prepared following reported procedures.[24] Compound **II** and **III** were already prepared in the group.

Tetrachloro silylcavitand (II).
To a solution of tetrahydroxy footed silylcavitand (0.5 g, 0.499 mmol) in dry 1,1,2,2-tetrachloroethane, few drops of DMF were added. The suspension was cooled to 0°C and thionyl chloride was slowly added (361 µL, 4.99 mmol,). The resulting suspension was stirred for 12h at 90 °C. The solvent was evaporated; the residue was dissolved in chloroform, washed with water and dried over $MgSO_4$. After evaporating the solvent the crude product was purified by silica gel column chromatography (hexane:ethyl acetate 8:2) to give the desired product as brownish solid (0.72 g, 0.464 mmol, 93%).
^{1}H NMR ($CDCl_3$, 400 MHz): δ (ppm) = 7.24 (s, 4H, Ar**H**), 4.69 (t, 4H, J= 8 Hz, ArC**H**), 3.68 (t, 8H, J= 8 Hz, $CH_2C\mathbf{H_2}Cl$), 2.50-2.38 (m, 8H, $CH_2C\mathbf{H_2}CH_2Cl$), 1.98 (s, 12H, Ar$C\mathbf{H_3}$), 1.92-1.76 (m, 8H, $C\mathbf{H_2}CH_2CH_2Cl$), 0.59 (s, 12H, Si$C\mathbf{H_{3,out}}$), -0.61 (s, 12H, Si$C\mathbf{H_{3,in}}$).

Tetrachloro resorcinarene (III)
An aqueous 36% HF solution (150 µL) was added to **II** (0.58 g, 0.538 mmol) dissolved in DMF. The suspension was stirred overnight at 55 °C. The product was precipitated by adding water to the reaction mixture. The white solid was collected by suction filtration. (0.45 g, 0.53 mmol, quantitative yield).
^{1}H NMR (Acetone-d_6, 400 MHz): δ (ppm) = 7.90 (m, 6H, ArO**H**), 7.33 (s, 4H, Ar**H**), 4.29 (t, 4H, J= 8 Hz, ArC**H**), 3.50 (t, 8H, J= 8 Hz, $CH_2C\mathbf{H_2}Cl$), 2.37-2.26 (m, 8H, $CH_2C\mathbf{H_2}CH_2Cl$), 1.91 (s, 12H, Ar$C\mathbf{H_3}$), 1.65-1.55 (m, 8H, $C\mathbf{H_2}CH_2CH_2Cl$).

Cavitand TSiiii [C_3H_6Cl, CH_3, Ph] (IV)
To a solution of resorcinarene **III** (0.255 g, 0.3 mmol) in dry pyridine, dichlorophenylphosphine (185 µL, 1.35 mmol) was added dropwise, under argon atmosphere. The solution was stirred at 60 °C for 1 h. Sulfur (0.61 g, 0.24 mmol) was added and the mixture was heated at 50°C for 2 h. The solvent was removed under vacuo and the solid was washed and sonicated with water, then filtered and dried. The crude product was purified by silica gel column chromatography (hexane:ethyl acetate 6:4) affording **IV** as white solid (0.275 g, 0.195 mmol, 65%)

^{1}H NMR ($CDCl_3$, 400 MHz): δ (ppm) = 8.21-8.06 (m, 8H, P(S)Ar**H$_o$**), 7.75 (s, 4H, Ar**H**), 7.65-7.44 (m, 12H, P(S)Ar**H$_m$**, P(S)Ar**H$_p$**), 4.70 (t, 4H, J= 8 Hz, ArC**H**), 3.59 (t, 8H, J= 8 Hz, $CH_2C\mathbf{H_2}Cl$), 2.62-2.44 (m, 8H, $CH_2C\mathbf{H_2}CH_2Cl$), 1.91 (s, 12H, Ar$C\mathbf{H_3}$), 1.82-1.64 (m, 8H, $C\mathbf{H_2}CH_2CH_2Cl$); **^{31}P{^{1}H}NMR** ($CDCl_3$, 161.9 MHz): δ (ppm) = 75.2 (s, P=S); **ESI-MS**: m/z 1422 $[M+K]^+$.

Cavitand TSiiii [$C_3H_6N_3$, CH_3, Ph] (V)

To a solution **IV** (0,25 g, 0.178 mmol) in DMF, sodium azide was added (0.12 mg, 1.78 mmol). The solution was stirred overnight at 55 °C for 12h. Then the solvent was evaporated and the crude was suspended in water and filtered affording **V** as a brown solid (0,25 g, 0.178 mmol, quantitative yield).

^{1}H NMR ($CDCl_3$, 300 MHz): δ (ppm) = 8.30-8.15 (m, 8H, P(O)Ar**H$_o$**), 7.70-7.50 (m, 12H, P(O)Ar**H$_p$**, P(O)Ar**H$_m$**), 7.24 (s, 8H, Ar**H**); 4.75 (t, J=8 Hz 4H, ArC**H**), 3.47 (t, 2H, J= 6.2 Hz $CH_2C\mathbf{H_2}N_3$), 2.51-2.35 (m, 8H, $CH_2C\mathbf{H_2}CH_2N_3$), 2.12 (s, 12H, Ar$C\mathbf{H_3}$), 1.81-1.65 (m, 8H, $C\mathbf{H_2}CH_2CH_2N_3$); **^{31}P{^{1}H}NMR** ($CDCl_3$, 161.9 MHz): δ (ppm) = 75.5 (s, P=S); **ESI-MS**: m/z 1468 $[M+K]^+$.

Cavitand TSiiii [C_3H_6-glucose-peracetate, CH_3, Ph] (VI)

A mixture of toluene/$CHCl_3$ (1:1) and DIPEA (210 μL, 1.18 mmol) was degassed 3 times with freeze pump thaw technique followed by addition of **V** (0.17 g, 0.12 mmol), propargyl glucose peracetate (0.23 g, 0.59 mmol) and the copper catalyst [$(EtO)_3PCuI$] (0.04 g, 0.059 mmol). The reaction mixture was stirred at 80 °C for 12h. Evaporation of the solvent yielded a crude that was purified by silica gel column chromatography (ethyl acetate) giving **VI** as white solid (0.245 g, 0.084 mmol, 70%).

^{1}H NMR ($CDCl_3$, 300 MHz): δ (ppm) = 8.27-8.07 (m, 8H, P(O)Ar**H$_o$**), 7.68 (s, 4H, **H**$_{triazole}$), 7.65-7.46 (m, 12H, P(O)Ar**H$_p$**, P(O)Ar**H$_m$**), 7.24 (s, 4H, Ar**H**), 5.25-5.14 (m, 4H, **H$_{3,glu}$**), 5.14-4.88 (m, 12H, **H$_{2,4,glu}$**, ArC**H**), 4.86-4.63 (m, 12H, **H$_{1,glu}$**, $C\mathbf{H_2}O$), 4.56 (t, 8H, $C\mathbf{H_{2,triazole}}$), 4.32-4.04 (m, 8H, **H$_{6,glu}$**), 3..81-369 (m, 4H, **H$_{5,glu}$**), 2.54-2.31 (m, 8H, $C\mathbf{H_2}CH_2N$), 2.14-1.82 (m, 68H, Ar$C\mathbf{H_3}$, $C\mathbf{H_2}CH_2CH_2N$, OCOC**H$_3$**); **^{31}P{^{1}H}NMR** ($CDCl_3$, 161.9 MHz): δ (ppm) = 75.8 (s, P=S); **MALDI TOF-TOF**: calcd. for $C_{136}H_{152}N_{12}O_{48}P_4S_4Na$ exact mass: 2995.7553, found: 2995.7760.

Cavitand TSiiii [C_3H_6-glucose, CH_3, Ph] (VII)

To a suspension of **VI** (0.03 g, 0.01 mmol) in methanol a cold solution of sodium in methanol (pH 9-10) was added dropwise. The mixture was stirred at room temperature for 2h until all the starting material was hydrolyzed. The

reaction was quenched by addition of Amberlite IR-120 resin. After 1h the resin was removed by suction filtration and the solvent was evaporated under reduced pressure affording the tetra glucose-cavitand **VII** as white solid (0,023 g., 0.01 mmol, quantitative yield).

^{1}H NMR (MeOD, 300 MHz): δ (ppm) = 8.33-8.18 (m, 8H, P(O)Ar**H$_o$**), 8.17-8.04 (m, 4H, **H**$_{triazole}$), 7.75-7.55 (m, 12H, P(O)Ar**H$_p$**, P(O)Ar**H$_m$**), 7.47 (s, 4H, Ar**H**), 5.11-4.69 (m, 12H, **H$_{2,3,4,glu}$**, ArC**H**), 4.40 (d, 4H, **H$_{1,glu}$**), 4.71-4.50 (t, 8H, C**H$_{2,triazole}$**), 3.97-3.55 (m, 8H, **H$_{6,glu}$**), 3.41-3.13 (m, 4H, **H$_{5,glu}$**), 2.58-2.35 (m, 8H, C**H$_2$**CH$_2$N), 2.10 (s, 12H, ArC**H$_3$**), 2.00-1.89 (m, 8H, C**H$_2$**CH$_2$CH$_2$N); **^{31}P{^{1}H}NMR** (MeOD, 161.9 MHz): δ (ppm) = 78.8 (s, P=S); **MALDI TOF-TOF**: calcd. for $C_{104}H_{120}N_{12}O_{32}P_4S_4Na$ exact mass: 2323.5863, found: 2323.5902.

Cavitand Tiiii [C$_3$H$_6$-glucose peracetate, CH$_3$, Ph] (VIII)

To a solution of **VII** (0.03 g, 0.01 mmol) in toluene a solution of H_2O_2 35% (0.65 mL, 6.66 mmol) in acetone was added dropwise. The mixture was stirred at 75 °C for 24h. The reaction was quenched by addition of H_2O. The aqueous phase was extracted with CH_2Cl_2. The organic phase was evaporated yielding compound **VIII** as yellow solid.

^{31}P{^{1}H}NMR (MeOD, 161.9 MHz): δ (ppm) = 11.6 (s, P=O); **MALDI TOF-TOF**: calcd. for $C_{136}H_{152}N_{12}O_{52}P_4Na$ exact mass: 2931.8467, found: 2931.8511.

Cavitand TSiiii [C$_3$H$_6$-lactose-peracetate, CH$_3$, Ph] (X)

A mixture of toluene/$CHCl_3$ (1:1) and DIPEA (245 μL, 1.39 mmol) was degassed 3 times with freeze pump thaw technique followed by addition of **V** (0.2 g, 0.139 mmol), propargyl lactose peracetate (0.471 g, 0.699 mmol) and the copper catalyst [(EtO)$_3$PCuI] (0.05 g, 0.069 mmol). The reaction mixture was stirred at 80 °C for 48h. Evaporation of the solvent yielded a crude that was purified by silica gel column chromatography (ethyl acetate:ethanol 98:2) giving **X** as white solid (0.346 g, 0.083 mmol, 60%).

^{1}H NMR ($CDCl_3$, 300 MHz): δ (ppm) = 8.27-8.12 (m, 8H, P(O)Ar**H$_o$**), 7.68 (s, 4H, **H**$_{triazole}$), 7.65-7.50 (m, 12H, P(O)Ar**H$_p$**, P(O)Ar**H$_m$**), 7.28 (s, 4H, Ar**H**), 5.40-5.33 (m, 4H, **H$_{1,lact}$**), 5.24-5.00 (m, 8H, **H$_{4',3,lact}$**), 5.00-4.86 (m, 12H, **H$_{2,2',lact}$**, ArC**H**), 4.85-4.64 (m, 12H, **H$_{3',lact}$**, C**H$_2$**O), 4.64-4.46 (m, 16H, **H$_{6,1',lact}$**, C**H$_{2,triazole}$**), 4.21-4.03 (m, 12H, **H$_{6,6,6',lact}$**), 3.98-3.76 (m, 8H, **H$_{4,5',lact}$**), 3.73-3.61 (m, 4H, **H$_{5,lact}$**), 2.52-2.38 (m, 8H, C**H$_2$**CH$_2$N), 2.22-1.91 (m, 104H, ArC**H$_3$**, C**H$_2$**CH$_2$CH$_2$N, OCOC**H$_3$**); **^{31}P{^{1}H}NMR** ($CDCl_3$, 161.9 MHz): δ (ppm) = 75.3 (s, P=S); **MALDI TOF-TOF**: calcd. for $C_{184}H_{216}N_{12}NaO_{80}P_4S_4$ exact mass: 4148,0933, found: 4148,1033.

Cavitand TSiiii [C_3H_6-lactose, CH_3, Ph] (XI)

To a suspension of **X** (0.03 g, 0.007 mmol) in methanol a cold solution of sodium in methanol (pH 9-10) was added dropwise. The mixture was stirred at room temperature for 2h until all the starting material was hydrolyzed. The reaction was quenched by addition of Amberlite IR120 resin. After 1h the resin was removed by suction filtration and the solvent was evaporated under reduced pressure affording the tetra lactose-cavitand **XI** as white solid (0,023 g, 0.007 mmol, quantitative yield).

^{1}H NMR (DMSO-d_6, 300 MHz): δ (ppm) = 8.25-8.13 (m, 12H, P(O)Ar**H$_o$**, **H**$_{triazole}$), 7.83-7.61 (m, 16H, P(O)Ar**H$_p$**, P(O)Ar**H$_m$**, Ar**H**), 5.40-5.33 (m, 4H, **H$_1$**$_{,lact}$), 5.24-5.01 (m, 8H, **H$_{4'}$**$_{,3,lact}$), 5.01-4.82 (m, 12H, **H$_{2,2'}$**$_{,lact}$, ArC**H**), 4.85-4.64 (m, 12H, **H$_{3'}$**$_{,lact}$, C**H$_2$**O), 4.60-4.45 (m, 16H, **H$_{6,1'}$**$_{,lact}$, C**H$_2$**$_{,triazole}$), 4.21-4.03 (m, 12H, **H$_{6,6,6'}$**$_{,lact}$), 3.98-3.76 (m, 8H, **H$_{4,5'}$**$_{,lact}$), 3.73-3.61 (m, 4H, **H$_5$**$_{,lact}$), 2.50-2.38 (m, 8H, C**H$_2$**CH_2N), 2.08-1.75 (m, 20H, ArC**H$_3$**, C**H$_2$**CH_2CH_2N); **^{31}P{^{1}H}NMR** (MeOD, 161.9 MHz): δ (ppm) = 74.7 (s, P(S)); **MALDI TOF-TOF**: calcd. for $C_{128}H_{160}N_{12}O_{52}P_4S_4Na$ exact mass: 2971,7975, found: 2971.8011.

Cavitand TSiiii [C_3H_6Cl, CH_3, CH_2CH_3] (XIII)

To a solution of resorcinarene **III** (0.4 g, 0.47 mmol) in dry pyridine, dichloroehtylphosphine (200 μL, 1.93 mmol) was added dropwise, under argon atmosphere. The solution was stirred at 60 °C for 1 h. Sulfur (0.12 g, 0.47 mmol) was added and the mixture was heated at 50°C for 2 h. The solvent was removed under vacuo and the solid was washed and sonicated with water, then filtered and dried. The crude product was purified by silica gel column chromatography (dichloromethane) affording **IV** as white solid (0.289 g, 0.47 mmol, 51%).

^{1}H NMR ($CDCl_3$, 300 MHz): δ (ppm) = 7.14 (s, 4H, Ar**H**), 4.51 (t, 4H, J= 7.4 Hz, ArC**H**), 3.72 (t, 8H, J= 7.1 Hz, CH_2C**H$_2$**Cl), 2.44-2.39 (m, 16H, CH_2C**H$_2$**CH_2Cl, CH_3C**H$_2$**P), 2.11 (s, 12H, ArC**H$_3$**), 1.86-1.83 (m, 8H, CHC**H$_2$**CH_2CH_2Cl), 1.52-1.43 (m, 12H, **CH$_3$**CH_2P); **^{31}P{^{1}H}NMR** ($CDCl_3$, 161.9 MHz): δ (ppm) = 92.2 (s, P=S); **ESI-MS**: m/z 1212 $[M+H]^+$, 1234 $[M+Na]^+$, 1250 $[M+K]^+$.

Cavitand TSiiii [$C_3H_6N_3$, CH_3, CH_2CH_3] (XIV)

To a solution **XIII** (0,29 g, 0.24 mmol) in DMF, sodium azide was added (0.18 mg, 0.28 mmol). The solution was stirred overnight at 55 °C for 12h. Then the

solvent was evaporated and the crude was suspended in water and filtered affording **XIV** as a brown solid (0,234 g, 0.189 mmol, 79%).
^{1}H NMR ($CDCl_3$, 400 MHz): δ (ppm) = 7.10 (s, 4H, Ar**H**), 4.55 (t, 4H, J= 7.4 Hz , Ar**CH**), 3.43 (t, 8H, J= 7.1 Hz, $CH_2C\mathbf{H_2}N_3$), 2.45-2.35 (m, 16H, $CH_2C\mathbf{H_2}CH_2Cl$, $CH_3C\mathbf{H_2}P$), 2.11 (s, 12H, Ar**CH$_3$**), 1.70-1.61 (m, 8H, $CHC\mathbf{H_2}CH_2CH_2Cl$), 1.53-1.43 (m, 12H, **CH$_3$**CH_2P); **^{31}P{^{1}H}NMR** ($CDCl_3$, 161.9 MHz): δ (ppm) = 92.4 (s, P=S); **ESI-MS**: m/z 1238 $[M+H]^+$, 1260 $[M+Na]^+$.

Cavitand TSiiii [C_3H_6-lactose-peracetate, CH_3, CH_2CH_3] (XV)
A mixture of toluene/DIPEA (1/1) (140 μL, 0.8 mmol) was degassed 3 times with freeze pump thaw technique followed by addition of **XIV** (0.1 g, 0.08 mmol), propargyl lactose peracetate (0.245 g, 0.36 mmol) and the copper catalyst [$(EtO)_3PCuI$] (0.027 g, 0.04 mmol). The reaction mixture was stirred at 80 °C for 48h. Evaporation of the solvent yielded a crude that was purified by silica gel column chromatography (dichloromethane:methanol 98:2) giving **XV** as white solid (0.288 g, 0.074 mmol, 93%).
^{1}H NMR ($CDCl_3$, 300 MHz): δ (ppm) = 7.56 (s, 4H, $\mathbf{H}_{triazole}$), 6.99 (s, 4H, Ar**H**), 5.28 (d, J= 5 Hz, 4H, $\mathbf{H_{1}}_{,lact}$), 5.16-4.98 (m, 8H, $\mathbf{H_{4'}}_{,3,lact}$), 4.95-4.76 (m, 12H, $\mathbf{H_{2,2'}}_{,lact}$, Ar**CH**), 4.75-4.53 (m, 8H, $\mathbf{H_{3'}}_{,lact}$, Ar**CH**), 4.52-4.36 (m, 16H, $\mathbf{H_{6,1'}}_{,lact}$, $C\mathbf{H_2}$triazole), 4.15-3.93 (m, 12H, $\mathbf{H_{6,6,6'}}_{,lact}$), 3.88-3.67 (m, 8H, $\mathbf{H_{4,5'}}_{,lact}$), 3.64-3.52 (m, 4H, $\mathbf{H_5}_{,lact}$), 2.41-2.14 (m, 16H, $CH_2C\mathbf{H_2}CH_2N$, $CH_3C\mathbf{H_2}P$), 2.15-1.76 (m, 104H, Ar**CH$_3$**, $C\mathbf{H_2}CH_2CH_2N$, OCO**CH$_3$**), 1.45-1.28 (m, 12H, **CH$_3$**CH_2P); **^{31}P{^{1}H}NMR** ($CDCl_3$, 161.9 MHz): δ (ppm) = 92.4 (s, P=S); **MALDI TOF-TOF**: calcd. for $C_{168}H_{216}N_{12}O_{80}P_4S_4Na$ exact mass: 3956.0934, found: 3956.0605.

6.7 References and Notes

[1] G. V. Oshovsky, D. N. Reinhoudt, W. Verboom, *Angew. Chem. Int. Ed.* **2007**, *46*, 2366-2393.

[2] S. M. Biros, J. Rebek Jr., *Chem. Soc. Rev.* **2007**, *36*, 93-104.

[3] D. A. Uhlenheuer, K. Petkau, L. Brunsveld, *Chem. Soc. Rev.* **2010**, *39*, 2817-2826.

[4] M. W. Peczuh, A. D. Hamilton, *Chem. Rev.* **2000**, *100*, 2479-2493.

[5] H. Zhou, L. Baldini, J. Hong, A. J. Wilson, A. D. Hamilton, *J. Am. Chem. Soc.* **2006**, *128*, 2421-2425.

[6] S. B. Larson, J. S. Day, R. Cudney, A. McPherson, *Acta Crystallogr.* **2007**, *63*, 310-318.

[7] D. T. Dang, H. D. Nguyen, M. Merkx, L. Brunsveld, *Angew. Chem. Int. Ed.* **2013**, *52*, 2915-2919.

[8] Y. Liu, Y. Chen, *Acc. Chem. Res.* **2006**, *39*, 681-691.

[9] a) V. Martosa, S. C. Bell, E. Santosa, E. Y. Isacoff, D. Trauner, J. de M. Martos, *Proc. Natl Acad. Sci. U.S.A.* **2009**, *106*, 10482–10486; b) O. Danylyuk, K. Suwinska, *Chem. Commun.* **2009**, *39*, 5799-5813; c) F. Perret, A. W. Coleman, *Chem. Commun.* **2011**, *47*, 7303-7319.

[10] a) D. P. Weimann,. H. D. Winkler, J. A. Falenski, , B. Koksch, C. A. Schalley, *Nature Chem.* **2009**, *1*, 573-577; b) D. Paul, A. Suzumura, H. Sugimoto, J. Teraoka, S. Shinoda, H. Tsukube, *J. Am. Chem. Soc.* **2003**, *125*, 11478-11479.

[11] J. M. Chinai, A. B. Taylor, L. M. Ryno, N. D. Hargreaves, C. A. Morris, P. J. Hart, A. R. Urbach, *J. Am. Chem. Soc.* **2011**, *133*, 8810-8813.

[12] R. E. McGovern, H. Fernandes, A. R. Khan, N. P. Power, P. B. Crowley, *Nature Chem.* **2012**, *4*, 527-533.

[13] M. R. Arkin, J. A. Wells, *Nat. Rev. Drug Discov.* **2004**, *3*, 301-317.

[14] a) C. L. Peterson, M. A. Laniel, *Curr. Biol.* **2004**, *14*, 546-551; b) R. Margueron, P. Trojer, D. Reinberg, *Curr. Opin. Genet. Dev.* **2005**, *15*, 163-176.

[15] K. D. Daze, F. Hof, *Acc. Chem. Res.* **2013**, *46*, 937-945.

[16] C. S. Beshara, C. E. Jones, K. D. Daze, B. J. Lilgert, F. Hof, *ChemBioChem* **2010**, *11*, 63-66.

[17] a) R. M. Yebeutchou, F. Tancini, N. Demitri, S. Geremia, R. Mendichi, E. Dalcanale, *Angew. Chem., Int. Ed.* **2008**, *47*, 4504-4508; b) R. M. Yebeutchou, E. Dalcanale, *J. Am. Chem. Soc.* **2009**, *131*, 2452-2453.

[18] M. Dionisio, G. Oliviero, D. Menozzi, S. Federici, F. P. Schmidtchen, E. Dalcanale, P. Bergese, *J. Am. Chem. Soc.* **2012**, *134*, 2392-2398.

[19] A. Lledo, J. Rebek Jr., *Chem. Commun.* **2010**, *46*, 8630-8632.

[20] O. Middel, W. Verboom, D. N. Reinhoudt, *Eur. J. Org. Chem.* **2002**, , 2587-2597.

[21] D. A. Ryan, J. Rebek Jr., *J. Am. Chem. Soc.* **2011**, *133*, 19653-19655.

[22] V. V. Rostovtsev, L. G. Green, V. V. Fokin, K. B. Sharpless, *Angew. Chem. Int. Ed.* **2002**, *41*, 2596-2599.

[23] J. M. Sanfrutos, M. O. Munoz, J. L. Jaramillo, F. H. Mateo, F. S. Gonzalez, *J. Org. Chem.* **2008**, *73*, 7768-7771.

[24] H. B. Mereyala, S. R. Gurrala, *Carbohydr. Res.* **1998**, *307*, 351-354.

Appendix A

Materials and Methods

Materials

All reagents and chemicals were obtained from commercial sources and used without further purification. Dry pyridine (supplied from Aldrich) was distilled over KOH and stored over 3 Å molecular sieves under Ar or used as received (pyridine absolute, over molecular sieves, $H_2O \leq 0.005\%$). Dichloromethane (purchased from Aldrich) was dried by distillation over CaH_2 according standard procedures and stored over 3 Å molecular sieves under Ar. Anhydrous chloroform (supplied from Aldrich) was prepared washing it twice with water and passed through a column of basic alumina oxide (supplied from Fluka) then it was distilled over CaH_2 and stored over 4 Å molecular sieves under Ar. Anhydrous toluene (supplied from Aldrich) was distilled over CaH_2 and stored over 4 Å molecular sieves under Ar. Dry DMF (DMF purissim. ≥ 99.5%(GC)) was provided by Aldrich and stored over 4 Å molecular sieves under Ar. Dry diethyl ether (diethyl ether purum ≥ 99.8%(GC), over molecular sieves) was purchased from Fluka and used as received.
Silica column chromatography was performed using silica gel 60 (Fluka 230-400 mesh ASTM), or silica gel 60 (MERCK 70-230 mesh).

Methods

- **NMR Measurements**

^1H NMR spectra were obtained using a Bruker AVANCE 300 (300 MHz) or a Bruker AVANCE 400 (400 MHz) spectrometer. All chemical shifts (δ) were reported in ppm relative to the proton resonances resulting from incomplete deuteration of the NMR solvents. ^{31}P NMR spectra were obtained using a Bruker AVANCE-400 (161.9 MHz) spectrometer. All chemical shifts (δ) were recorded in ppm relative to external 85% H_3PO_4 at 0.00 ppm.

- **MS Measurements**

(Chapters 2-3-4-6): Electrospray ionization ESI-MS experiments were performed on a Waters ZMD spectrometer equipped with an electrospray interface. Exact masses were determined using a LTQ ORBITRAP XL Thermo spectrometer equipped with an electrospray interface. MALDI was performed on a AB SCIEX MALDI TOF-TOF 4800 Plus (matrix, α–cyano-4-hydroxycinnamic acid).
(Chapter 5): ESI-MS was performed on a Thermo Scientific LTQ Orbitrap Velos mass spectrometer with an electrospray ion source in the positive ion mode.

Acknowledgments

Incredibile sono arrivato alla fine! Di persone da ringraziare ce ne sono parecchie, senza il vostro aiuto non avrei potuto fare niente di tutto questo.

Per prima cosa devo ringraziare i miei genitori, siete la mia guida e il mio supporto. Grazie per avermi sempre consigliato, aiutato a prendere qualsiasi decisione e ad affrontare qualsiasi sfida. Papà devi aprire una bottiglia di Pinot bella grossa questa volta!!! Un grazie anche a tutta la mia famiglia soprattutto i nonni gli zii e tutti i miei cugini, anche se non tutti hanno capito cosa ho fatto in questi tre anni (ma cosa fai in laboratorio?), sappiate che mi siete stati d'aiuto anche voi!

Un grazie ad Enrico per avermi permesso di trascorrere questa avventura nel suo gruppo ed avermi trasmesso la sua grande passione. Dovresti ringraziare me, fede e marco per tutte le scommesse che ti abbiamo fatto vincere sul milan.

Un grazie gigantesco a tutti i ragazzi del gruppo.
Per prima cosa tutti i ragazzi del lab. succursale 187 (illogic chemistry), come disse qualcuno per entrare al 187 bisogna possedere determinate qualità. Grazie a Marco, che dire la quantità di cose che mi hai insegnato nel tempo passato insieme è stato pari alle quantità di c. che abbiamo detto: ENORME. Grazie per tutti i consigli per 'sburlare' le reazioni. Discutere con te di chimica, idee varie, libri, cinema, milan, le f. di ole' diario deportivo, è stato un piacere, grazie amico!! Bedo, conoscitore assoluto di tutta la produzione mondiale di film e videogiochi (Bedo per caso hai visto quel film? domanda inutile), stare con te e Marco in laboratorio è stato incredibile, grazie anche per non avermi ucciso nel periodo di scrittura della tua tesi. Mattia altro grande componente del 187 (ma le reazioni dry con l'aria?). Fede (immigrato dal 213), dopo la specialistica anche il dottorato nello stesso lab., i momenti ignoranti hanno reso la scrittura della tesi un periodo non così stressante. Ale (pedros) ricordati che la chimica is a lieeeeeeeeeee. Grazie anche a Dario (ormai sei sempre al 187) Paola e Marta.
Un grazie anche a tutti i tesisti/e che hanno avuto la fortuna di passare al 187, Thomas (anche se hai devastato tutto il 187, entri nella storia del lab, ricordati di me quando aprirai il tuo gruppo di ricerca e diventerai professorone), Carola (grazie per l'allegria che porti in lab, se non ci fossi tu sai che noia solo con pedro ☺) Valeria (in bocca al lupo per la tua nuova avventura!) e Federico. Grazie di esistere 187!

Un grazie a tutti i ragazzi del 213. I super bulli polsky Kasjan e Kuba (miei compagni di sventura, andiamo a festeggiare in Polonia!! Kasjan aspetto un altro party per festeggiare nuovamente il matrimonio), la Dany (grande tuuuu, grazie per avermi corretto tutte le esse (s) mancanti della tesi, mi sdebiterò il prossimo aperitivo all'avis), Roby (grazie per tutti i consigli che mi hai dato in questi tre anni e per la tesi, peccato che sei juventina), Ely (grazie per tutto l'aiuto che mi hai dato e per la tesi), la Vero (super pallavolista), Tahnee e il nuovo arrivato Andreas.
Grazie amici, sono stato fortunato, siete i migliori compagni di laboratorio che potessi incontrare.

Thanks to Dr. Scherman for the opportunity to join his group in Cambridge for seven months, and special thanks to Silvia, Daniele, Ula, Setu, Sean, Matt, Louisa and all the guys of the group for the time we have spent together. I'd like to thanks also the lads of 11 a side (Magpies) and 5 a side football teams (Old School), thanks for the awesome time we spent together playing football and drinking beer (I felt at home in the pub with you).

Un grazie a tutti gli amici di sempre di Torre, San Lorenzo e Cappella, anche quelli che non vedo da un po' e tutti gli amici di Cingia. Non sono presente come prima alle nostre 'baracche' ma riusciamo sempre a divertirci come se non fosse mai passato del tempo, sappiate che siete dei ragazzi fantastici, siete una parte importante della mia vita. Un ringranziamento speciale a Manuel (ghengherеghen) che ha condiviso con me un anno e mezzo di appartamento a Parma, dovevamo registrare tutte le c. che abbiamo detto.

Infine voglio ringraziare tutte quelle persone che sono entrate nella mia vita, che hanno voluto credere in me per poco o molto tempo, che mi hanno lasciato bei ricordi o insegnamenti, che mi hanno arricchito, anche voi avete partecipato a rendermi la persona che sono oggi.

Grazie di cuore!

Daniele

The author

born in Asola (Mantova, Italy) on the 1st of November 1985

July 2003	**High School Diploma** ITIS Janello Torriani Cremona, Italy
March 2007	**Bachelor in Chemistry** University of Parma, Italy Supervisor: Prof. A. Arduini
April 2009	**Master in Chemistry** University of Parma, Italy Supervisor: Prof. A. Arduini
January 2011-December 2013	**Doctoral Research** University of Parma, Italy Supervisor: Prof. E. Dalcanale
January 2013-July 2013	**Research exchange** University of Cambridge, UK Supervisor: Dr. O. A. Scherman